A NUMERICAL MODELLING APPROACH TO STUDY THE IMPACT OF VENTILATION CONFIGURATIONS ON AIRBORNE TRANSMISSION IN INDOOR ENVIRONMENTS

ARMA KHAN

A THESIS SUBMITTED TO

THE FACULTY OF GRADUATE STUDIES

IN PARTIAL FULFILLMENT OF THE REQUIREMENTS

FOR THE DEGREE OF MASTER OF APPLIED SCIENCE

GRADUATE PROGRAM IN THE DEPARTMENT OF MECHANICAL ENGINEERING

YORK UNIVERSITY

TORONTO, ONTARIO

November, 2022

Abstract

The airborne transmission of COVID-19 has been a topic of significant controversy since the pandemic began. Research was needed to demonstrate the importance of airborne transmission and develop tools to recommend appropriate control measures. This study aimed to analyze the factors that impact airborne transmission, find techniques for infection risk minimization, and develop methods to compare different control measures on infection risk. Computational Fluid Dynamics (CFD) studies were conducted to analyze the impact of ventilation layout and infection source location in indoor spaces. A novel spatio-temporal risk model was further developed to quantify the risk in indoor spaces based on different control measures. Conclusions have been made that the ventilation layout and infection source locations can significantly impact the risk of airborne transmitted infection. Further research into building design and airborne transmission minimization techniques is urgently needed to prepare for airborne infectious diseases that may emerge in the future.

Dedication

I dedicate this thesis to my parents Nasima Khan and Mainur Khan, who have worked tirelessly to raise me and sacrificed so much to see me succeed. They are a constant source of inspiration, support, and guidance, and I would not have been able to achieve all that I have without them.

Acknowledgements

I would like to express my deepest gratitude to my supervisor, Prof. Marina Freire-Gormaly, who has been dedicated, encouraging and supportive throughout my thesis project, and provided me this opportunity to learn and grow.

I would like to also acknowledge the time and effort Prof. Ronald Hanson and Prof. Jude Kong have put in to serve as my committee members and provide me with valuable feedback and support.

I am an incredibly grateful for the support I have received from the Ontario Graduate Scholarship, the Donna Hayden Memorial Award, NSERC Missions Alliance Grant and NSERC Emerging Infectious Disease-OMNI One Health, as well as the collaborative efforts from DAIR, De Havilland.

I would like to thank my fellow lab mates for their valuable input, support, and friendship, especially Dorothy Piluk, Kishon Webb and Amanda Capacchione for their input and assistance with my thesis. I also acknowledge the efforts of Shehnaz Islam and Reetika Ali towards my thesis, their contributions were invaluable.

I would like to thank Dr. Hossein Hosseinimanesh, Alan Wong, Natalia Xantiev and David Kam, for their advice, assistance, and input.

I would like to extend a special thanks to our Technical services lead Robert Reynolds, who has helped me resolve countless technical issues while always being a ray of sunshine that brightens your day.

I am indebted to my parents Mainur and Nasima, and my brothers Sahil and Saqib for continuously motivating me and pushing me to accomplish any task I take on.

My utmost gratitude goes to my partner Sinan Olcun, who has never ceased to amaze me. He always finds a way to comfort, humor, and encourage me.

Table of Contents

List of Figures

List of Tables

Chapter 1 Introduction

1.1. Background

The SARS-CoV-2 virus (COVID-19) emerged from a seafood market in Wuhan, China in December 2019 [1]. At that point not much was known about the virus except that it was causing unexplained respiratory conditions (pneumonia) and was potentially human-to-human transmissible [1,2]. The virus spread rapidly with cases in almost every country, and by March 11, 2020, the World Health Organization (WHO) declared COVID-19 a pandemic [2]. Transmission of the virus was first recognized to be from close contact and fomite (contact with contaminated surfaces) transmission [3]. The potential for airborne transmission was vague during the early months of the pandemic, with back and forth statements from CDC (Centre for Disease Control and Prevention) [4] and a quick dismissal by WHO: adamant that claiming COVID-19 was airborne would be "misinformation" [5]. The only form of airborne transmission recognized was that from medical procedures such as intubation as of WHO's March 27, 2020 Scientific brief [3]. The validity of airborne transmission routes transpired into significant controversy among the scientific community; prominent scientists in aerosol transport—Dr. L. Morawska and Occupational health—Dr. D. K. Milton composed a letter signed by 239 other leading researchers (in the fields of aerosol transport, indoor air, building engineering, epidemiology, medicine, among others) with concerns that not addressing the risks of airborne transmission may worsen the already dire situation caused by COVID-19 [6]. As more evidence was compiled pointing to the validity of airborne transmission routes for COVID-19, WHO gradually modified their statements, to finally announce on December 23, 2021 (2 years after the virus emerged) that COVID-19 was in fact short-range airborne, and worsened in poor ventilation conditions [7]. The resistance to accepting airborne transmissibility of the virus was rooted in the history of disease transmission: Charles Chapin revolutionized "germ theory" in 1910 with the intention of moving away from the idea that disease mysteriously infected people through "miasmas" transported through the air [4,8]. The hope was to ensue more responsibility to the public to prevent disease, as they took on hygiene measures more consciously. This was effective for many years with diseases that were dominantly transmitted through close contact. However, germ theory propagated a momentum that made it difficult for diseases of airborne nature to be seriously considered [4]. Tuberculosis was accepted

to be airborne after tireless and detailed experimental work by Wells, Riley and Langmuir; and it took seven decades for measles and varicella (chickenpox) to be accepted as airborne [4,8]. This resistance in accepting airborne transmission routes resulted in little attention put towards control measures to prevent the spread of airborne transmitted diseases [9]. Furthermore, WHO may have feared declaring COVID-19 an airborne transmitted disease would worsen the existing paranoia among the public, especially considering the lack of specific solutions that exist to alleviate airborne transmission of the virus.

The history of negligence towards airborne transmission routes explains the lack of research and specific solutions that have been gathered till now, to minimize the effects of airborne transmitted diseases. Some solutions such as natural ventilation, filtration and UV disinfection have been used throughout history, however controlling airborne transmitted diseases is not regulated, and the control measures seem archaic in comparison to the measures and tools that exist for controlling water-borne diseases [10]. In terms of control measures for airborne transmission, ventilation has long played a role in clearing contaminants, delivering fresh air to occupants and keeping indoor conditions ideal for occupants. However, the role of ventilation to remove contaminants from occupants quickly and efficiently, without exposing these contaminants to other occupants, was a challenge only dealt with in airborne infection isolation rooms (AIIR) and hospitals where nosocomial infections needed to be minimized. Ventilation configurations play a major role in the transport patterns of indoor contaminants, including respiratory aerosols. However, the most ideal ventilation configuration is dependent on many factors, some of which are the setting of the room, occupant density, location of the infectious occupant with respect to the layout, heating vs. cooling mode, among many others [11–14]. Therefore, each unique setting requires a different solution. Current literature recognizes this issue and there have been many studies to investigate the impact of ventilation layout [12,15–19], ventilation type [14,20–24], infection source locations [25,26] and the usage of control measures (e.g., plexiglass barriers or air cleaners) [16,25,27,28]. The referred studies consider different settings and conditions, therefore, each of the studies is valuable, contributing towards an understanding of the routes of airborne transmission in those unique settings. However, the results from any one study cannot be extrapolated towards a rule of thumb for airborne transport patterns in all settings; the spatio-temporal distribution of aerosols is unique to each setting (with some overlap between different settings). So, to assess the airborne transmission risk in unique settings

and conditions, and to compare the effectiveness of different control measures to be implemented in the space, a spatio-temporal risk model is necessary. Existing risk models for airborne transmission consider many factors when modelling infection risk, such as the seminal Wells-Riley model [29,30], among other mathematical models [31–33]. However, these models neglect the spatial heterogeneity of airborne transmission, which is important when considering the range of risk distribution in a space. Certain spatio-temporal models solve this problem with coupled Computational Fluid Dynamics (CFD) and mathematical risk models [26,34,35]. This ensures spatial heterogeneity of infection risk is accounted for. Some models have also acknowledged the spatial heterogeneity of airborne transmission and tackled it by incorporating stochasticity [32,36], as they recognize the importance of proximity to the infection source location can change the infection risk to occupants. However, to date, no models have been encountered in literature to be independent of source location, when quantifying the spatially and temporally heterogeneous distribution of infection risk in a space. A model that can consider the risk of infection in an indoor environment with respect to changes in ventilation, added control measures and changes in occupancy, while removing the sensitivity of the infection source location to the results, can significantly benefit the approach towards infection risk determination in various indoor spaces.

1.2. Motivation

This thesis study was motivated by the ongoing COVID-19 pandemic that impacted the world in many ways. The pandemic resulted in more than 6.5 million deaths (as of September 2022) [37] and an estimated $500 billion in monthly losses to global gross domestic product (GDP) (estimated by the International Monetary Fund) [38,39], among a social, financial, and mental health crisis in the world. The routes of transmission for the virus became an immediate issue, and investigating methods for transmission mitigation were crucial. Airborne transmission was a largely controversial topic among scientists and public health organizations during the early months of the pandemic, which further added to the urgency of seeking airborne transmission risk mitigation strategies: if public safety measures to prevent airborne transmission were not being recommended, many COVID-19 outbreaks would occur through airborne routes, thus worsening the contagion. A seminal publication by Morawska et al. [10] has also declared that “a paradigm shift” needs to occur for the design, regulation and standardization of building ventilation to

prevent the devastating effects seen during the COVID-19 pandemic. Studying the impact of ventilation configurations and infection source locations in various public indoor settings provides insight into the dispersion patterns of respiratory aerosols. When transport and dispersion patterns of respiratory aerosols are better understood, control measures such as planning for optimized air cleaner placement, removing occupancy in certain zones of an indoor space, or upgrading the ventilation configuration altogether can be undertaken. This study is conducted with the goal of improving air quality and minimizing the risk of airborne transmission in various public indoor settings.

1.3. Objectives

The main objective of this thesis is to study airborne transmission pathways in ventilated indoor environments, to then identify factors that improve or worsen conditions. If the factors contributing to airborne transmission are better understood, effective control measures can be implemented to minimize outbreaks caused by airborne transmission of disease. Thus, understanding airborne transport patterns, finding control measures and identifying the optimal control measures for each space is valuable towards minimizing the effects of the COVID-19 pandemic. Specific objectives investigated in this thesis study are then to:

- Investigate the impacts of ventilation configurations and infection source locations on aerosols dispersion patterns and risk of airborne transmission.
- Identify combinations of possible ventilation and infection source locations that will contribute to minimal airborne transmission risk.
- Quantify the overall risk of airborne transmission through a spatio-temporal risk model that is adaptable to various spaces.

1.4. Thesis Outline

In Chapter 1, an introduction is provided to the topic of airborne transmission, the role of ventilation and the objectives and contributions of the thesis study. Chapter 2 provides an extensive literature review of airborne transmission, ventilation and risk modelling methods. Chapter 3 gives an overview of the main CFD methodology. In Chapter 4, a small office space is modelled to study

the impact of ventilation component location on aerosol spread patterns. Three different ventilation layouts are simulated: the existing ventilation layout, an added air outlet above the occupant, and an added air outlet away from the occupant. In Chapter 5, a lecture hall was modelled to study the impact of mixing and displacement ventilation configurations, as well as the impact of infection source location. Three different infection source locations were simulated for each ventilation type. In Chapter 6, a combined CFD-Mathematical modelling approach is used to develop a spatio-temporal risk model. The risk model considers the overall airborne transmission risk in a space through a derived reproduction number. Chapter 7 concludes the work completed in this thesis and provides directions for future research.

Chapter 2 Literature Review

2.1. Airborne Transmission and COVID-19

When concerned with airborne transmission risk modelling, several topics must be reviewed 1) to gain deeper insight on the routes of transmission, 2) the conditions that impact the risk of transmission and 3) the established measurement techniques for airborne transmission. The following sections are a review and discussion of viral transmission routes, the mechanics of airborne transmission, ventilation and its implications on airborne transmission, and airborne transmission risk modelling methods that exist in literature.

2.1.1. Transmission Routes

Viral transmission is known to occur through human-human routes, airborne routes and other routes involving endogenous, common vehicle or vector borne routes [9]. Respiratory infectious diseases such as influenza, rhinoviruses, coronaviruses, mainly transmit through three main routes: direct transmission, indirect transmission, and airborne transmission. Direct transmission occurs where an infectious individual has direct contact with a susceptible individual's droplets thus transmitting the disease through the susceptible individual's mucosae (nose and mouth) or conjunctiva (eyes) [3]. Indirect transmission occurs when an infectious individual's mucosa is deposited on surfaces (known as fomites) and a susceptible individual comes in contact with the fomite [3]. Airborne transmission is a route of infection transmission associated with the air carriage of infectious droplets that have evaporated to become infectious aerosols [40].

Airborne transmission is often confused with droplet transmission, hence distinguishing between droplets and aerosols will provide more insight into the two transmission routes. Droplets are generated through exhaling, speaking, coughing, sneezing among other exhalatory actions. While aerosols can result from those same actions, they are often formed from droplet breakup and/or through the evaporation of droplets (forming what is also known as droplet nuclei) [1]. For airborne transmission, both droplets and aerosols contribute to transmission routes, however they differ among several factors which include diameter, range of transmission, viral stability in various environmental conditions, as well as virulence and infectivity [13,41]. The defining factors to distinguish between droplets versus aerosols remain ambiguous in the scientific literature. The World Health Organization (WHO) and Centers for Disease Control and Prevention (CDC) define

particles with a diameter below 5 μm to be aerosols (aerosols tend to remain suspended in the air for longer periods of time) while particles with a diameter above 5 μm are recognized as droplets, which will deposit before surpassing a distance of 2 m [3]. In contrast, several studies reviewed by Bahl et al. [42] show that droplets as large as 50 μm in diameter can remain suspended (travelling horizontal distances beyond 2 m) and droplets with a diameter above 5 μm can travel horizontal distances up to 8 m. A moderately accepted definition in literature is that droplet transmission occurs with short-range (essentially face-to-face) interactions where expiratory droplets directly deposit on to a host's mucous membranes; while airborne transmission occurs when aerosols spread expansively within indoor environments and remain airborne until a susceptible individual inhales the aerosol laden air.

The severity of infection caused by large droplets versus by aerosols is an "unresolved dichotomy" [13]. Aerosols appear riskier, as they can be carried to distances significantly further from the source thus reaching more susceptible individuals than droplets (which would only be exposed to individuals in the immediate surroundings of the infectious individual) [9,41]. Aerosols can also contribute to more serious infection, as they are likely to deposit deep in the respiratory tract, thus causing a more severe infection in comparison to droplets, which deposit in the upper airways [41]. In contrast however, viral particles remain more intact in droplets, while aerosols tend to be diluted by the surrounding air and dry out by evaporation. Evaporation of the droplet exposes the viral particles to the environment which can speed up destruction of the viral particles [9,43].

2.1.2. Droplets vs. Aerosols

Droplets are distinguished by Xie et al. [44] into "small droplets"—that evaporate into aerosols, and "large droplets"—that quickly deposit before significant evaporation occurs. The size of large droplets ranges from 97 μm in diameter to 172 μm in diameter (for Relative Humidity (RH) ranging from 0%-90%), according to Wells [30], while Xie et al. [44] find a range of 60 μm to 125 μm, for the same range of RH [44]. They also report that at 50% RH (appropriate for recommended ambient RH) the large droplet diameter starts at 100 μm [44], which coincides with Duguid's data [45]. Duguid studied the suspension, deposition and evaporation characteristics of bacteria- carrying droplets and droplet nuclei ranging from diameters of 0.25 μm to 2000 μm. Duguid's experimental method explored how coughs, sneezes and loud speaking produced droplets. Duguid's experimental method of dyed droplet deposition on an oiled slide positioned in

front of the subject, and in other cases used a slit sampler for quantifying droplet nuclei. Duguid identified that droplets in the size range of 1 μm - 100 μm would become airborne, while droplets from 100 μm - 2000 μm would immediately deposit on the ground [45]. More recent studies have also attempted to distinguish between droplets and aerosols based on their diameters, with a focus of quantifying the fluid dynamics of airborne transmission specific to COVID-19 [42,46–49]. In a study by Rosti et al. [46] they perform Direct Numerical Simulations (DNS) for the propagation of droplets from a cough in various RH. Different diameter distributions were used based on experimental work by Duguid [45], Johnson et al. [49], Xie et al. [48], and Yang et al. [47], to study the evaporation and deposition of droplets. Rosti et al. [46] could not make any definitive conclusions on what percentage of droplets deposit to the ground, what viral loads were retained, nor how far small droplets could be transported, because the diameter distribution data from the four studies were drastically different. Bahl et al. [42] reviewed multiple studies (experimental, numerical modelling and mathematical modelling) that characterize the diameter distributions and resulting droplet propagation distances. The studies resulted in a range of conclusions for the horizontal distance travelled by droplets ranging from 2 m up to 8 m, with the majority of studies reporting distances further than 2 m. Furthermore, there were no distinguishing aspects between droplets and aerosols, as droplets can either deposit or dry out into droplet nuclei/aerosols given different conditions; they are not "mutually exclusive" [42]. Rosti et al. [46] and Bahl et al. [42] emphasized that more research is needed to acquire data for diameter distributions, while accounting for many variables that will impact the spread and evolution of the droplet diameters, such as the RH, the method of droplet ejection (cough, sneeze, breathing, etc.), the impact of turbulent jets, the thermal gradients present and the ventilation conditions of the room. Wells (1934) [30] and Duguid (1945-1946) [45,50] contributed seminal work to establish diameter distributions, evaporation rates and droplet deposition rates, but measurement and modelling technology has progressed significantly since then.

Current studies investigating the evaporation rates of droplets with respect to RH provide some insight about droplet evaporation and resultant distances travelled due to evaporative effects. Morawska [6] calculated the evaporation rates of pure water droplets in stagnant air with diameters 1, 10 and 100 μm in different RH levels (0%-80%). She concluded that 1 μm droplets evaporate within milliseconds, regardless of RH, 10 μm droplets evaporate within 0.1-0.5 seconds and 100 μm droplets take around 10 seconds to a minute. The Wells evaporation-falling curve [30]

shows the evaporation times for droplets that become droplet nuclei and remain suspended or fall after surpassing 2 m, while also showing the falling times for droplets that ballistically fall due to gravity and deposit on the ground/surfaces. Xie et al.'s analysis [44] is a revision of the Wells evaporation-falling curve [30] which confirms the evaporation times by Morawska [9], but also considers the falling rates of droplets. Xie et al. [44] additionally analyzed droplet evaporation-falling rates for different initial velocities, demonstrating that as initial velocity increases, droplets are more likely to surpass 2m instead of immediately falling; however, the evaporation time is not impacted by initial velocity. Liu et al. [51] investigated the evaporation times of a droplet with NaCl (salt) concentrations. They performed analytical calculations and experimental work quantifying a droplet's evaporation time (which was deposited on a Teflon-printed surface) for different RH conditions. Liu et al. [51] further evaluated the sensitivity in horizontal distance transport for droplet diameters in 0% and 90% RH, and for initial velocities of 5 m/s and 10 m/s. They reported that for droplet diameters 35 μm to 80 μm, at an initial velocity of 5 m/s, and diameters 50 μm to 80 μm, at an initial velocity of 10 m/s, the horizontal distance travelled by the droplets will be dependent on RH levels. Duguid's paper [45] showed that 88% of the airborne droplet nuclei are in the range of 1-32 um, which are considered independent of RH according to Liu et al.'s analysis [51].

2.1.3. Impact of environmental Conditions on Airborne Transmission

Many studies have overlapping conclusions about the impact of temperature and humidity on airborne transmission rates. There is clear agreement that low RH and low temperatures contribute towards higher risks of transmission for enveloped viral pathogens such as coronaviruses and influenza viruses [9,52–55]. Mecenas et al. [53] performed a thorough review study, analyzing papers that discuss the impacts of both humidity and temperature on the transmission of COVID-19. Sixteen of the seventeen reviewed papers showed that warmer temperate environments were less favorable towards the spread of COVID-19, and fourteen of fifteen reviewed papers concluded that more humid environments inhibited the spread of the virus. The review was, however, more focused on outdoor climactic conditions. Yang and Marr [56] modelled influenza A virus' airborne transmission effects with RH in residential settings. They reported that higher RH reduced the risk of transmission by both increasing the droplet settling rate and reducing the infectivity of influenza by 2.4 times when changing RH from 10% to 90% [56]. The effects of humidity are more nuanced for airborne transmission. It has been

acknowledged that lower humidity levels allow droplets to quickly evaporate, resulting in viral-laden aerosols suspended in the air [9,44,51]. In addition, RH can biologically impact hosts' immune systems: a higher RH ensures a host's mucous membranes remain intact, thus able to repel viral particles [57]. Furthermore, RH levels can impact the survivability of viral material within droplets. Lin and Marr [58] observed that lower RH (<40%) and higher RH (> 60%) would retain viral viability, but intermediate RHs (40% < RH < 60%) would drastically reduce the survival of viruses. They also observed that the solute concentrations were higher in intermediate RHs, and it is known that salts can damage the viral membranes, inactivating the virus. Lin and Marr [58] concluded that in higher humidity levels a droplet has higher water content, hence the salts within the droplet are diluted and do not impact the viral particle, thus retaining viral viability. Low humidity facilitates rapid evaporation causing the salts to crystalize and separate from the droplet which also retains viral viability. Only, RH levels of 40% to 60% keep an outer layer of the droplet that is concentrated with salts close to the viral membrane, which can inactivate the virus. ASHRAE recommends indoor RH levels of 40%-60% as it has benefits of inactivating viral material and maintaining mucous membranes in occupants [59].

Other environmental factors such as ozone, UV radiation and particulate matter in the air can also affect the stability and transmission of viral particles. UV radiation, specifically UV-C is known to damage viral DNA, and inactivate virus particles [60–62]. Ultraviolet germicidal irradiation (UVGI) is recommended by ASHRAE in upper room air and duct air disinfection and has been widely researched and used before the COVID-19 pandemic [43]. In terms of UV radiation impacts on the SARS-CoV-2 virus, Schuit et al. [63] studied the exposure of sunlight to simulated saliva and culture medium of SARS-CoV-2 in aerosol form. They reported that the half-lives of the SARS-CoV-2 virus was reduced significantly to less than 6 minutes, while the half-life in absence of sunlight was around 1.1 hours—similar to that reported by van Doremalen et al. [64]. Ozone, mostly found in outdoor air (considered a toxic indoor pollutant) also has transmission limiting effects. Yao et al. [65] performed data correlation analysis and reported that correlations exist between an increase in outdoor ozone levels and reduced spread of COVID-19. Furthermore, correlations have been observed between higher air pollution levels and increase in case counts, suggesting that viral particles are suspended and entrained with a higher density of particulates in the air [66].

2.1.4. Physics of droplet transport

Droplets are known to transmit through various exhalatory processes such as coughing, sneezing, breathing, talking, among others. Coughing is the most commonly modelled process in literature, with analytical models [67,68], experimental visualization and data collection [48,69–73], and numerical models [72,74]. Bourouiba et al. (2014) [68] describe cough and sneeze events as multiphase momentum driven jets that evolve into "buoyant puffs" as momentum dissipates, and the expelled cloud expands. Their study consists of observational studies of cough and sneeze events using light scattering and high-speed cameras, experimental measurements in a salt-water tank, and analytical model development for the sedimentation rate of droplets from the cough/sneeze cloud. Bourouiba et al.'s 2014 study [68] concluded that droplets are entrained within the emitted puff cloud after a cough/sneeze, and carried by buoyant forces, while the larger droplets fall from the cloud at rates depending on their settling speeds and cloud characteristics. The smaller droplets can then be carried long ranges from the source. However, the distance that the small droplets/aerosols are carried is dependent both on the airflow conditions in the room and on the initial momentum from the exhalatory event; after the initial momentum dissipates, the buoyant cloud can be impacted by local advection, stratification and diffusion from the ventilation induced conditions within an indoor space [68,75].

Further characterizing coughs, Gupta et al. [69] performed experiments characterizing coughs in human subjects, which showed cough flow rates can be modelled as a gamma-probability distribution, with an initial peak in flow rate and then a gradual decay. Wei and Li's paper [71] experimentally investigates the dependency of various boundary conditions (*i.e.*, temporal exit velocity, cough duration and velocity scale) on cough flow penetration. The experiments were conducted with an ambient fluid of water, and three cases for cough jets were investigated: pulsation, sinusoidal and real-cough (based on Gupta et al.'s results [69]). Through their observations it was hypothesized that the cough duration is an important factor in droplet propagation distance. This was claimed because, 1) a longer cough period (which can be defined as a steady cough) would propagate larger droplets further away, due to the continuous velocity source, and 2) there would be no leading vortex formed to hinder the droplets (often formed in an interrupted cough). Therefore, when considering cough boundary conditions in CFD applications, it is important to set realistic cough periods to accurately model the propagation of cough droplets.

The transport and deposition of droplets/aerosols can be influenced by gravity, inertia, buoyancy, drag and lift forces, inertial separation, thermophoresis, Brownian motion, basset force, virtual mass effect, coagulation, breakup, hygroscopicity and evaporation [76,77]. Respiratory droplets and aerosols have a higher density than the surrounding air, which leads to gravitational settling [78]. However, gravitational effects can be overcome by 1) buoyancy effects from the warm and humid air surrounding the droplets as they are expelled [68], and 2) drag and lift effects from the particle motion with respect to the surrounding air [78]. Drag effects are modelled with Stokes drag law when the particle Reynolds number is less than unity [76]. Inertial separation occurs when particles fall out of the fluid flow stream when quick changes occur to the stream such acceleration, deceleration or change in flow direction [76]. Thermophoresis effects are seen in small particles in the existence of a temperature gradient [76,77]. Basset force and virtual mass effect force are considered for particles whose density is lower than that of the ambient fluid [77]. Brownian motion is considered for micrometer ranged particles [76,77]. Saffman's lift force is applicable in the viscous sub-layers where the boundary layer shear effects cause the resultant lift force in particles [79]. Respiratory droplets can be susceptible to breakup, coagulation, hygroscopicity and evaporation as they are impacted by the particle-particle interactions, and the environmental conditions such as the RH and vapor pressure in the surroundings [80].

Several aspects can be considered when modelling the transport, processes and deposition of respiratory droplets and aerosols. However, as more detailed physics are incorporated into the model, the simulation process will become slower and prone to more sources of error. Determining the dominant factors that affect the transport and deposition of particles, to achieve the main goals of the simulation, is an important step when modelling particle-laden flow.

2.1.5. Evidence of airborne transmission

Many infectious diseases were investigated for their viability of transmitting through airborne routes. The predominance of airborne transmission routes for certain viral diseases is widely acknowledged, such as for: measles [81–83], varicella (chickenpox) [83,84], and tuberculosis (TB) [85]. Viruses such as influenza have also shown airborne transmissibility [86–89], but it is claimed that conditions need to be conducive for airborne transmission to be the dominant mode of transmission [40,87]. Evidence of airborne transmission for respiratory syncytial virus (RSV) [90], human rhinovirus (hRV) [91], Middle East Respiratory Syndrome coronavirus (MERS-CoV) [92], and Severe Acute Respiratory Syndrome (SARS) [93–95] have

also been collected. A community outbreak of SARS in Hong Kong, during the SARS epidemic (2003) was investigated and modelled [93]. The study showed the possibility of SARS transmission through airborne routes, which occurred between buildings through the sewage system. The virus transmitted to several floors and buildings from the index building and concentrated on middle and upper levels due to rising plumes. Other possible routes such as person to person contact, and vector transmission through rats were considered. Those hypotheses were falsified due to the peak infection (187 confirmed cases) being within a 1-3 day window, which suggests one superspreading source.

The airborne transmissibility of SARS-CoV-1 and SARS-CoV-2 were shown in an experimental study with ferrets, separated to prevent contact, fomite or droplet transmission [96]. The ferrets inoculated with the virus were kept on the bottom cage and a multiple-bend pipe system connected to the top cage, which was housing the susceptible ferret. The setup allowed airborne infectious particles to travel upwards, causing 4 out of 4 of SARS-CoV-1 infections, and 2 out of 4 of the SARS-CoV-2 infections. Adding to the evidence, a seminal experimental study conducted by van Doremalen et al. [64] showed the viral stability of SARS-CoV-1 and SARS-CoV-2 in aerosol form. A three-jet Collison nebulizer was used to generate viral aerosols (with diameters of less than 5 μm) to explore the viral stability. They quantified the viral stability by analyzing air samples and surface samples of these viral aerosols. The results showed a viral half-life (for both viruses) of 1.1 hours to 1.2 hours while suspended in air, results of which are also confirmed by Smither et al. [97] who report a half-life of 1.25 hours.

Evidence from experimental studies provides a convincing case for airborne transmission as a viable route of transmission for SARS-CoV-2, which is further supported with sample studies and COVID-19 outbreaks. In the context of COVID-19 outbreaks, a restaurant in Guangzhou, with an index patient (in table A) infected customers within their two neighbouring tables (B and C) but did not infect any of the waiters or 68 other customers in the restaurant. No evidence of close contact had occurred between the families during the lunch. The airflow from an air conditioner is hypothesized to have catalyzed the spread of viral particles from the index patient, as the airflow created a “contaminated recirculation envelope” [5]. In another instance, a Skagit Valley choir rehearsal with 61 choir members, where only one member (index patient) appeared to have cold-like symptoms, resulted in 53 members contracting the SARS-CoV-2 virus. The virus is suspected to have transmitted through respiratory aerosols because the choir rehearsal was held indoors in

an inadequately ventilated space. Social distancing precautions were followed in the choir rehearsal so the index patient could not have possibly come into close contact with all 53 attendees [6]. Other instances of COVID-19 outbreaks: in a call-centre [98], meatpacking plant [99] and cruise ship [100] have also pointed towards airborne transmission as the likely culprit, because the number of secondary cases of infection were significant enough to rule out droplet and fomite transmission.

In a sample study, Santarpia et al. [101] sampled thirteen COVID-19 infected patient rooms with surface samples of commonly touched items, the floors, windowsills, and air samples. The results showed 63.2% of in-room air samples tested positive for RT-PCR. Based on a scientific brief released on the 27th of March, WHO argued that PCR positive results do not indicate viral transmissibility, even though certain surface samples with PCR positive results showed growth of the SARS-CoV-2 virus after 3 days of cell culture [4]. The viral replication in cell cultures indicates the transmissible nature of the viral samples [7]. Other sample studies have also found viable viral material in air samples and air outlets [101–104] suggesting viral-laden droplet nuclei/aerosols disperse in the air and settle in the air outlets when the room air is exhausted out. Aerosolization of virus particles is also likely from activities such as flushing toilets and resurfacing of settled droplets. A field study by Liu et al. [105] detailed the results of collecting airborne and deposited viral samples of the SARS-CoV-2 virus in two Wuhan hospitals. They found a high number of RNA copies in washrooms and medical personnel change rooms, which they claim was due to the lack of sanitation and aerosolization nature of actions within those rooms: flushing and changing (which resurfaces deposited particles). Liu et al. [105] also found that outdoor hospitals and outdoor areas had very few to no viral copies, suggesting outdoor ventilation is an effective technique to reduce airborne transmission.

2.2. Ventilation

Building ventilation is one of the most important measures in dealing with airborne transmission risk [9,10]. Ventilation is the method of supplying air into indoor spaces, which helps dilute and flush out contaminants, odours, moisture and heat, thus keeping the Indoor Air Quality (IAQ) safe and comfortable for occupants. Methods of natural (passive) and mechanical (active) ventilation are commonly used in buildings to ensure good IAQ. Natural ventilation has been seen in historic buildings with air flow pathways designed to enter and exit from windows, doors, openings and other architectural designs [106]. Mechanical ventilation has been adapted and is more common, being especially crucial in hot or cold climates where Heating, Ventilation and Air Conditioning (HVAC) are required to maintain habitable temperatures indoors.

Using ventilation to curtail the spread of viral-laden aerosols from indoor air has been recommended and emphasized by several authors [10,11,23,107,108] and regulatory organizations [43]. In fact, Morawska et al. [10] have urged that a "paradigm shift" in design, management and specific guidelines for ventilation is necessary to reduce the risk of airborne transmission. Before the pandemic, ventilation practices and guidelines were geared towards thermal comfort and removal of bioeffluents, but infection prevention had not been considered—with exception to Airborne Infection Isolation Rooms (AIIR). Morawska et al. [10] propose tackling airborne infection with ventilation that accounts for 1) risk based on infection viral load, 2) demand controlled and, 3) additional UV disinfection and filtration measures in place. It should further be noted that each indoor space is different, from: the occupant locations, ventilation type and location, furniture layout and other obstructions, which is why one ventilation solution cannot be applied to all settings [11–14]. An important aspect to further consider for airborne transmission of viral particles is the location of the infection source with respect to the ventilation. The interaction between the ventilation induced air pathways, and the respiratory aerosol from the infection source, can have drastically different outcomes for the airborne transmission risk in a room depending on the ventilation layout and infection source location [15,25]. There are three main scenarios observed from previous studies:

i) the aerosols can quickly be removed from the room by the return outlets (ideal case)—resulting in little risk of airborne transmission,

ii) the aerosols can dilute and spread all over the indoor space—which exposes a high number of occupants to the virus, but everyone may not be exposed to enough viral concentration to induce infection [42,108,109]

iii) the aerosols can circulate and concentrate in certain zones of the space—leading these zones to be high risk for airborne transmission, causing severe infection to the occupants in those zones [25,110] .

There have been other discussions and examples of variation in airborne infection risk distribution in an indoor space dependent on: location of HVAC components [12,15–19], ventilation configurations [14, 20–24] and infection source locations [25,26].

Most ventilation related advice focuses on appropriate Air Changes per Hour (ACH) [111,112]. Increasing the air change rate essentially flushes out any particles in the room and replaces it with filtered, or a mix of new and filtered air, which helps reduce the stagnation of viral particles. Thus, considering the ACH in a space is important for good air quality. However, Liu et al. [113] have shown that the ventilation rate is only effective in certain ventilation configurations, and Villafruella et al. [114] conclude that there is no relationship between increasing ACH and lower transmission risk, (in fact the risk increases in some cases with higher ACH). Furthermore, Memarzadeh and Xu's [111] study demonstrates how an optimally planned ventilation configuration has significantly more impact on the contaminant removal rate (hence risk of infection to susceptible occupants in the room) than the air change rate. The outbreak in a restaurant in Guangzhou was a prominent example during the emergence of COVID-19, of how airborne transmission can be exacerbated by a poorly placed ventilation configuration [110].

Other ventilation related advice recommends effective filtration with MERV 13 or higher rated filters [43,115], UV disinfection [20,43,116], minimizing air recirculation [116] and adding air cleaners (portable or fixed) in the space [16, 43,116]. Air recirculation can be dangerous when the air is contaminated with infectious aerosols and proper filtration and/or disinfection is not incorporated: contaminated air can reach zones that would not have otherwise been exposed to the infection, and lead to an outbreak in the building [116]. Using air cleaners is shown to add extra air change rates by helping the ventilation system cleanse/change the indoor air [43,117,118]. However, air cleaner placement is also an important factor: if not placed correctly, the air cleaner can disturb the ventilation air flow pathways, causing worse IAQ conditions and possibly increasing infection risk [10,118]. He et al. [16] performed CFD studies to analyze the effects of

air cleaner location, infector location with respect to air cleaner placement, room size and thermal effects in a small classroom. They concluded that placing air cleaners closer to the infector provides the most effective results in terms of particle removal, and the next most optimal method is placing the air cleaner near the ventilator which reduces recirculation in the domain. Lindsley et al. [118] also recommended placing air cleaners close to the infectious/droplet generating occupants.

The following is an introduction to different ventilation designs describing their benefits and working principles.

2.2.1. Mixing Ventilation

Mixing Ventilation (MV) is the most commonly used air distribution configuration [119]. Mixing ventilation induces mixing of new and old air, through high velocity air release, which contributes to the dilution of contaminants. The ventilation strategy locates both supply inlets and return outlets near, or at the ceiling of an indoor space [120]. During the dilution of contaminants, the contaminants are discouraged from concentrating, but the caveat is they are allowed to spread and circulate around the indoor space which could increase risk of transmission to zones far from an infected occupant [108]. However, certain studies conclude that MV performs well as it dilutes the contaminants rather than concentrating them in the breathing zone of other occupants [15,121].

2.2.2. Displacement Ventilation

Displacement Ventilation (DV) is a more energy efficient and effective air distribution strategy for delivering fresh air to occupants' breathing zones [120]. In displacement ventilation, the air supply inlets are located on the floor, or on walls near the floor and the air return grilles are located near the ceiling. The goal of this strategy is to pool cold air from the supply over the floors, after which air will rise up at the locations where high heat loads exist [120,122]. This configuration allows thermal stratification of air as cooler fresh air displaces the warm polluted air surrounding occupants and heat sources; the warmed air travels towards the top of the room as buoyancy takes effect. In this case, contaminants released from occupants can move upwards with the warm air and stagnate near the ceiling, or get removed from the room through the return grilles/exhaust located near the ceiling [23,113,114]. One challenge with the displacement ventilation configuration is the possibility of "lock-up phenomenon" which has been noted in

previous CFD studies of airborne transmission in displacement ventilation settings [114,121,123]. In the "lock-up phenomenon" the exhaled contaminants stagnate in the breathing zone of occupants or right above the infectious occupant's breathing zone. This would further increase the transmission risk when other occupants are elevated, for example, the source occupant sitting or lying down versus the susceptible occupant standing (often the case in health care settings), or in a terraced floor settings (e.g. lecture halls, auditoriums and stadiums).

2.2.3. Other Ventilation Configurations

Novel ventilation configurations are attracting more attention, with innovative techniques to improve thermal comfort while reducing contaminant exposure to occupants. Studies on the effectiveness of ventilation designs such as personal ventilation, stratum ventilation, among others are resulting in optimistic results.

Personal ventilation as the name suggests, is a configuration where each occupant has separate air inlets and exhausts [21]. This method allows clean air to be directly delivered to the occupants and has shown effectiveness in protecting susceptible occupants from infection [24]. On the other hand, if the occupant is infected, the ventilation design helps to spread the infected droplets further, thus amplifying the risk of transmission [24]. He et al. [24] have shown that personal ventilation is useful when combined with total ventilation design if the total ventilation is designed as a mixing ventilation configuration; however, it does not perform as well if displacement or underfloor ventilation is used as the total ventilation design.

Stratum ventilation (SV) is another novel ventilation design, which is mainly used for cooling purposes in small to medium sized rooms. The design consists of air inlets placed at the breathing level of occupants, delivering supply air directly to the breathing zones. SV is shown to tackle airborne transmission to occupants by inducing good air quality in the breathing zone, as well as increasing the deposition rate of droplets and aerosols. Lin's paper [124] investigates three different scenarios under two different ventilation configurations (DV and SV), for scenarios when the teacher is the source, when a student near the supply air is a source and when a student near the return is a source. They conclude that in all three scenarios SV performs most optimally to remove particles from the breathing zone, because: 1) SV allows for fresher air in the breathing zone, and 2) their higher horizontal air velocity allows for particle depositions onto surfaces. Tian et al. [125] also discuss the benefits of SV. They conclude that the particle concentrations in the entire room and the breathing zone were lesser in SV than DV. They report that more particles

were deposited with SV but more escaped with DV. In contrast, another study reports that DV performs most optimally for overall IAQ in the room, but SV still performs the best for IAQ in the breathing zone [126].

2.2.4. Recommended Ventilation Configurations

In terms of ventilation and its effects on droplet aerodynamics, Somsen et al. [127], studied expired droplets for their falling time and retention time in a room. Experimental systems with laser diffraction and laser scattering were used to investigate the droplet aerodynamics. It was found that 5 um droplets with the consideration of gravity and drag stayed in still air for 9 mins until they reached the floor. Three cases were considered: 'a room with no ventilation,' 'with mechanical ventilation' and 'with ventilation combined with an open door and window.' The highly ventilated room's droplets were halved within 30 s, the mechanically ventilated room took 1.4 mins, and the non-ventilated room took 5 mins. Hence, they stressed the importance of ventilation. Another example of the effects of ventilation can be noted by Yin et al.'s [128] experimental study which was conducted to see the difference between varying ventilation methods, different auxiliary exhaust heights, different released particles and for CFD validation. A steady state experiment was conducted (steady continuous particle exhalation). Solid particles were considered for tracing as water droplets released by the patient are negligible for airborne transport and dispersion. That is because heavy droplets either fall in the immediate surrounding due to its weight or evaporate in a matter of seconds (compared to the longer time taken for droplet nuclei to disperse) [9]. The experiments were performed with MV, (where air is distributed uniformly through a room) and DV (which facilitates natural convection by inserting cool air from the lower areas of the room and exhausting warmer air from the ceiling/ upper areas of the room). It was noted that when the auxiliary exhaust was placed in the lower part of the room, displacement ventilation performed poorer than mixing ventilation. Although when the exhaust is located at higher levels of the room displacement ventilation at 4 Air Changes per Hour (ACH) performs equivalently to mixing ventilation at 6 ACH. Overall, displacement ventilation provided the highest air quality levels at patient breathing zones with maximum air changes per hour [128].

Other studies have also acknowledged more optimal performance with DV configurations, in reducing particulates in the breathing zone [19,24,113,126]. Liu et al.'s study [113] performed CFD work and experimental validation for a small open plan office space to compare MV and DV configurations. Liu et al. [113] concluded that DV performed better than MV, as DV stratified

droplets to the top of the room while MV mixed the droplets all over the office space. Furthermore, Tian et al. [126] conducted experimental work in a small office space with DV, MV and SV configurations, and evaluated the three configurations using contaminant removal effectiveness (CRE) and air change effectiveness (ACE) parameters. Tian et al. [126] concluded that DV performs best, followed by SV, then MV in overall IAQ, but SV performs best, followed by DV then MV when only the breathing zone is considered. Zhu et al.'s paper [19] studied four different ventilation configurations in an occupied bus with multiple infectors. It was concluded that displacement ventilation and filtration are effective measures to reduce the risk of transmission. He et al.'s paper [24] studied the effects of exhaled droplet dispersion and transmission with total ventilation and personal ventilation combined. The total ventilation strategies used were mixing (MV), displacement (DV) and underfloor air distribution ventilation (UFAD). They used CFD and experimental work with tracer particles (with 0.8 μm, 5 μm, 16 μm diameter sized particles). They made several conclusions among which were: 1) MV had uniform droplet distribution unlike DV and UFAD which had concentration stratification, 2) for the size range of 5 μm and below, DV and UFAD had significantly lower fraction of particles inhaled in comparison to MV, and 3) for 16 μm particles DV performed the best, followed by MV, then UFAD, which was the worst because it prevented 16 um particles from settling. Reviewing the following studies, the most optimally performing ventilation design to reduce airborne transmission risk points to DV, however most of these studies were performed in office or bus settings where most/all occupants have the same breathing level.

Studies performed in patient ward settings claim that DV is not preferred and may even be more dangerous in health care settings, where the patient's breathing level is below the Health Care Worker's (HCW). Villafruela et al.'s study [114] examines the effects of exhaust location, ACH and radiant wall location for displacement ventilation in a patient ward setting. They evaluate with metrics of CRE, ACE and cross transmission to the HCW. They do not recommend displacement ventilation in healthcare settings due to the lockup phenomenon, as exhaled air from the infector stagnates at the HCW's breathing zones. A review by Qian and Zheng [129] discuss that when the infector is facing upwards, the DV system works well to remove the expelled droplets. However, when the infector is facing forward the expelled droplets penetrate and disperse widely in a thermally stratified layer (known as the "lock-up layer"), which can contribute to a high risk of infection if the lock up layer is in the breathing zone of HCWs. On the other hand,

certain ventilation configurations are recommended for health care settings. Cheong and Phua's [14] CFD study compares pollutant removal effectiveness between 3 different ventilation strategies, and they conclude that having supply grilles at the ceiling close to the patient and exhaust grilles on the lower wall near the patient to allow a clean to dirty air flow pattern is most effective at particle removal. Thatiparti et al. [17] performed detailed CFD simulations in an isolation ward with a coughing patient for two different ventilation designs, 1) with the air supply above the patient and air exhaust away, and 2) with the air exhaust above the patient and air supply further away. The results showed that 7% of the particles were removed in the first second with setting 1, and 24% of particles were removed within the first second with setting 2. Thus, according to Thatiparti et al. [17] and Cheong and Phua [14], in settings where the infection source is known, a clean to dirty air flow pathway seems to be the most efficient and safest option to quickly remove particles.

CFD and experimental studies of different ventilation configurations were modelled in literature [14,19,24,113,121,126,128,130–132] for displacement, mixing, stratum and underfloor ventilation. Some studies suggest that mixing ventilation allows for better airborne transmission risk management, because of the air dilution capabilities [121], and the ACH can be altered to accommodate cases of higher infection [113] (for example, the ACH can be increased during the pandemic). Others have demonstrated the benefits of displacement ventilation in energy efficiency, ventilation effectiveness and airborne transmission safety [19,24,113,126,133]. Some studies have also shown the benefits of more novel ventilation designs such as stratum ventilation [125,132]. Cetin et al. [15], and Qian and Zheng [129], have performed thorough literature reviews on the impacts of varying air inlet and outlet locations, on ventilation effectiveness, and on contaminant removal effectiveness. There is an overall lack of consensus on which ventilation configuration works best; the optimal ventilation configuration varies upon setting, heating vs. cooling, volume of domain, direction of contaminant release, heat fluxes among other variables. Thus, well validated and detailed studies for each new setting are valuable to providing insight regarding the most optimal ventilation configuration for a setting.

2.3. Risk Analysis of Airborne Transmission

Risk analysis of airborne transmission in indoor spaces often involves mathematical models, CFD studies and experimental work to characterize the aerosol spread, and risk of infection. The following is an overview of the different risk analysis methods and results from each method.

2.3.1. Experimental Models

Earlier work has involved experimental studies to find droplets' diameter distributions [45], and evaporation rates [30]. More recent experimental work has also studied upon the transport of droplet nuclei with PIV [72,73,134,135], smoke visualization [15,136,137] and particle/gas sampling techniques [113,128,138,139]. In Cetin et al.'s study [15] a 1:5 scaled down environmental chamber was used to model 5 different inlet/outlet locations and 3 different particle source locations, which were then replicated in CFD simulations. Smoke visualization was used to observe the particle transport and air flow. From Cetin et al.'s results [15], it was noted that having the inlet and outlet on the same wall induces the most particle removal and placing inlets on the ceiling result in the lowest particle concentration in the breathing zone. A concern with placing inlets and outlets in the same wall is air short-circuiting, but it was only seen to be an issue when inlets and outlets were placed facing each other. Proper circulation can be achieved with inlets and outlets on the same wall, thus providing optimal air flow scenarios for the room. Liu et al. [113] used a to-scale experimental chamber to simulate a 4-occupant open plan office space for MV and DV configurations. They atomized saline particles from different locations and measured the temperature and particle concentrations in the space. They concluded that DV performed better than MV, as DV stratified droplets to the top of the room while MV mixed the droplets all over the space. Liu et al. [113] also noted that droplet dispersion was dependent on infection source for DV but not MV. Experimental work can provide insightful information on airborne transmission and the implications of ventilation; however, experimental setups can be costly, and limited to certain probe points, measurement parameters, settings, and environmental conditions.

2.3.2. Mathematical Models

Mathematical models for infection risk have been prevalent with quantifying the airborne transmission risks of COVID-19, such as the seminal Wells Riley model [29,140] from which many sub-models are derived [141], modifications of the Susceptible-Exposed-Infected-Removed (SEIR) model [142], and dose-response model [33]. The models consider infection probabilities through various metrics such as inhalation/exhalation rates, viral infectivity, as well as viral

removal rates from the indoor space. Existing mathematical models for airborne transmission are effective and time-efficient tools for approximating the airborne transmission risk in a space, however, when considering ventilated spaces with turbulent flows, partial mixing, or complex air flow patterns, viral-laden particles can distribute unevenly causing mathematical models for estimating airborne transmission risk to fall short of an accurate representation of the airborne transmission risk. The Wells-Riley model [29] has been valuable to the progress of airborne infection quantification, however, the models generalize ventilation rate, and infection concentration or quanta (1 quantum is the infectious dose needed to infect 63% of the susceptible population) [143] distribution in a space, which does not incorporate any spatial heterogeneity of airborne infection risk. A comparison of the Wells-Riley model [29] with CFD by Foster et al. [144] resulted in high accuracy with laminar flow fields but as turbulence increased when simulating forced ventilation, the Wells Riley model underpredicted the risk with an error of 29%. Noakes and Sleigh [145] identify this limit in the Wells-Riley model as well as identifying how the model does not consider infection risk based on proximity to the infection source. They develop a model that incorporates stochasticity to the Wells-Riley model and combines it with zonal-mixing ventilation equations (to incorporate air mixing heterogeneity). Noakes and Sleigh [145] also conclude that the simple Wells-Riley model significantly underestimates the risk of infection in cases where the space is not fully mixed.

2.3.3. Computational Fluid Dynamics (CFD) Models

Computational Fluid Dynamics is a numerical method for solving flow fields and fluid interactions with objects, heat transfer and chemical changes. A set of partial differential equations are solved computationally to result in a visual demonstration of the fluid flow fields. CFD techniques have been used in the context of infection transmission through airborne routes in literature to solve for cough and sneeze flow dynamics, aerosol dynamics and ventilation performance. Methods such as Direct Numerical Simulations (DNS), Large-Eddy Simulations (LES) and Reynolds Averaged Navier-Stokes (RANS) have all been used in the context of droplet and aerosol transport. DNS is the most computationally expensive method [146], thus, has been applied by Rosti et al. [46] to a small domain for a short period, when a cough is ejected and dissipated (approximately 1 to5 seconds). DNS is known for its accuracy, as the Navier-Stokes equations are solved directly. This allows a cough's detailed transport physics to be observed. LES solves the large eddies, but models the smaller fluctuations in turbulence, which makes it less

computationally expensive than DNS. Liu et al. [147] used LES to solve for particle-laden flow in a restaurant with turbulence and thermal effects. RANS is computationally the cheapest as it performs time-averaged flow simulations. It is the most commonly used method in airborne transmission modelling literature, with several recent studies using RANS to model particle-laden and multiphase flow simulations [18,26–28,148]. Considering the abundance and well documented methods for RANS simulations, as well as the low computational expenses, RANS modelling is applied in the current thesis.

In terms of modelling airborne infection spread and ventilation performance in different spaces, patient wards/isolation wards have been modelled the most in literature [17,114,128,132,149,150]. This is the most important location as most infections do spread in health care settings. Additionally, nosocomial infections are dire because of the risk to other vulnerable patients and health care workers who are essential to the operation of the health care facilities. The next most modelled spaces are high density vehicles and public spaces, such as airplane cabins[26,27,151,152], buses [72,148], restaurants [131,147] and supermarkets [18,28]. Furthermore, amid the return to work/school efforts without disease eradication, concerns of infection spread are tackled with airborne transmission simulations in classrooms [18,25,144] and office spaces [24,113].

Use of CFD for estimation of airborne transmission has been prevalent, especially after the emergence of the SARS-CoV-2 virus. Various studies are resulting in useful information regarding the transport patterns in different settings [16,18,25,27]. For instance, Cui et al. [28] perform a CFD simulation of particle/droplet spreading in a supermarket. It was noted that increasing attachment efficiency reduced the long-term suspension and dispersion of particles. Further iterating that particle deposition is an effective method, in Talaat et al.'s study [27] computational fluid-particle dynamic simulations were carried out in a Boeing 737 cabin area to evaluate the effectivity of reducing cabin capacity versus installing sneeze guards/shields. They concluded that the sneeze shields reduced droplet deposition per passenger by 30-35% and inhalable fraction to around 50%. Similarly, Abuhegazy et al. [25] reported from their CFD study that adding glass barriers between students in a classroom reduced 92% of droplet transmission between susceptible students located 2.4 m away from the infected student. Yang et al. [24] investigated droplet dispersion and evaporation with varying humidity and air flow directions in a ventilated coach bus. The study demonstrated that high RH (95% RH), backward supply direction and passengers sitting

at nonadjacent seats could significantly reduce the infection risk of droplet transmission in buses. Although, it is important to note that while increasing humidity in a space limits long-term suspension of respiratory droplets, it is impractical when considering the thermal comfort of occupants. Yang et al.'s simulation results [148] indicate droplets are transported above the seats, in which case installing shields/barriers between rows and including air outlets or open windows could create zonal separation thus reducing transmission risk.

Another transmission limiting strategy in literature is creating zonal separation with air flow. For example, Khankari [12] demonstrates adding two separate exhausts instead of a shared exhaust limits the dispersion of contaminants to two adjoining office booths. The transmission risk is further improved when separate supply and exhausts are dedicated to each adjoining office booth. Several studies have also concluded that it is highly effective to locate exhausts and air cleaners near the contaminant source, or high-volume exhaling occupant [16,17,19]. Further considering the effects of HVAC component location, Shao et al. [18] demonstrates considerable variation in airborne transmission risk in a domain, when varying ventilation unit location. In contrast, Abuhegazy et al. [25] vary infection source location while keeping the ventilation model constant and made similar conclusions to Shao et al. [18]: infection source location with respect to the ventilation can affect the spatial distribution of airborne transmission risk hence affect the location of infection risk hot spots. It can then be extrapolated that the spatial heterogeneity of risk in a domain can be further amplified by varying ventilation configurations as well as infection source locations.

2.3.3.1. CFD Methods for airborne transmission studies

This section reviews six CFD based airborne transmission studies to specifically study the CFD setup and risk measurement methods. Reviewing common methods in literature will help to develop an accurate and validated methodology for the thesis.

Cui et al. [28] perform a CFD simulation of particle/droplet spreading in a supermarket. They used the Ansys FLUENT software to solve for the air flow fields, and subsequently conducted Lagrangian particle tracking with their in-lab software. Their main goal was to solve particle spread with variable deposition rates. While they focused on droplets smaller than 50 µm (i.e. 5 and 20 µm); the evaporation of droplets is recognized to be insignificant towards the change in size hence aerodynamic properties of the droplets will be insignificant for the chosen droplet diameters. They studied particle dispersion around the store with 0%, 25%, 50%, 75% and 100%

surface attachment rates of particles. The turbulent dispersion of particles was considered using eddy diffusivity with a Schmidt number of 0.7 (in the range of 0.3 to 1.2 for indoor airflows) and a random walk approach. The droplets formed into a plume and the method of moments was used to compute the plume centroid and spreading of particles. It was noted that increasing attachment efficiency reduced the long-term suspension and dispersion of particles. Furthermore, low rated MERV filters were shown to be ineffective at filtering the droplets, and since they penetrated the ventilation channels.

Within Talaat et al.'s study [27] computational fluid-particle dynamic simulations were carried out in a Boeing 737 cabin area to evaluate the effectivity of reducing cabin capacity versus installing sneeze guards/shields in the context of reducing COVID-19 and other airborne diseases from spreading throughout the cabin. The study was designed with three cases: cabin at full capacity, cabin at 66% of full capacity and full capacity with sneeze shields in place. The numerical study was conducted with RANS RNG k-epsilon turbulence modelling and Lagrangian particle tracking for the discrete phase. The particles were in the range of 1 – 50 μm, simulated in several monodisperse simulations (only a single diameter simulated in each case) due to the concern of skewing mass-averaged values due to larger sized particle outliers. In terms of pressure-velocity coupling, the SIMPLE algorithm was used with first-order pressure interpolation. The cabin environment was initialized with ventilation boundary conditions run in transient simulation till convergence was achieved around 10^{-4} for turbulence, momentum and continuity parameters. Even though Lagrangian particle tracking incorporates particle size effects on drag and gravity, a large particle count was needed to determine particle distributions independent of the particle count itself. The study used 300,000 particles. Talaat et. al. concluded that reduced capacity and installation of sneeze shields reduced the risk of contamination by equivalent measures. The sneeze shields reduced droplet deposition per passenger by 30-35% and inhalable fraction to around 50% although it should be noted that reduced capacity also reduces the probability of passengers with the infection.

Yang et al. [148] investigated droplet dispersion and evaporation aspects of droplets due to breathing in an adequately ventilated coach bus. They performed detailed CFD studies. Several aspects from their study inspired my study in terms of their validation techniques and controls. The aim was to see how to minimize the suspension of droplets in the air from an infectious exhalation. This is most effective with larger particles and high RH. This is because larger droplets

deposit faster and high RH ensure evaporation doesn't play a big role in shrinking the droplets. For their CFD setup, they used RANS modelling with the RNG k-epsilon turbulence model which is cited in their paper as ideal for modelling indoor environments. The SIMPLE algorithm is used for pressure and velocity decoupling and second order upwind scheme for convection and diffusion-convection terms. They applied drag, gravitational, Brownian and Saffman's lift force. Their droplets were considered as a mixture of water liquid and sodium chloride and used the mass weighted mixing law to define the density and specific heat values. Relative humidity was heavily considered for their effects on droplet evaporation through the Ranz-Marshall correlation. The total simulation time was 600 s after a steady-state simulation was used to initialize the coach bus. Their simulation was validated by Yin et al.'s experimental study [128] simulating droplet dispersion in an airborne infection isolation room. The study demonstrated that high RH, backward supply direction and passengers sitting at nonadjacent seats could significantly reduce the infection risk of droplet transmission in buses.

Shao et al. [18] performed both in situ experimental measurements and CFD simulations to assess the risk, and observed the evaporation and residence times of respiratory droplets from asymptomatic hosts. They used Schlieren imaging and digital inline holography (DIH) to visualize the droplet motion in normal breathing patterns and collected data for CFD inputs. They conducted CFD using OpenFOAM software for a small elevator, a classroom, and a supermarket. Their goal was to assess the time-dependent variance in particle size, concentration, and spatial distribution, with the focus of analysing the risk of airborne transmission. Their results showed that for the elevator and supermarket, droplet removal rate was very minimal due to stable circulation regions formed. For the supermarket, the emitter was moving, hence less likely to cause stable circulation regions and droplet removal rate was higher. This research is similar to my current research focus of iterating simulations for various emitter locations to see the implications of HVAC design, although an office space was not modelled, and the number of locations was limited to two iterations/location instances only. The study concluded that there is high "spatial heterogeneity for risk" and suggested that ventilation can prove to be advantageous in particle removal, but the caveat was, that HVAC can sometimes worsen indoor environments by creating local hot spots or spreading particles extensively.

Liu et al. [147] performed a CFD based investigative study of the prominent restaurant outbreak that occurred in the Guangzhou district in China [110]. The goal was to identify what

main factors contributed to the airborne transmitted cases within the three affected tables. The model reconstructed the restaurant layout, with 5 Air-Conditioning (AC) systems with filtration and heat flux producing table areas. They solved the flow field with Large Eddy Simulations (LES) and flow interactions on solid surfaces with immersed boundary method. The AC air flow rate and temperature difference (between the tables and the AC) were varied. Particles of 1.5 μm diameter were tracked with the Lagrangian particle tracking algorithm, and were reduced based on filtration effects in the AC. The particle exposure was mapped with iso-planes based on the normalized concentration of particles with maximum concentration. The results showed that air recirculation and low filtration efficiency caused particles to recirculate and induce higher exposure to the occupants. They concluded that the thermal effect from thermal plumes is important to consider in models as they can significantly change the streamlines, cause air recirculation and increase infection risk. They also noted that filtration efficiency is important as the AC recirculation caused 30% higher infection rates.

Yan et al. [26] performed a CFD study in an aircraft cabin with a Wells-Riley based risk measurement approach. Their CFD domain was larger (seven rows) than what is usually modelled for aircraft cabins (three rows), thus they were able to see the long-range turbulence impacts in the cabin. They used RANS modelling with a k-epsilon RNG turbulence model, and particles were tracked with the Lagrangian particle tracking algorithm. The particle concentrations and residence times were able to be collected because the Lagrangian method was used. Yan et al. then used this data in the particle in cell (PSI-C) method to then calculate the risk of infection, which was dependent on the mass flow rate, residence time and cell volume. They varied their infection source locations based on middle or aisle seats. As a result, they found that particles travel much further when the infection source is sitting close to the window, where air flow is the heaviest, and particles tend to stagnate when the infection source is seated near the aisle. Yan et al.'s risk measurement approach based on Wells-Riley's percent of infection risk per seat is very effective at visualizing the spatially heterogenous distribution of risk and will be implemented in the current thesis.

The following tables (Table 2-1.1 and Table 2-1.2) summarize the settings of the reviewed literature.

Table 2-1.1: Details of numerical setup by Cui et al. [28], Talaat et al. [27], Yang et al. [148], Shao et al. [18], Liu et al. [147] and Yan et al. [26].

Author(s)	Location /Setting	Software	Turbulence Model	Multiphase-model
Cui et al. (2021) [28]	Supermarket	Ansys FLUENT + NEMO3D	RANS Realizable k-ε	Lagrangian particle tracking
Talaat et al. (2021) [27]	Airplane cabin	Ansys FLUENT 19.1	RANS RNG k-ε	Lagrangian particle tracking
Yang et al. (2020) [148]	Coach bus	Ansys FLUENT	RANS RNG k-ε	Eulerian-Lagrangian
Shao et al. (2020) [18]	Elevator, classroom, and supermarket	OpenFOAM-6	RANS Realizable k-ε	Lagrangian particle tracking
Liu et al. (2020) [147]	Restaurant	In-house CFD solver	LES (incompressible flow)	Lagrangian particle tracking
Yan et al. (2017) [26]	Airplane Cabin	CFX 16.2	RANS RNG k-ε	Lagrangian particle tracking

Table 2-2.2: Details of numerical setup by Cui et al. [28], Talaat et al. [27], Yang et al. [148], Shao et al. [18], Liu et al. [147] and Yan et al. [26].

Author(s)	Forces/other interactions on particles	Steady/Transient	Validation	Other details
Cui et al. (2021) [28]	Stoke's drag law, turbulent diffusion Neglect thermophoretic forces and evaporation	Steady-state RANS equations	N/A	5μm and 20 μm droplets were studied. Eddy diffusivity +DRW applied.
Talaat et al. (2021) [27]	Stokes-Cunningham drag model, gravity.	Transient initialization then particle injection	N/A	Monodisperse simulations conducted, with 300,000 particles

Yang et al. (2020) [148]	Stoke's drag, gravitational, Brownian and Saffman's lift force + evaporation	Transient (with steady initialization)	Yin et al.'s data [128]	Mass weighted mixing of water and NaCl
Shao et al. (2020) [18]	Stoke's drag, gravitational + evaporation. Neglect Brownian, forces, Kelvin effect and turbulent dispersion	Transient (with steady initialization)	N/A	Rosin-Rammler distribution is used for the particle diameters. A risk model is used based on particle passing counters in cells.
Liu et al. (2020) [147]	Turbulence, flow–aerosol interaction, effect, Brownian motion, effect of subgrid-scale (SGS) flow structures, stokes-Cunningham drag, thermal effect, and filtration	Transient	Posner et al. [153] and Bay et al.'s data [154]	Risk exposure index is quantified by normalized particle concentration. The importance of thermal and filtration effects was demonstrated.
Yan et al. (2017) [26]	Stokes-Cunningham drag, buoyance force, virtual mass force	Steady-state	Li et al.'s data [134]	Particle sensitivity tests with normalized particle concentration is conducted. Risk was assessed with "particle source in cell (PSI-C) method.

The reviewed CFD studies above are shown to have diverse methods for domain of analysis, particle and flow physics, diameter distribution of particles and risk measurement. This review of methods has also provided some understanding of the common methods used, such as to model turbulence in indoor environments the RANS RNG k-epsilon model seems to be common among many studies. Furthermore, Stokes-Cunningham drag law is the conventional drag law used, and Lagrangian particle tracking is prevalent and used in all the above reviewed studies. This review has provided a sense of what is often followed and in agreement to literature for CFD modelling of airborne transmission, and what differs based on each study and their rationale behind the choice of method, thus helping develop a validated methodology for the simulation studies in the thesis.

2.4. Conclusion

In this chapter, the specific characteristics of airborne transmission are defined, the physics and environmental factors that impact airborne transmission are reviewed, evidence of airborne transmission by COVID-19 and other diseases are presented and a review of the main control measure of airborne transmission—ventilation—is included, with ventilation associated recommendations in literature. Furthermore, the methods of airborne transmission risk modelling are reviewed, which included experimental work, mathematical modelling, and a detailed review of CFD based models and methods.

From the literature review of various CFD and experimental studies, it was noted that the location of ventilation components, the design of the ventilation configuration and the location of infection source can all impact the spatial and temporal distribution of infectious aerosols. However, evaluating the variation of airborne transmission risk based on both the ventilation type and the infection source location for a space were not seen in literature. Furthermore, very few studies investigated the impact of infection source location, and no risk models included infection source location. Overall, there has been little research on the dispersion patterns of airborne infectious particles within pre-COVID-19 literature, thus, more investigative and modelling studies into the transmission dynamics of airborne particles will add value to the topics of airborne transmission in indoor environments and ventilation measures for infection control. This in turn will assist health organizations, building designers and building operators to protect the public from future airborne diseases.

Chapter 3 Methodology

A breakdown of the methodology sub-sections, firstly the general meshing and CFD methods applied to all sections for the continuous and discrete phases is described. Then a validation study is presented to validate the CFD methods used in the simulation studies. Specific boundary conditions, initial conditions and risk measurement methods is left to be discussed in the specific chapters (chapters 4-6).

3.1. General CFD Methods

3.1.1. Meshing

For all the CFD domains in the thesis, uniform mesh size is applied with exceptions to prism layers near the walls and higher mesh resolutions on inlet, outlet, and occupant surfaces. Uniform mesh sizing is implemented because the spatial distribution of particles in the domain is unknown for all cases, thus having uniform mesh sizing prevents fluctuations in tracking accuracy in different areas of the domain. Additionally, in the lecture hall domain there are three different source locations for each setup, implementing high mesh densities near the injection sources would be time consuming (if three different meshes were generated), or computationally expensive (if three different areas had high mesh densities in the domain). It should also be noted that from most observed results, the particles do not remain near the source location's expulsion zone for a significant part of the simulation time; the particles are mixed quickly and, in many cases, distribute throughout the domain, making it difficult to identify zones in the domain to increase mesh resolution in.

3.1.2. Numerical Modelling Setup

Ansys Fluent 20.2 [155] was used to simulate all the different cases, with the use of Reynolds Averaged Navier-Stokes (RANS) modelling. A pressure-based solver was used. Turbulence was modelled with the RNG $k-\varepsilon$ turbulence model with standard wall functions, as seen in equation 1 below:

Kinetic energy, k:

$$\frac{\partial}{\partial t}(\rho k)+\frac{\partial}{\partial x_i}(\rho k u_i)=\frac{\partial}{\partial x_j}\left(\alpha_k \mu_{eff}\frac{\partial k}{\partial x_j}\right)+G_k+G_b-\rho\epsilon-Y_M+S_k \quad (1)$$

Dissipation rate, ϵ

$$\frac{\partial}{\partial t}(\rho\epsilon) + \frac{\partial}{\partial x_i}(\rho\epsilon u_i) = \frac{\partial}{\partial x_j}\left(\alpha_\epsilon \mu_{eff}\frac{\partial \epsilon}{\partial x_j}\right) + C_{1\epsilon}\frac{\epsilon}{k}(G_k + C_{3\epsilon}G_b) - C_{2\epsilon}\rho\frac{\epsilon^2}{k} - R_\epsilon + S_\epsilon \quad (2)$$

α_k and α_ϵ are the inverse Prandtl numbers for kinetic energy and dissipation rate, respectively. G_k represents the turbulent kinetic energy generated by the mean velocity gradients, and G_b represents the turbulent kinetic energy generated by buoyancy. $C_{1\epsilon}$ is 1.42, and $C_{2\epsilon}$ is 1.68. The k-epsilon RNG turbulence model is preferred for indoor models as it can simulate both high and low Reynolds numbers efficiently [156,157]. According to turbulence comparison studies the RNG k-epsilon model compares with the experimental data more accurately in comparison to other turbulence models [153] and requires less computational resources to converge [131].

It is assumed that the boundary layers are turbulent in specific regions, specifically near the high velocity inlets, hence the prism layer meshing is designed for turbulent ranges in y+ (*i.e.* 30-300). Standard wall functions were used because the y+ required for accurate boundary layer modeling is higher than that for enhanced wall functions: standard wall functions require y+ between 30 and 300, while enhanced wall functions require a wall y+ less than 5 [158]. Thus, with standard wall functions the process for mesh refinement is easier, as cells do not have to be reduced to capture y+ ranges as low as 1 and be compatible with the free-stream mesh size (which could be significantly larger).

The energy equation was activated, because thermal effects can have a significant effect on pathlines and particle trajectories, such as creating air recirculation due to natural convection [147]. Energy related components can then be integrated into the setup, such as, ambient temperature conditions, heat flux boundary conditions on occupants and temperature boundary conditions to air inlets and infection sources. In the context of thermal effects buoyancy is implemented with the Boussinesq model. Appropriate Boussinesq density and thermal expansion terms were added.

In terms of solution methods, pressure-velocity coupling was solved with the coupled method, pressure was solved with PRESTO!, Least Squares cell based gradient discretization was used and all the other parameters were solved with second order upwind method. To solve the particle trajectories transiently, the flow field solution was initialized in steady-state, and after the velocity and temperature monitors stabilized, the particles were injected, and solved with transient

particle tracking. Modelling viral-laden aerosol flow within air is recognized as a particle-laden flow, therefore a Euler-Lagrange approach is considered [159]. The Discrete Phase Model (DPM) feature in Ansys Fluent is used [159]. The model allows the ambient air to be solved as a continuum (in the Eulerian reference frame) and the aerosols solved as discrete particles in the Lagrangian reference frame [159]. See equations (3-5) below for the equation of motion used to track the particles in the Lagrangian reference frame and equations (6 -7) showing the Stoke's law settling velocity and particle Reynold's number [77].

$$\frac{d\,u_p}{dt} = F_D\left(u - u_p\right) + \frac{g\left(\rho_p - \rho\right)}{\rho_p} + F_a \tag{3}$$

Where the drag force F_D is,

$$F_D = \frac{18\mu}{\rho_p d_p^2 C_c} \tag{4}$$

C_c is the Cunningham correction to Stokes' drag law.

$$C_c = 1 + \frac{2\lambda}{d_p}(1.257 + 0.4e^{-(1.1 d_p/2\lambda)}) \tag{5}$$

The settling velocity equation based on Stoke's law,

$$v_t = \frac{d^2 g(\rho_p - \rho)}{18\,\mu} \tag{6}$$

The particle Reynold's number,

$$Re = \frac{\rho v_t d_p}{\mu} \tag{7}$$

The terms present in the equations above are u and u_p, represent the air and particle velocities, ρ and ρ_p, represent the air and particle density, μ represents the molecular viscosity of air, d_p, is the particle diameter λ, is the molecular mean-free path, and v_t, is the terminal velocity of particles [157].

The inertia of the particle was equated to the forces applied on the particle [77]. The forces applied on the respiratory aerosols were then: the drag force, using the Stokes-Cunningham drag law, gravity, and additional forces. Stokes-Cunningham drag law was used because it was determined that more than 98.2% of the particle diameters in Table 3-1 resulted in Reynold's

numbers below 1. The terminal velocity for all particle diameters were calculated using the settling velocity equation based on Stokes law (see equation (6)). The respective settling velocities were then used to calculate the Reynolds numbers for all particle diameters 1 μm to 100 μm (see equation (7)). Other forces that could be considered in the "F_a" term are thermophoretic force, virtual mass force, Saffman's lift force and Brownian force. Thermophoretic force was considered, since the ventilation induced temperature gradients could affect particle trajectories. Saffman's lift force accounts for the particle lift effects that occur due to near wall shear forces. Saffman's lift force was considered because it may affect the deposition rate of particles on surfaces. The virtual mass force was neglected, as it was assumed the density of particles will always be greater than the density of air. Brownian motion was neglected as only sub-micrometer diameters are affected [78]. Two-way coupling was activated as unsteady particle tracking with steady-state continuum is in use. Other assumptions made were that the respiratory aerosols do not breakup or coalesce, and evaporation effects are negligible to the long-term dispersion effects of droplet nuclei, as shown by Morawska [9].

For the current study, the particle diameters are modelled with a Rosin-Rammler diameter distribution, with a minimum of 1 μm and maximum of 100 μm (see Figure 3-1), referenced from Duguid's paper [45]. The particle diameter data below was fitted with a Rosin-Rammler/Weibull fit resulting in a mean of 28.83 μm, and shape factor of 1.30. See Figure 3-1 and Figure 3-2 for the probability distribution function and the cumulative distribution function with fitted Rossin-Rammler distribution curves. The distributions were fitted using MATLAB's distribution fitter.

Table 3-1: Binned airborne droplet diameters from J.P. Duguid.

Droplet Diameter (μm)	Number of droplets from one cough with mouth 'closed'
1-2	50
2-4	290
4-8	970
8-16	1600
16-24	870
24-32	420
32-40	240
40-50	110
50-75	140
75-100	85

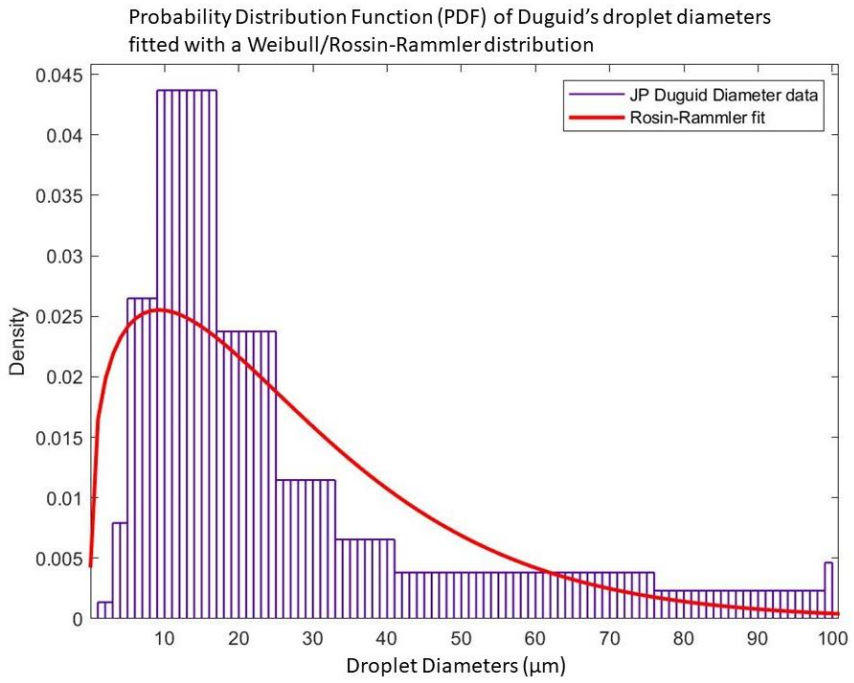

Figure 3-1: Probability Distribution Function of Duguid's diameter distribution with a Rossin-Rammler fit.

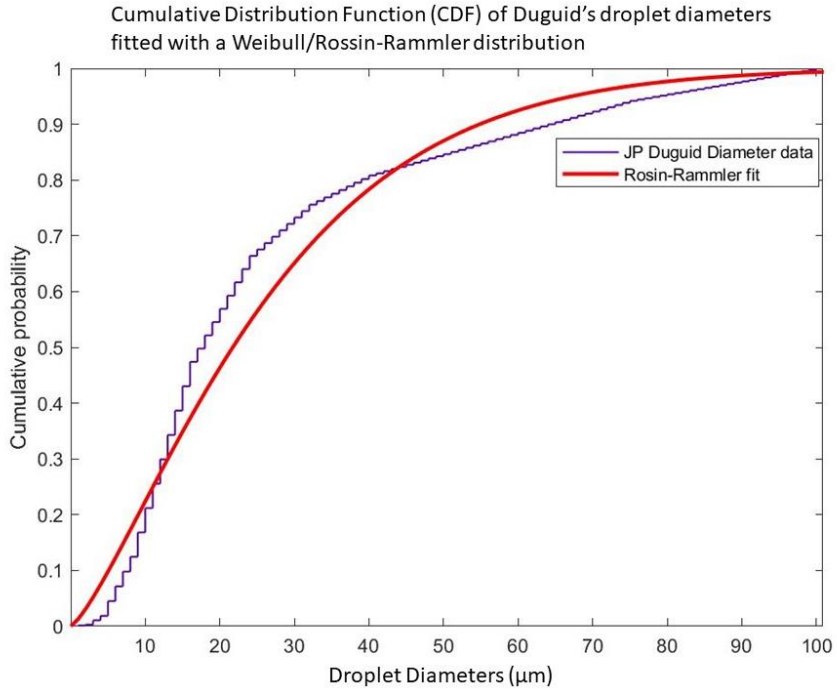

Figure 3-2: Cumulative Distribution Function of Duguid's diameter distribution with a Rossin-Rammler fit.

From the probability distribution function (Figure 3-1), it is seen that the number density for droplet diameters increases rapidly, to a peak number density for 8 μm - 16 μm sized droplets. After the peak, the density of droplet diameters greater than 16 μm gradually reduces, with droplet diameters after 32 μm accounting for less than 10% of the number density. The Weibull curve fit has a peak around 10 μm, which then gradually reduces towards 0 for the number density.

3.2. Validation

A validation study based on Yin et al.'s data [128] has been carried out to validate the CFD methods discussed in sub-chapter 3.1. Due to time, budget and pandemic related lab access constraints, an in-lab experimental validation study was not feasible. Yin et al.'s study is based on an experimental study of particle dispersion in a patient ward for mixing and displacement ventilation conditions, with varying exhaust locations and air change rates. The study was designed specifically for CFD validation and is ideal for ventilated indoor air CFD studies as the experimental study was carried out in an insulated and ventilation induced patient ward with high precision sensors and instruments. They placed omnidirectional anemometers (which were verified by two ultrasonic anemometers) to measure the temperature and velocity distributions, and a multigas particle sampler to measure the particle concentrations.

For the current validation study, only temperature and velocity measurements were used. Particle concentration validations were attempted, but resulted in significant values of relative error, which could be because of many reasons: 1) the particle size distributions and number densities were different between the experimentally produced particles and the aerosols simulated in the model, resulting in different airborne patterns, 2) the particle measurement methods of both the experimental and CFD study had significant sources of error, 3) due to lack of computational resources, the particle concentrations could not reach steady state.

3.2.1. Methodology

Yin et al.'s experimental ward was modelled, with the dimensions provided in the study, see Figure 3-3 for the replicated model of the patient ward. The ward had simplified geometries (cuboids) for a bed, a patient, a caretaker, medical equipment, and a TV from which all except for the bed produced heat fluxes. The ward had two air inlets, one at the ceiling to induce the mixing ventilation setting, and a diffuser on the bottom wall opposing the patient, to induce displacement ventilation. There were two air exhausts, one the left wall (with respect to the patient), one on near

the ceiling and one near the floor. The study measured temperature and velocity at 8 pole locations and 7 probe heights, of which 5 pole locations were provided: pole 1, pole 3, pole 5, pole 7 and pole 8. The authors were contacted for the remaining pole locations, but without success. The pole locations for the five poles are indicated in Figure 3-4.

The Displacement Ventilation, High auxiliary Exhaust, 4 Air Changes per Hour (DV HE 4ACH) configuration, was used to validate the CFD setup. The heat fluxes were applied as calculated from the total power and surface area provided in Yin et al.'s study, see Table 3-2 for the heat flux values. The diffuser inlet was set as a velocity inlet BC with 0.14 m/s for the inlet velocity to produce 114 cfm of air into the room. Both the main and auxiliary exhaust were active with outflow BCs applied to both. The walls had adiabatic no slip conditions, and the ambient temperature was set as 23.9°C.

Table 3-2: Validation study boundary conditions

Component	Boundary Condition
Ambient temperature (°C)	23.9
Inlet air temperature (°C)	19.5
Patient heat flux (W/m^2)	66.25
Caretaker heat flux (W/m^2)	49.1
Medical equipment heat flux (W/m^2)	24.32
TV set (W/m^2)	67.07
Diffuser	Velocity-inlet (0.14 m/s)
Main exhaust	Outflow
Auxiliary exhaust	Outflow
Walls	Adiabatic, no slip
Floors	Adiabatic, no slip
Ceiling	Adiabatic, no slip

In terms of meshing, a 5 cm unstructured tetrahedral mesh was used. A mesh sensitivity study was conducted to show that that there were no significant deviations in temperature results between 10 cm, 5 cm, and 2.5 cm mesh sizes. For the velocity results the 5 cm mesh and 2.5 cm mesh performed similarly, thus the 5 cm mesh was used. The first prism layer height and number of prism layers (increasing in mesh size by 1.2) were calculated: with the Reynold number based on the air velocity from the diffuser and ambient air conditions, and the characteristic length based on the patient length.

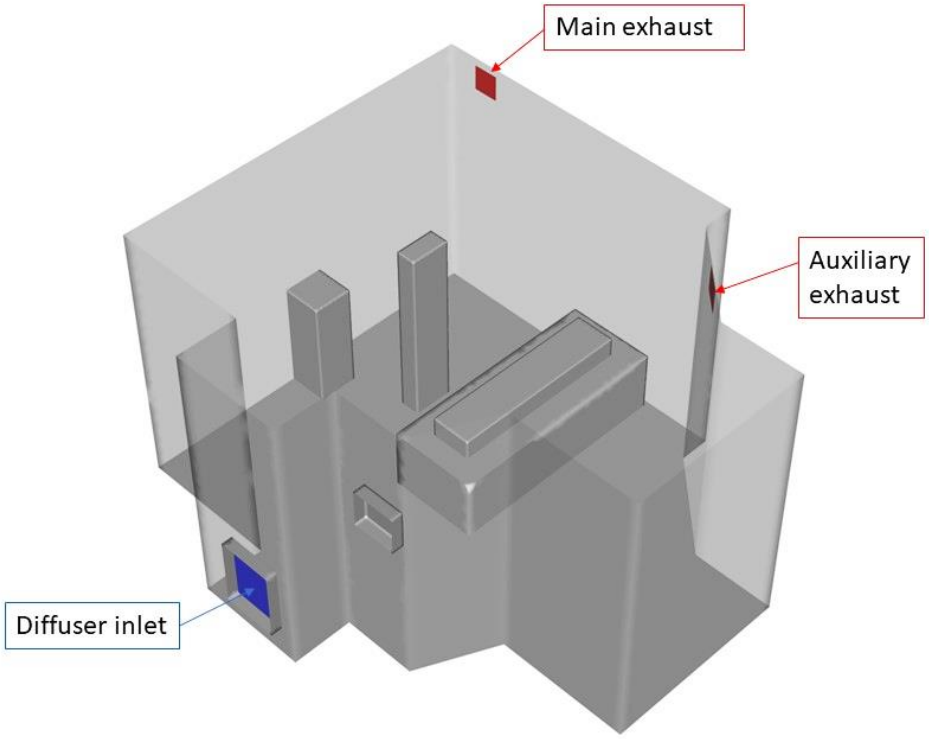

Figure 3-3: Patient ward CFD domain replicated based on Yin et al.'s [128] study. The domain is ventilated with a diffuser air inlet, and two air outlets: main exhaust and auxiliary exhaust. The domain contains a bed, a lying patient, a standing caretaker, medical equipment, and a TV.

The simulations were run in steady-state, with hybrid initialization. The data was collected after the residuals, temperature and velocity monitors stabilized. The continuity residuals stabilized at 0.5 and the all the other residuals stabilized at around $1x10^{-2}$. The residual values were comparatively higher than what is recommended in literature ($1x10^{-3}$ or less), but the accuracy limitation was mesh dependent i.e., a higher mesh resolution would allow the residuals to reduce further to provide more accurate results. However, the chosen mesh resolution sufficed for the current study.

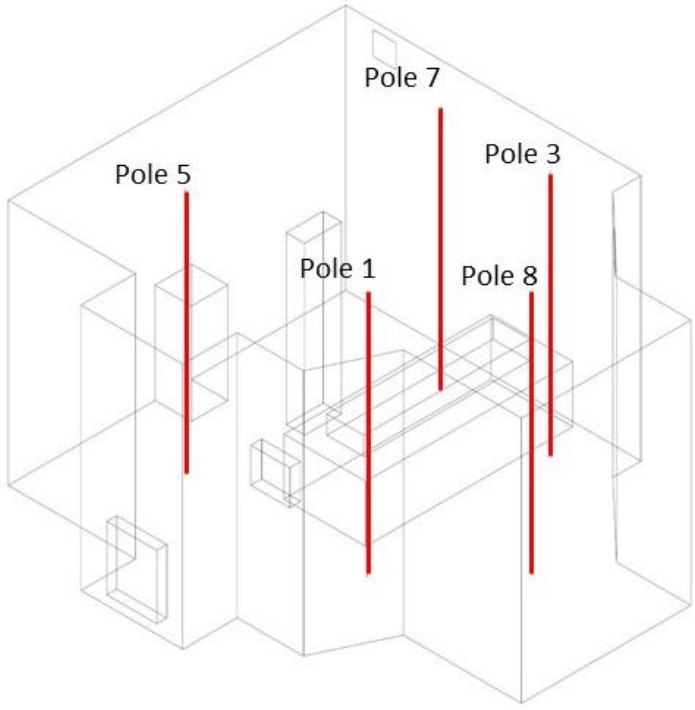

Figure 3-4: Patient ward pole locations for temperature and velocity probe measurements

3.2.2. Results

The following plots (see Figure 3-5) show the temperature distributions from the CFD post-processed pole results compared with the experimental data points from Yin et al.'s paper [128]. The temperature data has been normalized based on the supply and exhaust temperatures, as seen in equation (8).

$$\theta = \frac{T - T_s}{T_e - T_s} \tag{8}$$

Hence θ is applied on the x-axis to ensure the data is normalized even if there are temperature discrepancies between the poles, and between experimental and CFD data. The y-axis is the height in meters.

The temperature results conform well with the experimental data for the points closer to the ceiling, however deviations are seen as the temperature curves reach towards the floor. According to the experimental study, the sources of error were the wall insulation, where the temperature deviated by up to 0.3 K, and the sensor accuracy, which was tested to be 0.2 K.

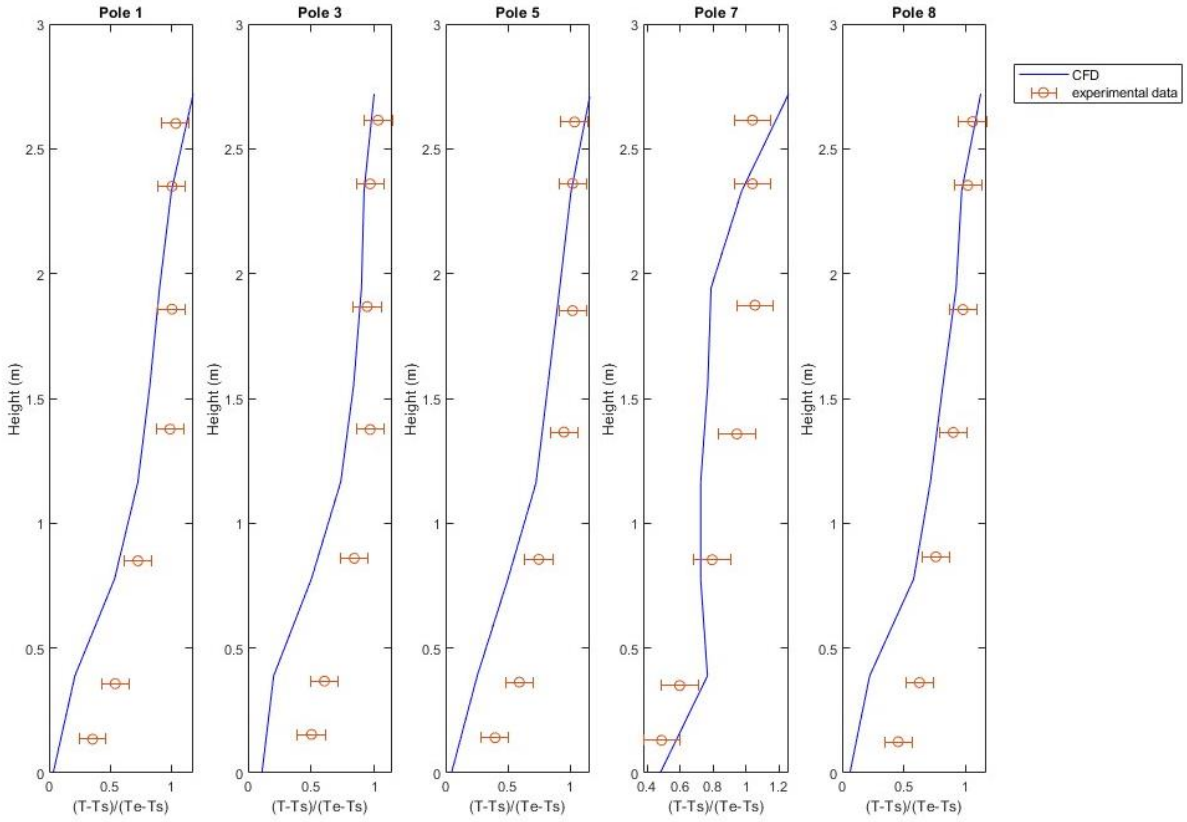

Figure 3-5: Temperature validation plots for poles 1,3,5,7 and 8 with Yin et al.'s experimental data.

The total temperature error is set to be 0.5 K, which is then normalized and applied to the plots. The results are within the error bars for more than 80% of the data. The temperature deviations towards the bottom of the plots/room may be due to several reasons: either the adiabatic boundary conditions were not appropriate because in the experimental chamber the floor and walls were transferring some heat through conduction or radiation, the air was not constantly supplied at 19.5°C during the experiment, there was some turbulent mixing when the air was supplied causing warmer air to mix with the cold incoming air or the mesh needed further corrections near the floor.

The following plots (see Figure 3-6) show the velocity distributions from the CFD post-processed pole results compared with the experimental data points from Yin et al.'s paper [128]. The x-axis is the velocity data in meters per second, and the y-axis is the height in meters. The error bars are based on the sensor tolerance of 0.02 m/s.

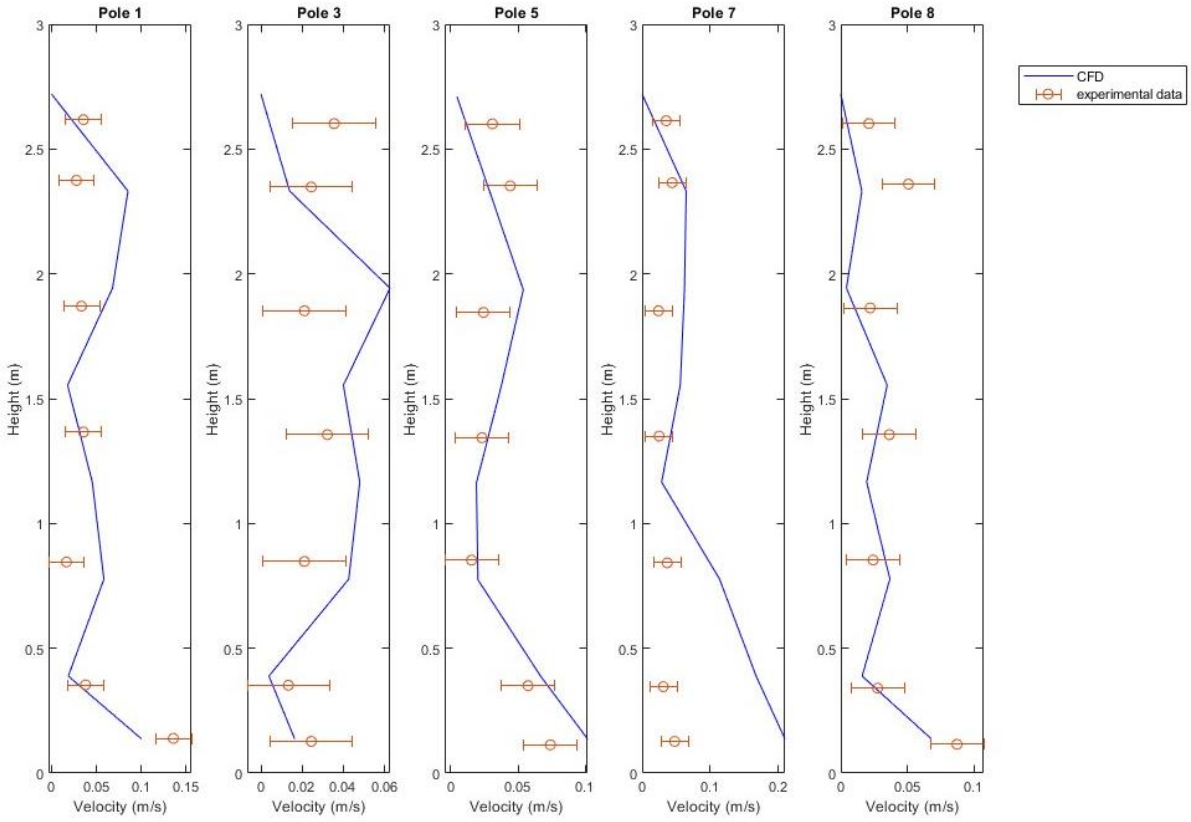

Figure 3-6: Velocity validation plots for poles 1,3,5,7 and 8 with Yin et al.'s experimental data.

The velocity distributions over the 5 poles have very good convergence with the experimental data. Poles 7 which is furthest from the diffuser and closest to the main exhaust (see Figure 3-4) has the most deviations. Specifically, towards the floor the maximum relative error goes up to 339%, which is quite significant. A probable cause for this error may be because of the high velocity fluctuations near the exhaust for the simulation. An additional hypothesis is that the geometry and HVAC components were simplified for the simulation; for example, as seen from the experimental chamber photos in Yin et al.'s paper the bed would allow air flow underneath, while the modelled bed in the simulation domain is a cuboid perfectly attached to the floor. This difference in bed geometry could affect the airflow patterns near the bottom of pole 7. All other poles provided good convergence to validate the CFD method. Based on the temperature and velocity distribution validation results presented above, the validation study was deemed acceptable to proceed with the chosen CFD methodology.

Chapter 4 CFD studies to Investigate the impact of Ventilation Layout in a Small Office.

4.1. Introduction

Small single-occupancy offices are not considered high risk spaces for airborne transmission, with the obvious reason that there is no secondary occupant in the room to transmit infection to. However, it was noticed that certain offices are not equipped with air outlets/return grilles, an example being the faculty offices in the Bergeron building in York University campus. These faculty offices have supply inlets to ensure they remain ventilated, but the air is then designed to escape through the doors into the main hallway to a common return grille. Khankari [12] has shown that inducing air containment, by having separate air outlets for each zone is an effective strategy to limit airborne transmission to different zones of a space. Zhang has also re-iterated this advice for classrooms and offices [21]. Small offices have been evaluated for ventilation effectiveness and airborne transmission risk in literature [24,121]. The current setup is designed to observe the aerosol spread from a single cough, to evaluate if adding an air outlet to a small office is effective at reducing the risk in the room (for secondary occupants that can come into the space) and preventing aerosols from exiting the space through the door slip or an equivalent. The following simulation study contains three cases,

- Case 1: the existing ventilation layout, with no air outlets, but includes a rectangular opening to simulate the slip opening under a closed door (No outlet).
- Case 2: an added air outlet placed right above the occupant (Overhead outlet) with the existing configuration.
- Case 3: an added air outlet placed further away from the occupant (Far-off outlet) with the existing configuration.

4.2. Methodology

The office space simulation methodology involves constructing the geometry, meshing the domain, and simulating the air and particle flows, to then qualitatively determine the areas of the office that are higher in aerosol concentration. Three cases were studied to compare the effects of outlets on aerosol dispersion. A note, “aerosol” and “particle” is used interchangeably throughout this chapter and the thesis.

4.2.1. Meshing and Geometry

The office space is based on York University’s Bergeron building faculty office 437C, see Figure 4-1. The office space was modelled in SolidWorks, with maximum room dimensions of (3.54 m x 3.31 m x 1.97 m) in length, width, and height respectively, see Figure 4-1 for the major dimensions of the space. The air supply inlets are located in the ceiling with active area dimensions of (1.17 m x 0.03 m) per slot. There are two slots in each supply inlet, and two supply inlets total in the office, i.e., there are four air supply slots. The supply air produces 57 L/s of total air to the space as assigned in the ventilation plans of the building.

For case 1, the slip opening under the door has dimensions of (1.02 m x 0.02 m), and for cases 2 and 3, the outlet is a square with sides of 0.3 m each. The occupant is simplified with an ovular torso, and a cylindrical head. The shoulders and top of the head have 10 cm edge fillets applied. The occupant’s torso has a height of 0.9 m, the long side of the oval is 0.6 m, and the short side is 0.4 m. The height is comparatively short, with the assumption that they are seated. The occupant’s head is 0.63 m in diameter and 0.18 m in height. There is also a PC included on the desk to provide heat flux. The dimensions of the PC are (0.5 m x 0.18 m x 0.5 m) in (L x W x H).

Uniform tetrahedral meshing was applied to the domain, with a mesh size of 6.25 cm. The inlets had a mesh size of 0.93 cm, and the outlets had a mesh size of 5 cm. The total number of mesh elements were 936,182 elements. A mesh sensitivity study was not conducted, as the mesh size was adapted based on the mesh sensitivity results from the lecture hall study section 5.2.1. Both simulations were designed in parallel, and the lecture hall design had higher inlet velocities (for the mixing ventilation configuration), thus it was assumed that the mesh sensitivity results were adaptable to the current office space mesh. For future studies, to provide more confidence in the results a mesh sensitivity study should be conducted for each new simulated space.

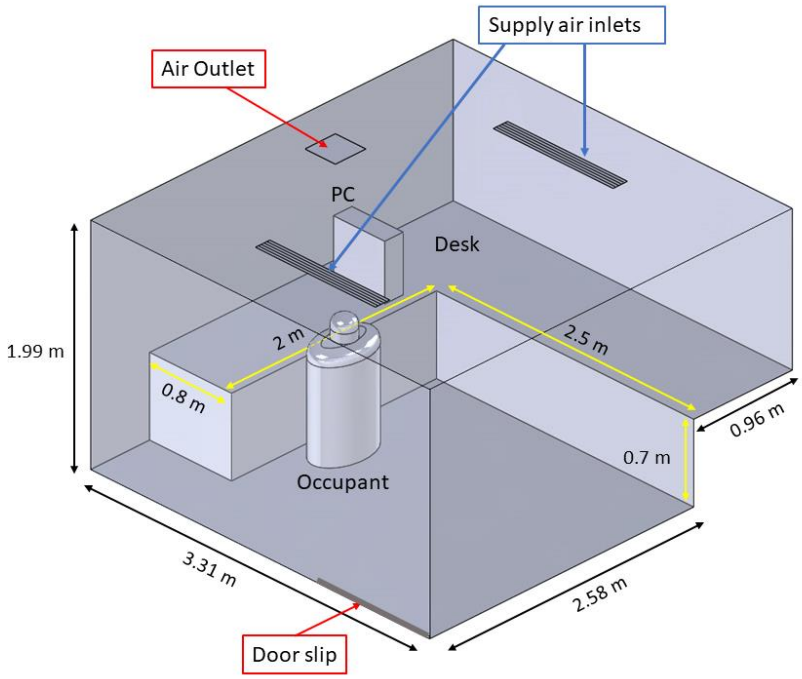

Figure 4-1: Dimensions of the office space for the overhead outlet case in meters, and labels indicating the air inlet, air outlet, door slip, occupant, PC and desk.

4.2.2. Numerical Modelling Setup

The general setup followed the same methodology as described in section 3.1.2. Boundary conditions and particle injection details are provided below.

4.2.2.1. Boundary Conditions

The three cases were run with the same conditions except for the conditions pertaining to the return grille and its location, i.e., the return-grille was not applied for case 1, and the location of the return grille was different between case 2 and case 3.

Table 4-1: Boundary Conditions for each component in the Small Office's CFD domain.

Component	Boundary Condition
Ambient temperature (°C)	23
Inlet air temperature (°C)	18
Occupant heat flux (W/m^2)	64.6
PC heat flux (W/m^2)	71.4
Diffuser	Velocity-inlet (0.85 m/s)
Door slip	Pressure-outlet
Return grille (case 2 and 3)	Pressure-outlet
Walls	Adiabatic, no slip

Floors	Adiabatic, no slip
Ceiling	Adiabatic, no slip
Desk	Adiabatic, no slip

4.2.2.2. Particle Injection Details

The initial velocity was set to 6 m/s to simulate the risk for a minimum momentum expulsion, which ensure the main dispersion of particles is due to ventilation rather than cough momentum driven. The mass flowrate is set to $5x10^{-7}$ kg/s with 2 streams to produce 8040 droplets. The droplets were assigned a density of 998.2 kg/m^3, representing 100% liquid water droplets. The cough period was set to 0.4 seconds according to Gupta et al.'s data [6]. The source diameter was set to 2 cm with a cone shaped expulsion and the release angle was 22 degrees [7]. The injection temperature was set to 307.15K (34°C) to match the temperature of droplets that would be expelled from the human body [68].

4.3. Results and Discussion

The following sets of figures show the dispersion of particles in the office room for three ventilation cases: no air outlets in the room, an air outlet (case 1) on the overhead of the occupant (case 2) and an air outlet far-off from the occupant (case 3). The occupant's cough particles were tracked based on their diameters, as seen by the bar on the left of the figures with the diameters ranging from 1 μm to 100 μm. The variance in particle colours correlate to the particle diameters.

Figure 4-2 below, shows the ventilation configurations for the three cases with respective air inlets highlighted in blue, and air outlets and door slip highlighted in red. The particles are shown to be expelled from the occupant, who is faced away from the desk and towards the wall. This occupant orientation was chosen for maximum dispersion of particles; if the occupant was facing towards the desk, most particles would collide with the wall in front of the desk and deposit quickly on the wall, desk and occupant's clothing. The cough trajectories for each case began to look different as soon as the particles were expelled, with the case with no outlets rising in a slow puff due to buoyancy, the case with the overhead outlet rising as well, and the case with the far-off outlet rising and moving towards the front of the occupant.

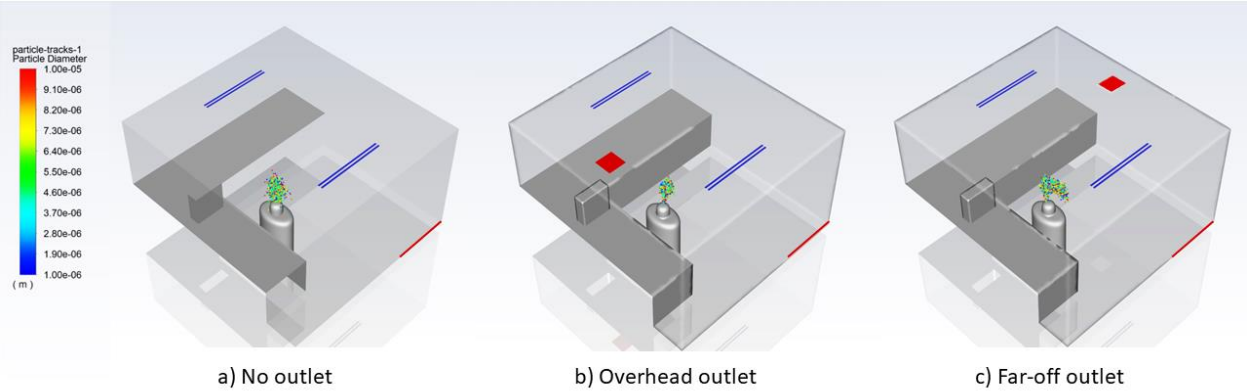

Figure 4-2: The Small Office CFD domain 3 seconds after the occupant coughs for cases 1-3, a) No outlet in the domain, only the door slip b) with an overhead outlet and c) with a far-off outlet.

After 30 seconds since the cough was expelled, the particles had dispersed extensively (see Figure 4-3). Case 1 with no outlets, had the least number of particles circulating in the room, which was because many of the particles deposited or exited through the door slip. The particles were able to quickly deposit or exit because the air flow allowed for one directional flow. The air from the inlets pushed the particles down, which lead to 77% of the particles to deposit on the occupant (see Table 4-2). The remaining particles moved through the room and the negative pressure from the door slip was able to bring out some of the particles that were pushed towards the floor from the inlet air trajectories. For case 2 with an overhead outlet, the particles are seen to exit through the outlet, while several particles lingered in the area near the door slip and the right wall (with respect to the occupant). Particles were extensively dispersed, because when the cough was directed forwards, the air from the inlet and the pull from the overhead outlet led to a mixing phenomenon for the air and particles. Case 3 with the far-off outlet, attracted most of the particles towards the outlet, as seen by the cough particles gradually spreading away from the occupant and towards the outlet. This also means a high concentration of the particles were spreading towards the door which is close to the outlet. The widespread of particles near the door poses a high risk in case a secondary occupant walks into the room within a few minutes of a cough event.

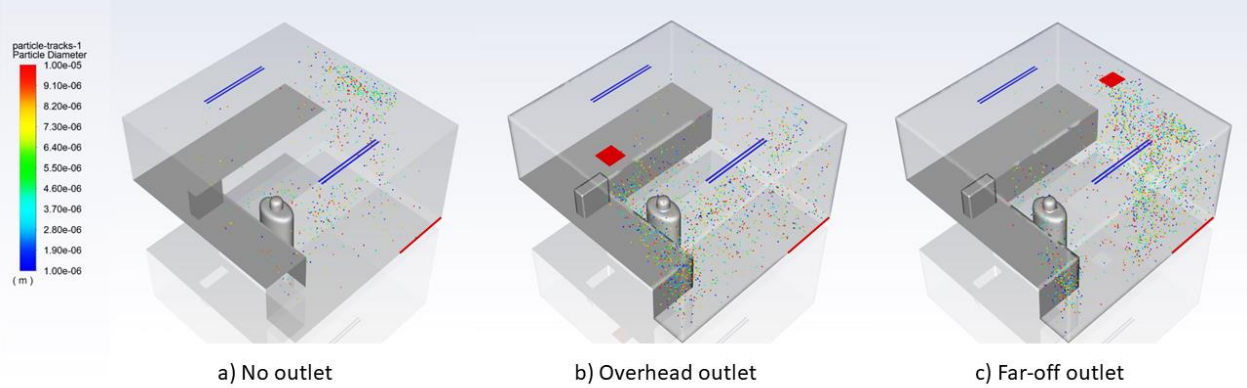

Figure 4-3:The Small Office CFD domain 30 seconds after the occupant coughs for cases 1-3, a) No outlet in the domain, only the door slip b) with an overhead outlet and c) with a far-off outlet.

By 1 minute (see Figure 4-4), the particles reduced in concentration by either depositing on surfaces or escaping through the outlet and/or door slip.

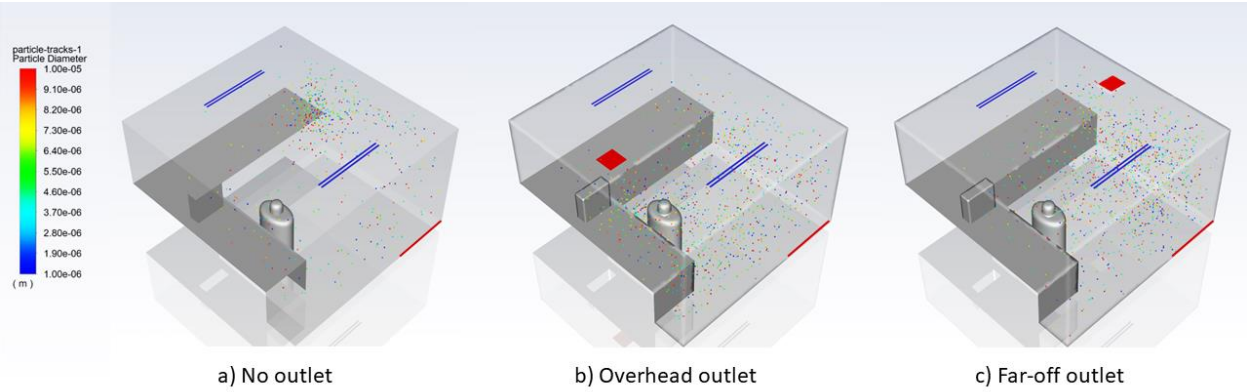

Figure 4-4: The Small Office CFD domain 1 minute after the occupant coughs for cases 1-3, a) No outlet in the domain, only the door slip b) with an overhead outlet and c) with a far-off outlet.

At 2 minutes (see Figure 4-5), the particles near the door slip and underneath the outlet for all three cases mostly cleared out. Only some particles out of reach from the door slip or outlet stagnated in ambient air.

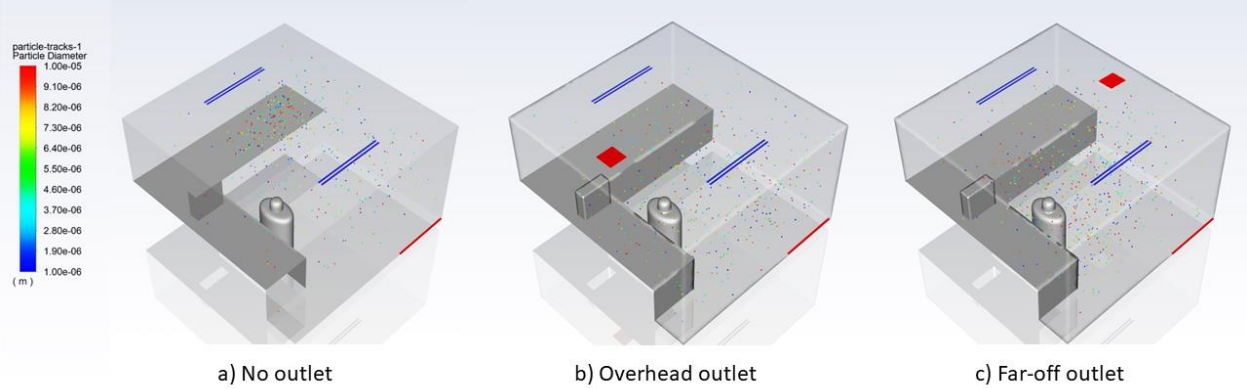

Figure 4-5: The Small Office CFD domain 2 minutes after the occupant coughs for cases 1-3, a) No outlet in the domain, only the door slip b) with an overhead outlet and c) with a far-off outlet.

At the 5-minute point (see Figure 4-6), which is the end of the simulation, less than 1% of the initial number of particles survived as stagnated particles in the ambient air. This signifies that the ventilation in the room for all three cases was effective at recycling the air and removing contaminants. However, the three cases need to be distinguished, which can be done from the particle summaries for the three cases. See Table 4-2 for the particle summary for all three cases, describing the number of particles that escaped or were trapped in each zone of the domain.

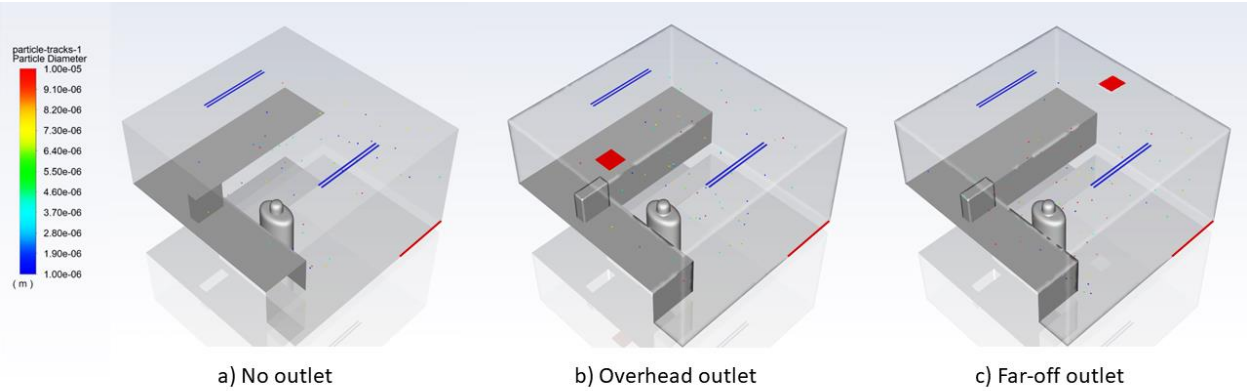

Figure 4-6: The Small Office CFD domain 5 minutes after the occupant coughs for cases 1-3, a) No outlet in the domain, only the door slip b) with an overhead outlet and c) with a far-off outlet.

Examining the particle summaries from Table 4-2: for case 1, it is seen that most particles deposited on the occupant, while a smaller proportion deposited on the walls and floor. This was caused by the high velocity of air pouring through the inlets in the ceiling, which pushed the

particles downwards and onto the occupant. Case 1 was unlike case 2 and 3, where the outlets were able to re-direct the flow leading to a lower number of particles trapped on the occupant. Without any outlets for case 1, around 5% of the particles escaped through the door slip and into the hallway, and less than 1% of particles deposited on the desk.

Table 4-2: Particle Summary—number of particles that escaped or got trapped in each zone for cases 1-3.

Zone	Trapped/Escaped	No outlet (Case 1)	Overhead outlet (Case 2)	Far-off outlet (Case 3)
Outlet	Escaped	--	562	1742
Door slip	Escaped	376	290	354
Walls and Floor	Trapped	1327	3820	3954
Occupant	Trapped	6225	3090	1766
Desk	Trapped	51	212	153
In fluid	--	61	66	71

For case 2, with the outlet over the occupant, 7% of the particles escaped through the outlet. A significant number of particles had also deposited onto the occupant, walls, and floor for case 2. In terms of case 3, with the outlet farther away from the occupant, a higher number of particles (around 22% of particles) were able to escape through the outlet. Case 3 had the smallest proportion of particles deposited on the occupant as the particles were carried away from the occupant quickly and effectively. Most of the particles then deposited onto the far wall and floor.

Within the three cases, the air and particle flow varied, resulting in different distributions for the particle summaries. For case 1, as there were no outlets on the ceiling, the air flow was strictly downwards, which resulted in the particles depositing on the occupant as soon as they were expelled, and the remaining particles slowly drifted to then deposit on the walls, floor or escape through the door slip. Case 1 had the most particles exit through the door slip, which introduced a risk to the occupants directly outside the office. However, the case with an overhead outlet and far-off outlet were not significantly better at reducing the particles that escaped from the door slip. The particle proportions that exited from the door slip ranged from 3.6% (case 2) to 4.7% (case 1). For case 2 and 3, there were outlets on the ceiling, along with the ceiling located inlets, which formed a mixing ventilation scenario. Mixing ventilation designs often vigorously mix the old and new air, which also mixes the contaminants in the air. When the air contaminants are mixed, they are spread all over the room (as seen in Figure 4-4 and Figure 4-5, b and c), before they are eventually diluted and removed from the room. When considering the risk of infection due to the

ventilation layout for the three cases, case 1 with the existing ventilation layout and no outlets performed the best, because there were fewer particles stagnating and circulating in the air. If a secondary occupant were to enter the room, they would first be exposed to the air; the higher number of particles that are widespread and circulating in the air, the higher the risk of infection through airborne transmission. Thus, it can be concluded that adding outlets to the ceiling did not improve the overall risk in the room. Additionally, as all three cases had differing particle distributions throughout the space, it can also be concluded that the impact of ventilation components and location can have significant effects on the particle dispersion patterns in a space.

Recommendations for airborne transmission safety can also be derived from the results above. The impact of outlets was observed, with particles tending towards the location of outlets. In the scenarios above if an outlet, or more realistically an air cleaner (which functions similar to an outlet by attracting air flow through and cleansing the air of contaminants, but cheaper and more feasible to install) were placed near the occupant and on the floor, the particles would go through the air cleaner. The particles that escaped through the door slip (outside the office) and circulated in the air would reduce significantly. Other ventilation configurations may also be investigated, for example, displacement ventilation, which could efficiently remove contaminants from the space through a bottom-to-top airflow direction. This flow orientation would also prevent deposition of particles on the occupant and other surfaces, thus reducing the risk for indirect and fomite transmission.

4.4. Conclusions and Future Work

This chapter of the thesis investigated the dispersion patterns of aerosols from a single cough within the exisitng ventilation layout for York University's Bergeron building faculty office 437C, in addition, also compared the aerosol dispersion results with those of the office when an outlet is added to the ceiling. Three cases were considered, case 1 was the exiting layout with no outlets, case 2 was a ventilation layout with an added overhead air outlet, and case 3 was a ventilation layout with an added far-off air outlet. The objective of the chapter study was to evaluate whether an added outlet in the office would reduce the overall risk of cough aerosols circulating in the room, and the risk of those aerosols escaping from the room into the hallway.

It was concluded that adding outlets to the space did not significantly reduce the number of particles that escaped from the space. The particle proportion that was escaping through the

door slip into the hallway in the existing configuration was 4.7%, while it was reduced to only 3.6% and 4.4% after the overhead outlet and far-off outlet were added, respectively. Furthermore, it was observed that adding ceiling located outlets to the office induced vigorous mixing in the space, which lead the particles to disperse extensively and circulate in the air. This widespread dispersion contributes to higher risk, as a secondary occupant (that walks into the room) has a higher probability of being exposed to the infectious particles.

Some measures that can potentially reduce the risk of infection in the space, is adding well located air cleaners and changing the ventilation type. Adding air cleaners to the space allow cough particles to be removed from the room efficiently and prevent particle stagnation. The most ideal outlet location is closer to the occupant(s), thus in cases where the infectious person is idenitified, they should be placed close to them. This advice is in agreement with studies in literature that suggest "clean-to-dirty" air pathways are safest to prevent airborne transmisison [14,17]. Furthermore, ventilation configurations that allow for uni-directional transport of cough particles, and prevent deposition on surfaces, such as displacement ventilation—which transports air contaminants towards the ceiling, would reduce the risk of infection exposure to secondary occupants.

The office space simulation study was perfromed during the beginning of the thesis study to, 1) evaluate the funcionality and convergability of the CFD method, and the aerosol tracking perfromance, 2) qualitatively analyze the sensitivity of particle spreading with respect to different ventilation layouts. An office space was chosen because of the small domain and simplified geometry, in addition to being a public indoor space where there is potential risk of transmisison to secondary occupants (office visitors and neighbouring occupants). Since the simulation study was perfromed early in the thesis study, a quantitative risk model had not yet been developed. To add value to the results for this study, a spatio-temporal risk assessment can be applied to the space. The variance in risk for the three cases (or more) can then be compared quantitaviely, depending on the spread of the particles, the concentration of particles in certain areas and the residence time of particles in the space.

Chapter 5 CFD studies to Investigate the impact of Ventilation and Infection Source Location in Lecture Halls

5.1. Background and Introduction

As COVID-19 case numbers reduce, and return to campus efforts begin for institutions, the airborne transmission safety of classrooms and lecture halls should be considered. Classrooms and lecture halls are some of the most densely packed public spaces where occupants stay in a single location for long periods of time (typical class durations are 1-3 hours). There is also the risk of high occupancy turnover rates, as multiple classes use the space during the day. Outbreaks caused by airborne transmission in such spaces is a likely possibility. Thus, a study to analyze the effects of ventilation configuration and infector source location in a lecture hall can assist in prioritizing different outbreak prevention measures. It should be noted that concerts and sports events are also densely packed settings, and many of those venues follow a terraced floor set up: therefore, the following set of simulations can also be extended to those settings.

CFD and experimental studies of different ventilation configurations were extensively modelled [14,19,24,113,114,121,126,128,131,132] such as for displacement, mixed, stratum and underfloor ventilation, resulting in an overall lack of consensus on which ventilation configuration works best; the optimal ventilation configuration varies upon setting, heating vs. cooling, volume of domain, direction of contaminant release, heat fluxes among other variables. When considering the risk of airborne transmission in a large, terraced floor setting such as a lecture hall, results may vary in comparison to smaller, leveled floor settings. A study by Cheng, Niu and Gao [160] investigated the performance of stratified ventilation (e.g. displacement ventilation) in a lecture hall. They observe a thermal comfort issue that could arise with stratified temperature distributions in a terraced floor setting: the cold air will tend to move downwards and to the front, while displacing the warmer air upwards and backwards. This can lead to disproportional cooling for the occupants, and a higher risk for occupants at the back (who are receiving more contaminated air). However, the airborne transmission risk for the occupants was not considered in the study. In terms of airborne transmission risk, an experimental study by Ruud et al. [161] calculated the Wells Riley based infection risk using the carbon-dioxide concentrations in the occupied lecture hall. They performed measurements in a singular location at the front of the lecture hall, from which

they determined the infection risk to be 0.098%. Their limitations were that they did not investigate the spatial heterogeneity of infection risk, and they limited their study to one ventilation configuration.

Airborne transmission and ventilation studies based on lecture hall settings are not extensive in literature, and the aforementioned studies do not directly investigate the impact of ventilation configurations on airborne infection transmission. Therefore, investigating the effects of infector location, and airflow distribution patterns can lead to new, and valuable information amid return-to-campus efforts. This current study used CFD to investigate the varying airborne transmission risks of two main types of ventilation for cooling: mixing ventilation (MV) and displacement ventilation (DV) (refer to section 2.2 for more details on MV and DV), and three different infection source locations in a lecture hall. The measurement of infection risk through airborne transmission routes was simulated with particle distributions in the CFD domain. The concentration and distribution of particles in the breathing zone of occupants were incorporated into a spatio-temporal Wells-Riley based risk equation modified by Buonanno et al. [143]. The main objective was to determine the most effective configuration to limit airborne transmission in large, terraced floor settings, which is a common architectural design of lecture halls, auditoriums, and concert halls.

5.2. Methodology

5.2.1. Geometry and Mesh

The dimensions of the lecture hall in the current study were modelled based on the Curtis Lecture Halls at York University campus. The lecture hall's dimensions based on maximum length, width and height are (14.37 x 14.33 x 4.88) m, and a total volume of 718.84 m^3. The lecture hall can hold a maximum occupancy of 188 persons. For the simulation, the hall was modelled with 40% occupancy (i.e., 76 people) to include physically distanced seating (see Figure 5-1). The occupant (mannikin) models are simplified as slots with semi-circular sides, and a cylindrical shape for the head. The rectangular slot has a length of 0.35 m, and each semi-circle side has a radius of 0.15 m, resulting in a maximum body width of 0.65 m. The occupants are assumed to be seated, hence the torso height is set as 0.89 m. The head height is 0.25 m. The overall dimensions for the mannikins are then (1.14 x 0.65 x 0.3) m for the height, width, and thickness, respectively. The surface area of the manikin is 1.99 m^2. Curvature is included on the occupant's model to

roughly imitate a human body. The instructor's mannikin is modelled similar to the occupant mannikin, but the torso is shortened, and two cylindrical legs are added to represent the instructor as standing. The instructor's mannikin has an updated torso height of 0.75 m, and the cylindrical legs have a length and diameter of 0.75 m and 0.22 m respectively, all other dimensions are kept consistent to the occupant model.

The ventilation strategies are modelled for cooling purposes only, and are designed as follows:

1. Mixing ventilation (see Figure 5-1), which is the existing configuration in place and was replicated in the model with appropriate effective areas for the supply inlets and return grilles. The inlets are located on the ceiling, and the return grilles on the upper corner of the left wall (from the reader's perspective), as seen in the figure. The inlet dimensions are (0.5 m x 0.025 m) for each slot, and each inlet has 2 slots, with a total of 26 inlets (52 slots). The two return grilles have dimensions of (0.91 m x 0.45 m). The airflow rate through each inlet is designed for a maximum of 200 Cubic Feet per Minute (CFM) to provide a total of 5200 CFM in the lecture hall space. For the current simulation the mixing ventilation cooling load is assumed to work for 75% occupancy (assuming full occupancy is 189 occupants) hence 3900 CFM is supplied to the space.

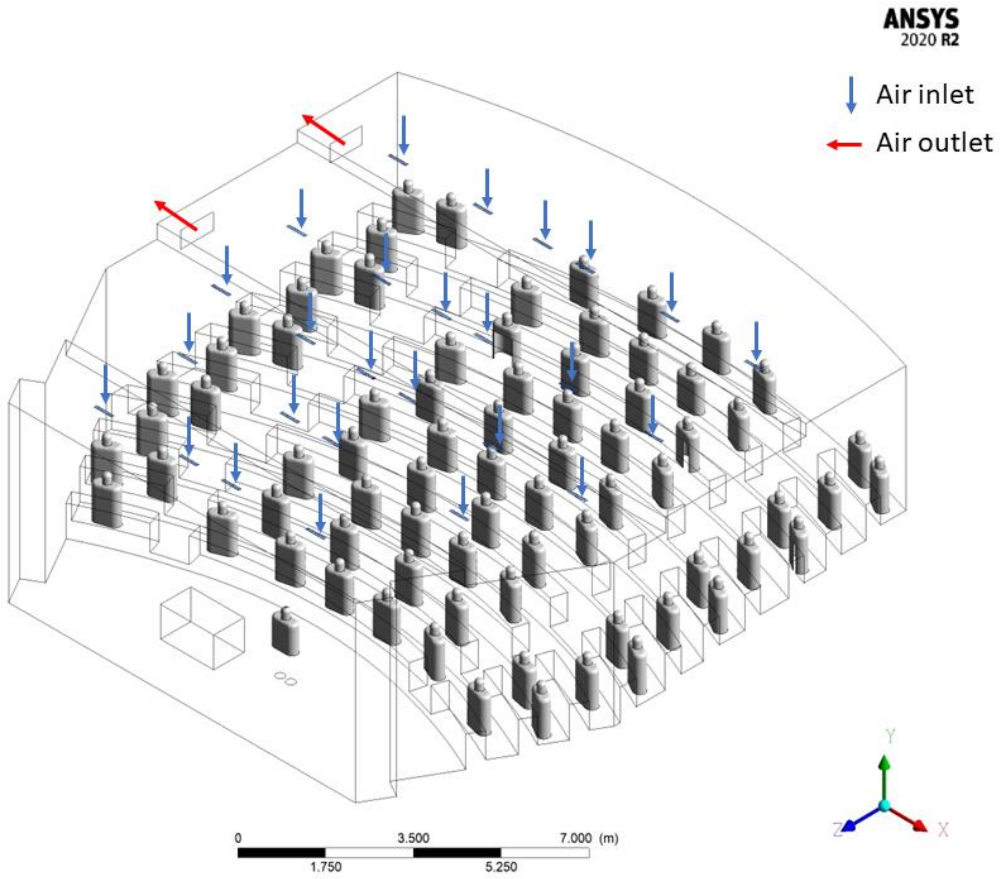

Figure 5-1: Mixing ventilation configuration with the blue arrows indicating air inflow into the lecture hall from the ceiling inlets and red arrows indicating air outflow from the lecture hall through side wall outlets.

2. Displacement ventilation (see Figure 5-2), for which the inlets are located on the stair risers, with dimensions of (30 in x 6 in) replicated from the Price Displacement Flow Recessed (DFR) Diffuser series, specifically designed for risers [133]. The volume flow rate from each inlet is 50 CFM, to supply a total of 2200 CFM with 44 inlets, which is an appropriate displacement ventilation cooling load for 73.5% occupancy (assuming full occupancy is 189 occupants). The required cooling load calculations are performed considering heat loads from occupants and lighting, through the price displacement ventilation design software "Room Designer" [162]. The return grilles are located at the upper corners on both side walls, with the same dimensions as in the mixing ventilation configuration (0.91 x 0.46) m. The return grilles were designed this way to also observe the impact of outlet location on particles dispersion.

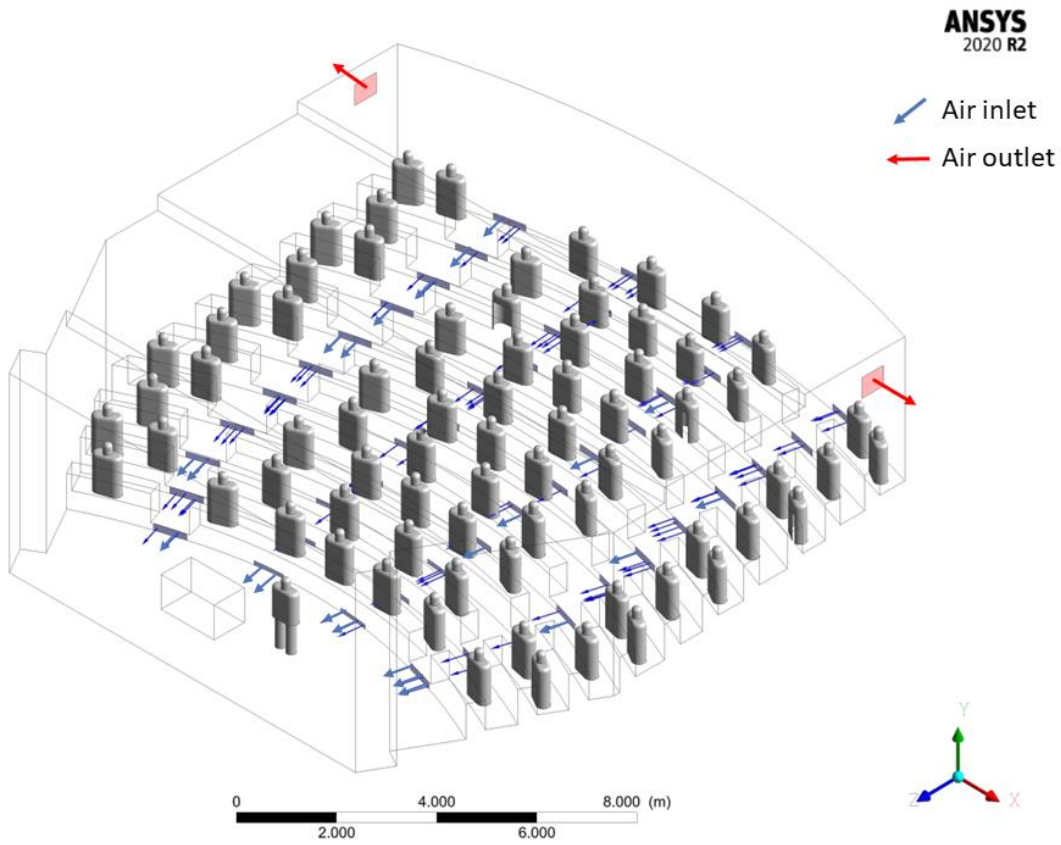

Figure 5-2: Displacement ventilation configuration with the blue arrows indicating air inflow into the lecture hall from the stair riser diffusers and the red arrows indicating air outflow from the lecture hall through the side wall outlets

The domains for the three ventilation configurations were run with unstructured tetrahedral meshes, generated through ANSYS meshing. The lecture hall was meshed with element sizes of 6.25 cm for the ambient region, and refined grids on the occupant surfaces, air inlets and outlets. The occupant surfaces were meshed with 2 cm element size, and the inlets and outlets were meshed with: 2 cm and 3 cm for DV, and 0.75 cm and 3 cm for MV, respectively. The near wall cells were refined with prism layers to ensure the y + remained < 30. The total number of elements in the domain were then 32.5 million elements.

5.2.1.1. Mesh Sensitivity Study

Mesh sensitivity analysis was performed for all three ventilation configurations. Steady-state simulations without particles were run for 4 cm, 6.25 cm, and 9.77 cm cell sizes. Each mesh

size is a factor of 1.56 from the next mesh size. The mesh sensitivity was evaluated using the 1) normalized temperature distributions (see equation (8)), based on the simulation specific location, supply and exhaust temperatures, 2) the velocity distributions (in m/s) in the probe locations. The temperature and velocity results based on mesh size were evaluated specifically at four pole locations (see Figure 5-3). Pole 1 was oriented vertically, parallel to the y-axis, which was placed in front of the central occupant in the lecture hall. It was not placed directly at the centre to avoid intersection with the occupant. Poles 2 and 3 were also oriented vertically and were placed symmetrically on the centres of each stairwell of the lecture hall. Pole 4 (in red) was oriented horizontally, parallel to the x-axis, and ran through the middle of the upper and lower rows of occupants.

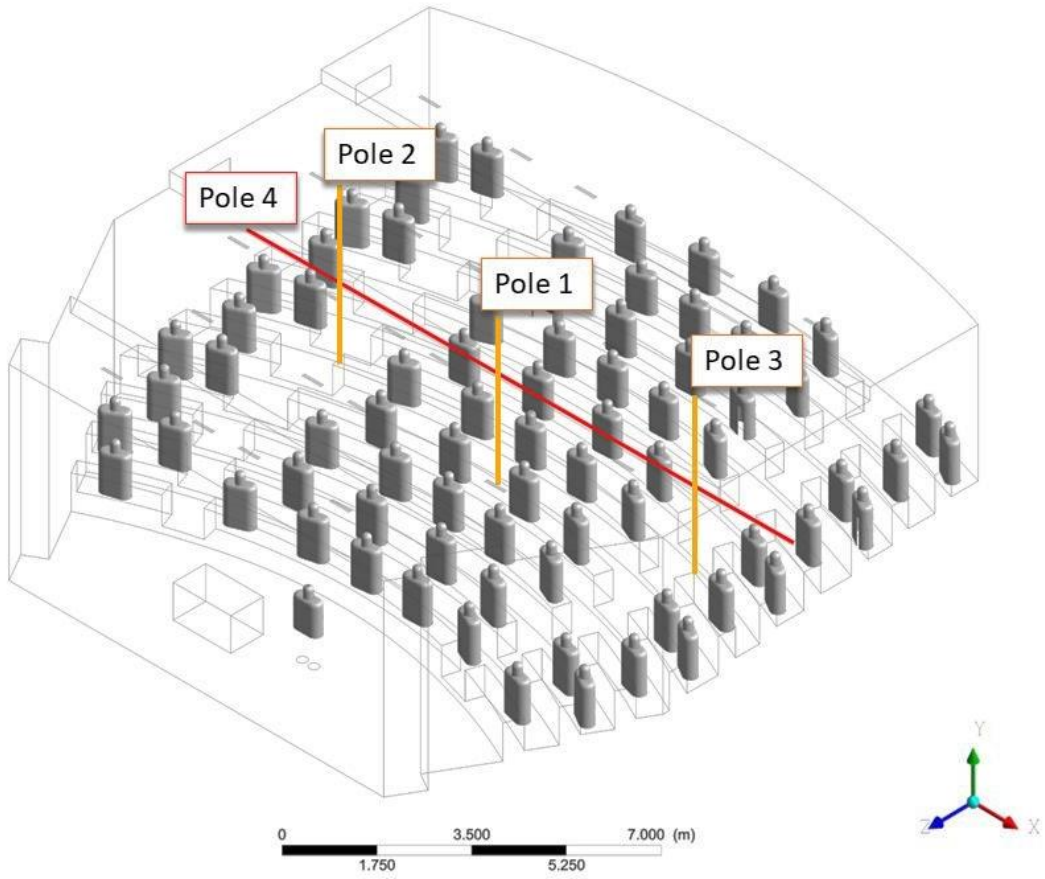

Figure 5-3: Lecture Hall pole locations for mesh sensitivity analysis on both MV and DV configurations. Poles 1,2,3 (vertical) and 4 (horizontal) measure temperature and velocity distributions over their height/length for all three evaluated mesh sizes (9.77 cm, 6.25 cm and 4 cm).

The following sets of plots show the mesh sensitivity results for MV and DV configurations, evaluating the temperature and velocity results for each mesh size: 9.77 cm, 6.25 cm and 4 cm.

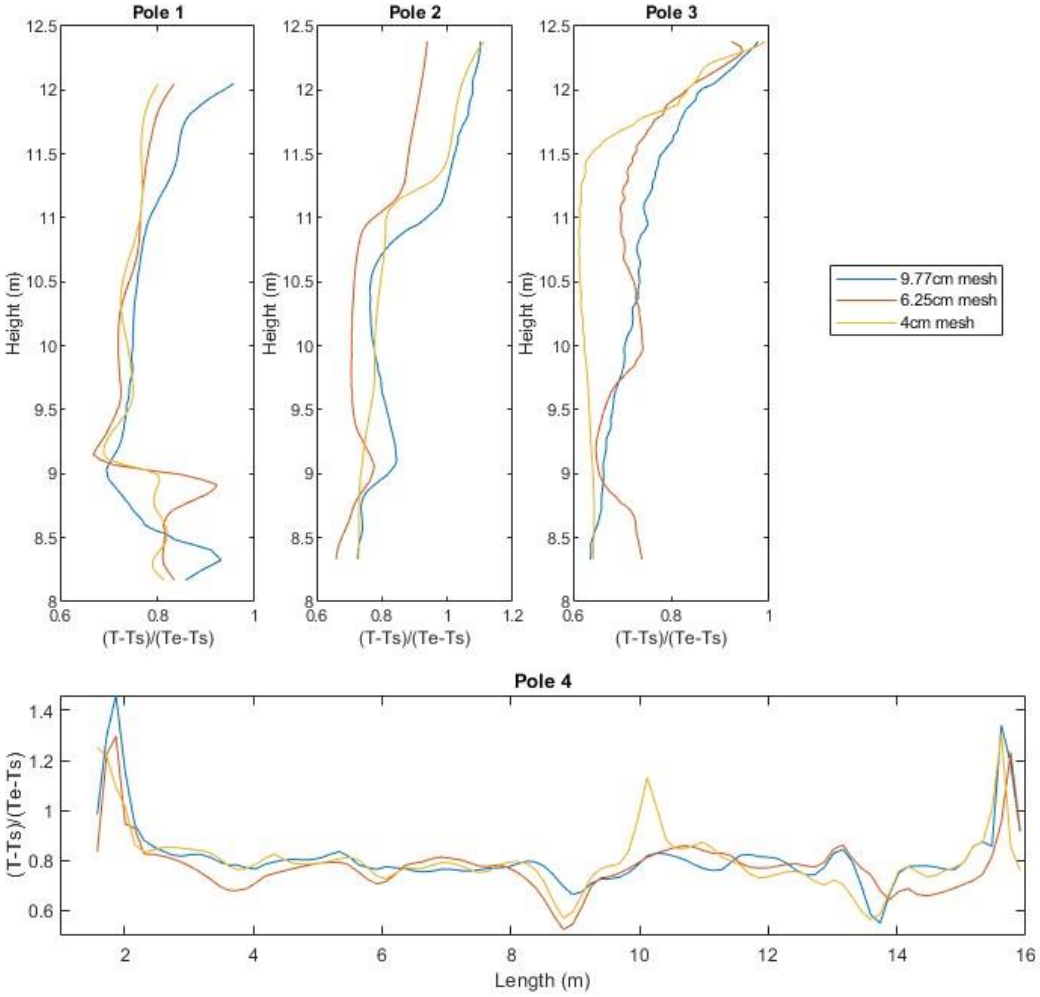

Figure 5-4: Temperature mesh sensitivity results for the mixing ventilation configuration.

Figure 5-4 above shows the mesh sensitivity results for temperature in the MV configuration. The results follow similar trends with some deviations. For instance, in pole 1, the 6.25 cm and 4 cm mesh results overlap well, except at the 9 cm height, where the peak temperature in the 6.25 cm mesh case is larger than in the 4 cm mesh case. The 9.77 cm mesh case also does not seem to match well. This could be due to the difference in mesh resolution, as well as higher fluctuations near the floor, where the air drafts from the inlets and heat flux from the occupants

vigorously mix. The average relative error between the 6.25 cm and 4 cm mesh sizes were 1%,7.6%,10% and 2.2% for poles 1-4, respectively.

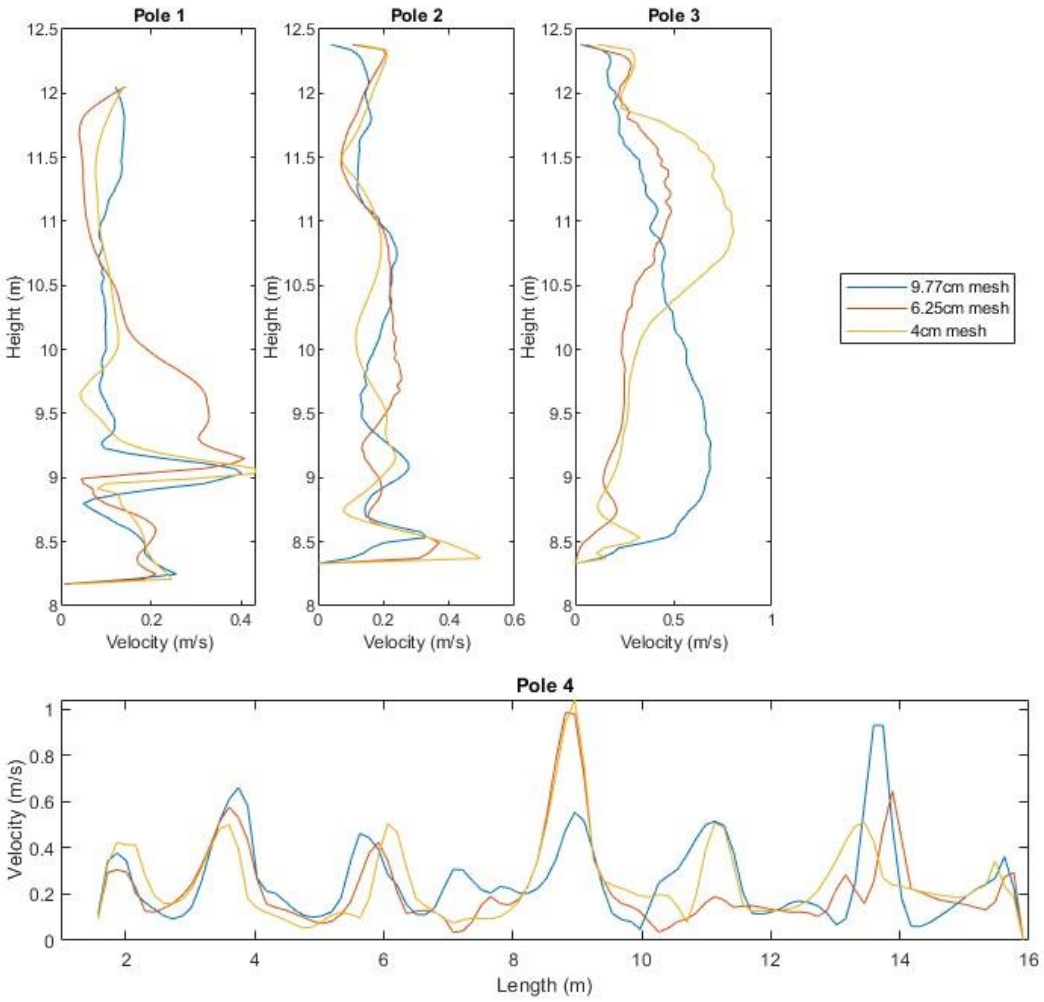

Figure 5-5: Velocity mesh sensitivity results for the mixing ventilation configuration.

Figure 5-5 above shows the mesh sensitivity results for velocity in the MV configuration. There are large deviations in certain regions of the vertical poles (pole 1-3) which again can be due to the stochastic mixing that occurs with the high velocity inflow of air from the ceiling inlets, leading to different air flow patterns in each run case. Looking at the horizontal pole (pole 4) the bigger picture of velocity distributions can be observed. The peaks and troughs in velocity are synchronized, with the 6.25 cm mesh and 4 cm mesh having good alignment. The average relative error between the 6.25 cm mesh and 4 cm mesh is 1.42% for pole 4.

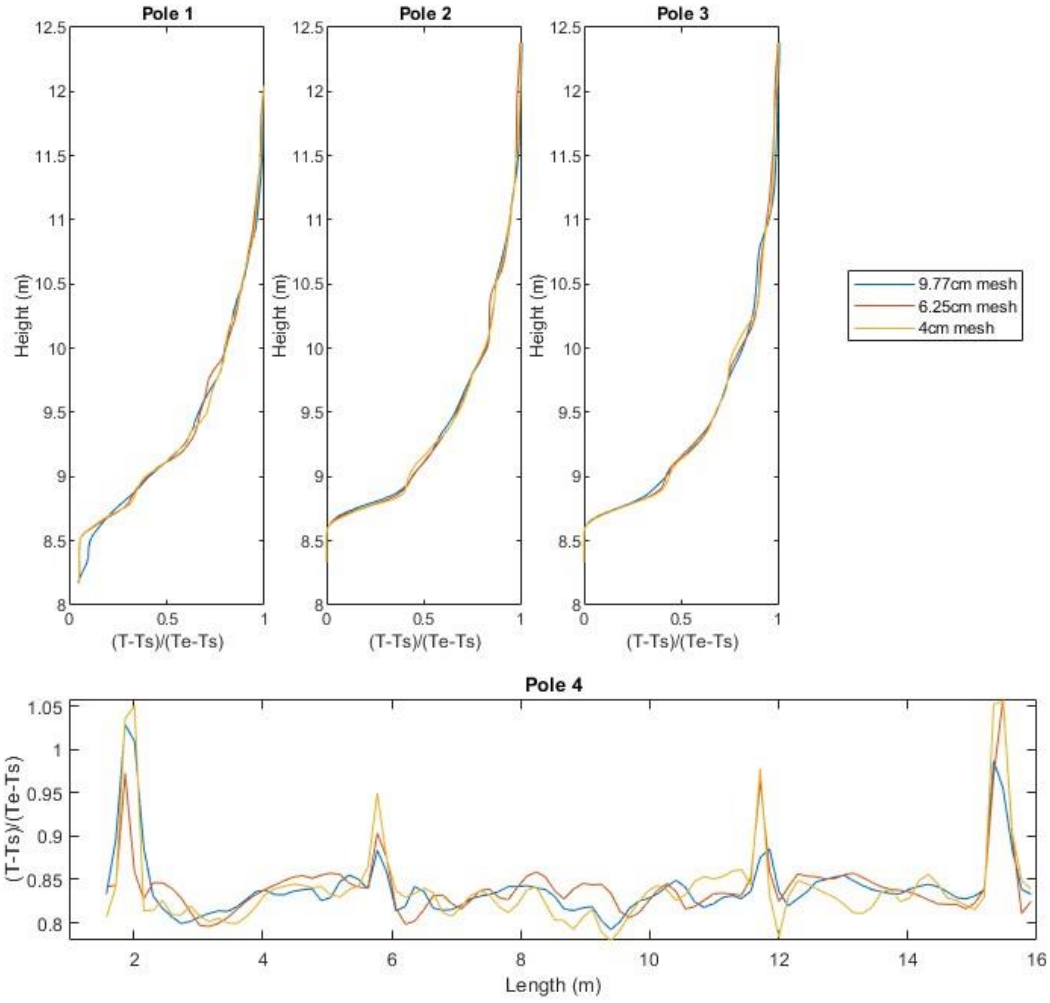

Figure 5-6: Temperature mesh sensitivity results for the displacement ventilation configuration.

Figure 5-6 above shows the mesh sensitivity results for temperature in the DV configuration. The results have very good convergence, especially in the vertical poles (pole 1-3). This is due to the low velocity induced displacement ventilation configuration that ensures a stabilized temperature stratification. The temperatures do not mix much and remain stable through the course of the simulation, resulting in good convergence and demonstrating mesh independence.

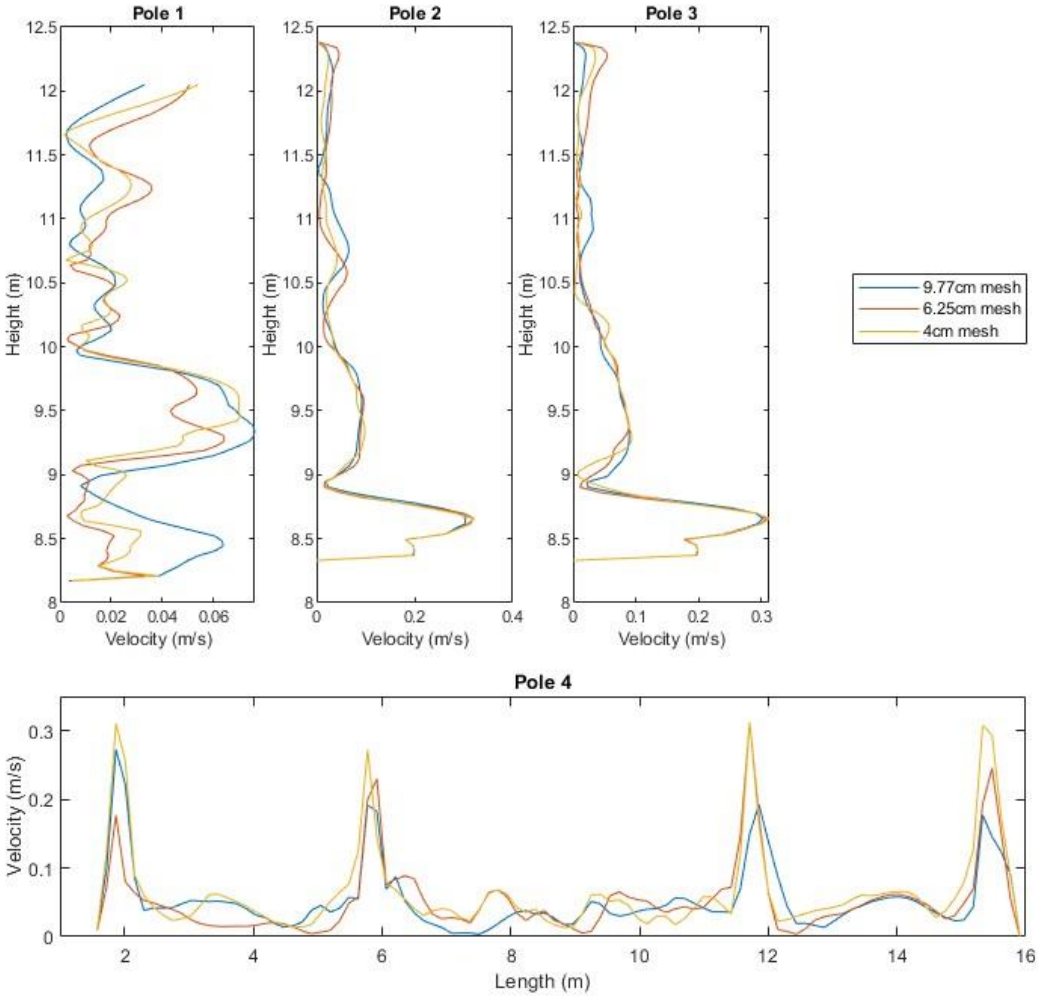

Figure 5-7: Velocity mesh sensitivity results for the displacement ventilation configuration.

Figure 5-7 above shows the mesh sensitivity results for velocity in the DV configuration. Pole 1 has good results, but some of the velocity fluctuations do not get captured well as the mesh resolution decreases. Overall, however, the distribution patterns are synchronized. Results in poles 2-4 are very well aligned and provide confidence for mesh independency.

For all the cases, it was found that the 6.25 cm mesh performed comparatively to the 4 cm mesh domain, while the simulation time was significantly lower with the 6.25 cm mesh, relative to the 4 cm mesh domain, therefore all simulations were performed with the 6.25 cm cell size.

5.2.2. Numerical Modelling Setup

The numerical modelling method was followed as described in section 3.1.2. The specific boundary conditions and particle injection details are described below.

5.2.2.1. Boundary Conditions

The two ventilation configuration cases (MV and DV) had significantly different boundary conditions based on the design requirements of the ventilation configurations.

Mixed:

The ceiling supply diffusers in the ceiling were modelled as velocity inlets with inlet velocities of 2.9 m/s, per slot. The inlet temperature was set to 18°C (291.15K) The return grilles were simulated with an outflow boundary condition; hence particles were able to escape. The walls were no-slip and adiabatic, and particles reflected from the wall, and the coefficients of restitution were modelled by polynomial functions. The occupants in the room were modelled to produce a constant heat flux of 64.6 W/m^2 and reflect particles. Reflected particles were trackable by the user defined function unlike trapped particles, and it was seen that many particles would settle on surfaces with the reflection boundary condition, as their deposition velocity was low, preventing them from rebounding. (Tu Intensity= 21.2, hydraulic diameter = 0.047 m)

Displacement:

The supply diffusers located on the stair risers were modelled as velocity inlets with inlet velocities of 0.2 m/s. The return grilles were modelled as pressure-outlets. The walls and occupants' boundary conditions are same as in the mixing ventilation case.

Table 5-1: Boundary conditions for mixing and displacement ventilation cases

	Mixed	Displacement
Inlet location	Ceiling	Stair risers
Outlet location	Upper left side wall	Upper side walls
Inlet velocity (m/s)	2.9	0.2
Outlet boundary condition	Pressure-outlet	Pressure-outlet
Ambient temperature (°C)	23.5	23.5
Inlet temperature (°C)	18	17
Occupant heat flux (W/m^2)	64.6 W/m^2	64.6 W/m^2

5.2.2.2. Particle Injection Details

Particles were injected into the domain to simulate the transport of respiratory aerosols. The particle injection was modelled with reference to an average human cough. The SARS-CoV-2 virus can be spread through airborne routes by a variety of exhalatory activities, for instance, coughing, breathing, sneezing, talking among other many others [3]. Coughing, singing, and sneezing have significantly higher droplet expiratory volumes in comparison to simply talking or breathing [50]. Additionally, coughing is a primary symptom of COVID-19 infection [109], hence a cough is the chosen form of particle injection for this study.

Cough initial velocities range from 6 m/s to 22 m/s based on Particle Imaging Velocimetry and Interferometric Mie Imaging studies [4,5]. The initial velocity was set to 6 m/s to simulate the risk for a minimum momentum expulsion, thus evaluating the risk as ventilation driven rather than cough momentum driven. The mass flowrate was set to 5.2e-6 kg/s with 20 streams to produce 4000 droplets [4]. The droplets were assigned a density of 800kg/m^3. The cough period is set to 0.4 seconds according to Gupta et al.'s data [6]. Furthermore, the source diameter was set to 0.02 m with a cone shaped expulsion and the release angle to 22 degrees [7]. The injection temperature was set to 307.15K (34°C) as it is being expelled from the human body [68]. The particle diameters were modelled with a Rosin-Rammler diameter distribution, with a minimum of 1 μm and maximum of 100 μm based on Duguid's paper [45]. The particle diameter data were fitted with a Rosin-Rammler/Weibull fit resulting in a mean of 28.83 μm, and shape factor of 1.30.

The infector location was simulated at three different locations to investigate the effect of initial source location on respiratory aerosol spread. The locations of the infected occupants are indicated in Figure 5-8 below circled in red. The locations for the infected occupants were chosen based on variation in position with respect to the side walls, and the rows of seating. This allows each location to provide information for the impact of z (specific row), x (location in a row), and y (height of the row) on particle spread.

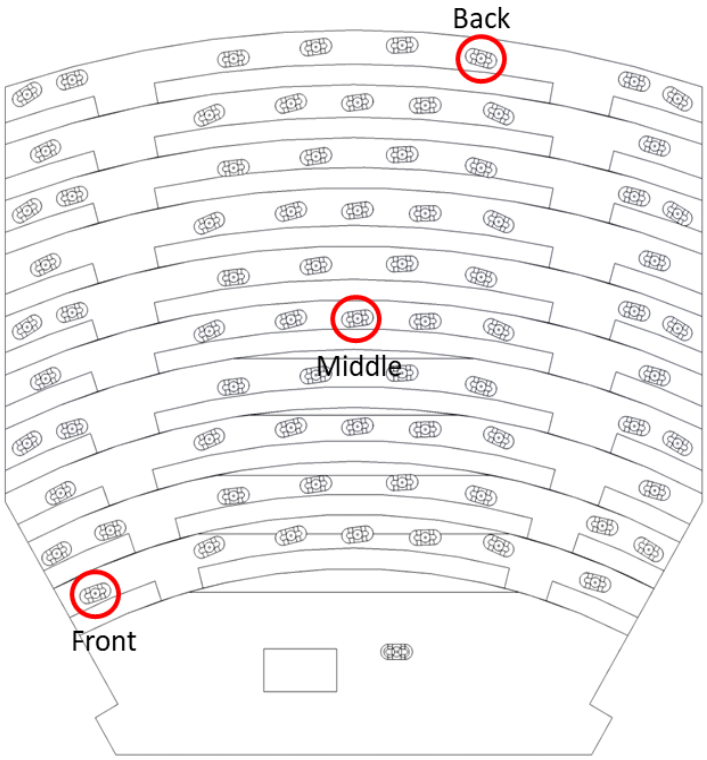

Figure 5-8: Top view of the lecture hall, with infection source locations circled in red for front, middle and back infection source cases.

3.3.1. 5.2.3. Risk Assessment

The lecture hall was divided into 22 zones with equal areas, to analyze how infection risk varies over different areas of the lecture hall (see Figure 5-9). These zones were further reduced to only include particles in the breathing zones of occupants, where most particles can be inhaled and cause infection. Each zone includes two rows (with elevation differences of 1 tier), hence the breathing zone was set from the top of the head of the upper row occupant till the desk of the lower row.

The risk of infection for the occupants were measured using a modified form of the Wells-Riley equation referenced from Buonanno et al. [143], see equation (9) below. The function for risk of infection (R, %) is dependent on time, and evaluated for each zone of the lecture hall.

$$R = \left(1 - \mathrm{e}^{-\mathrm{IR}\int_{T_i}^{T} n(t)dt}\right) (\%) \tag{9}$$

IR (m^3/s), represents the inhalation rate of the occupants, which is set to 1.36 x 10^{-4} m^3/s (0.49 m^3/h), based on the resting inhalation rate average for males and females [143]. In this study a unity infection term is assumed, so the quanta concentration in $n(t)$ (quanta/m^3), is equivalent to the particle concentration (number of particles/m^3) [26]. In other words, one particle will result in one quantum of infection. The quanta concentration is integrated over time, specifically by the residence time of each particle as it enters a zone at time T_i and leaves the zone at time T.

The risk value was then quantified by accounting for the total number of particles in the breathing zone every time step (*i.e.*, every 1 second for the current case), for a total of 300 seconds (5 minutes). The integral of quanta concentration from T_i and T was then reflected by the particle counter; a simple example, if the total number of particles in an occupant's breathing zone was 10 particles from 1-100 seconds, then 20 particles entered the breathing zone, thus the total particle count became 30 from 100-200 seconds, the counter would equal:

$$10(100) + 30(100) = 4000$$

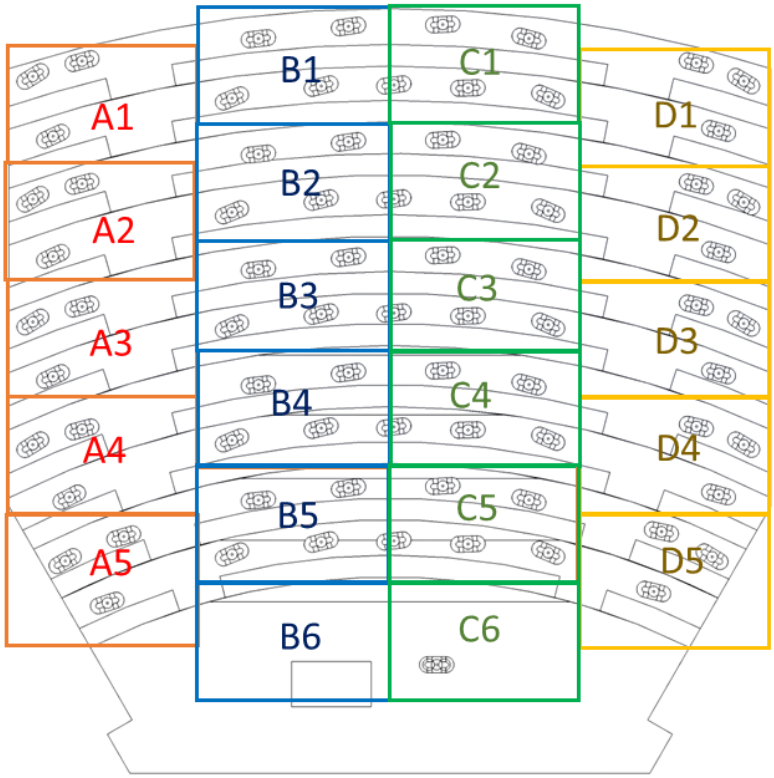

Figure 5-9: Top view of the lecture hall, divided into zones from A1 to D5.

5.3. Results and Discussion

5.3.1. Ventilation Performance Results

The following figures show the velocity vectors and temperature distribution contours as a result of the different ventilation configurations. The figures demonstrate the working principles of the mixing and displacement ventilation configurations.

The ventilation cases were designed based on different working principles. The existing mixing ventilation design is meant to function by mixing and dilution; the old and new incoming air is mixed uniformly to achieve the recommended ACH. This leads high velocity air to be inserted from the inlets located in the ceiling. The high velocity air comes down and vigorously mixes the heated/contaminated air with the new incoming air, leading to any aerosols or contaminants becoming diluted. This air movement is clearly depicted in Figure 5-10 below. The air is injected at 2.9 m/s, which slows down but still retains momentum as it reaches the occupants and the floor. After the jets reach different surfaces, vortices are created that propagate air mixing.

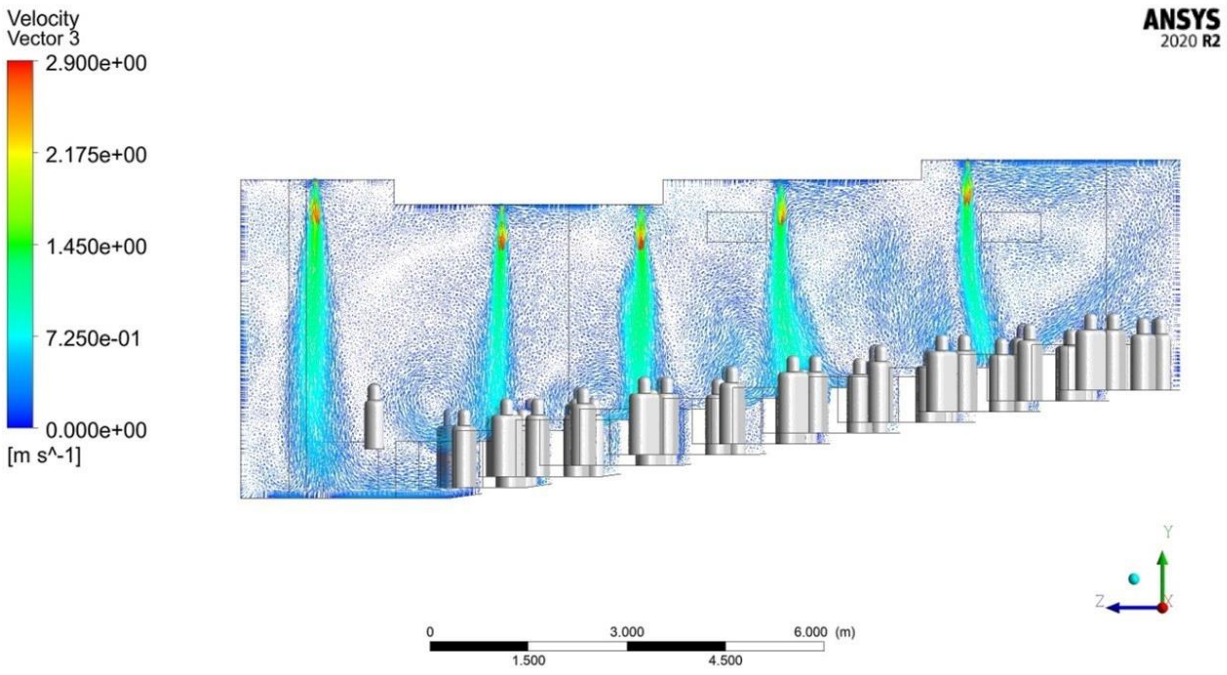

Figure 5-10:Velocity vectors for the mixing ventilation case, in side view

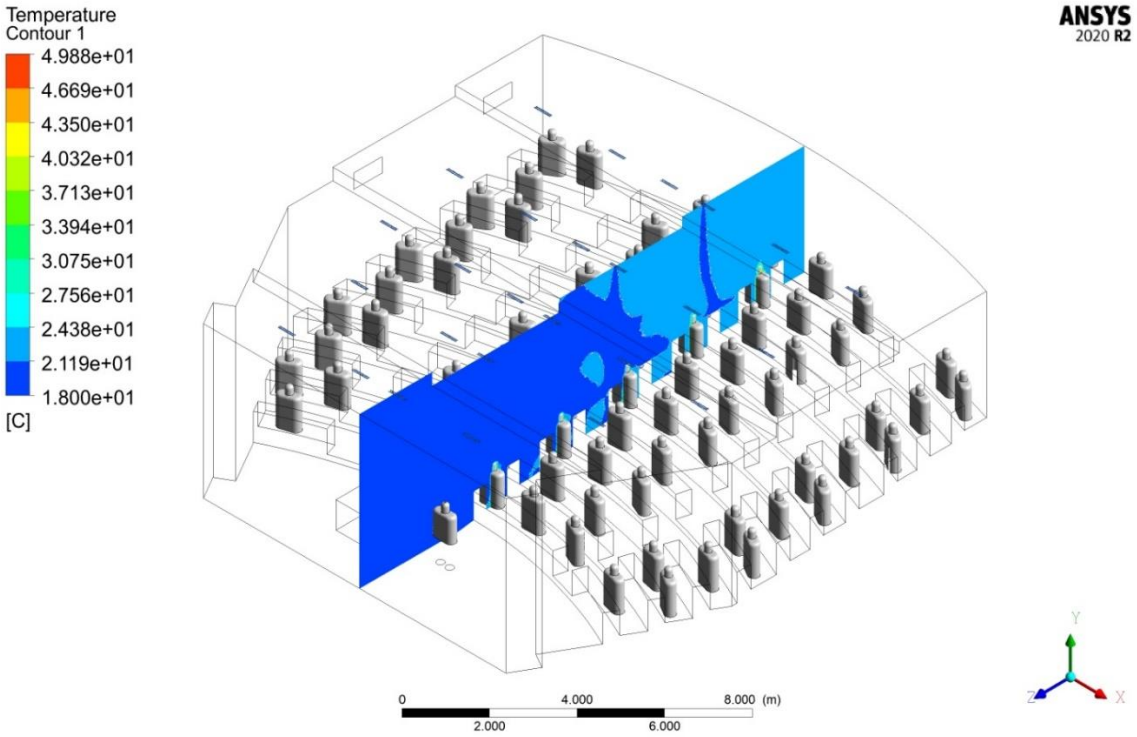

Figure 5-11: Temperature contour for the mixing ventilation case.

The results of the mixing phenomenon can further be seen in Figure 5-11, where the temperature contour through the middle of the lecture hall shows an almost homogeneous distribution of temperature. There is some difference in temperature between the front and back of the room: the front areas of the hall are around 18°C -21°C, while areas at the back are slightly warmer (21°C-24°C). This could happen because, even though the cooler incoming air is getting mixed and distributed within the space, some buoyancy driven effects are causing the cooler air to gather at the front while the warmer air drifts to the back. This effect was demonstrated well by Chen, Niu and Gao [160].

For DV configurations, the working principle is based on thermal stratification: the buoyant rising of warmer air displaced by the incoming cooler air results in air exchange in the space. The rising motion of air due to thermal stratification is driven by heat dissipation from occupants (and heat dissipating equipment), hence most air will rise near occupants. This upwards air motion is observed by the velocity vectors in Figure 5-12. There is a clear upwards motion and slight backwards motion of the velocity vectors coming from the occupants' heat fluxes.

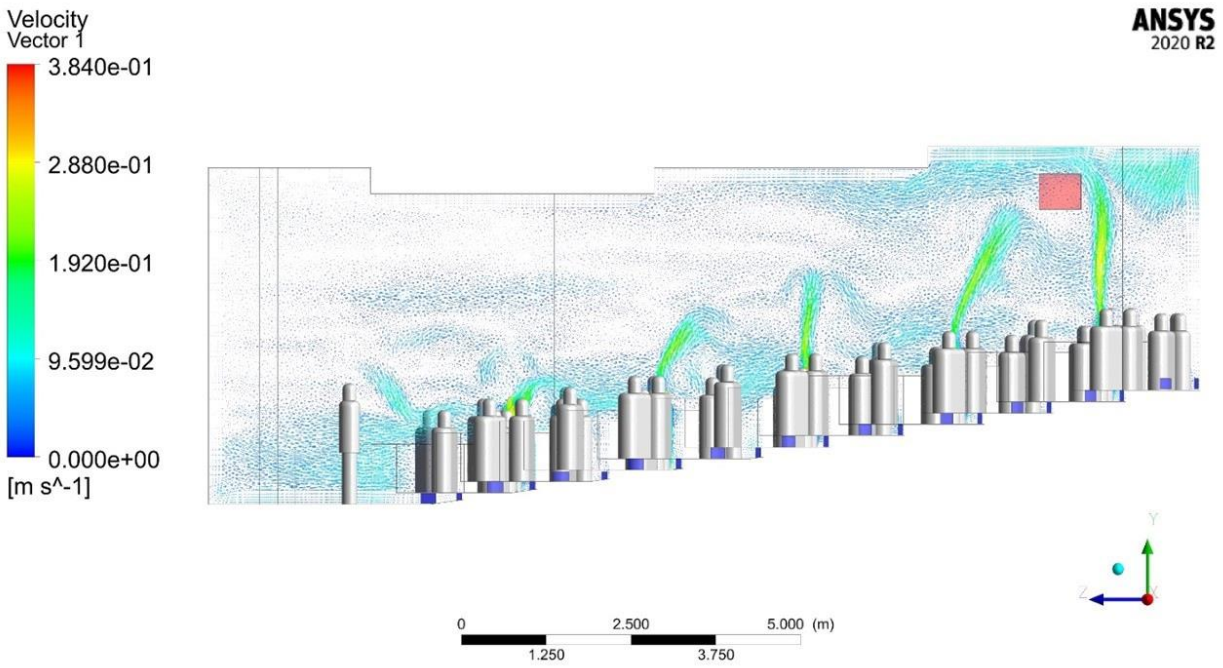

Figure 5-12: Velocity vectors for the displacement ventilation case in, side view.

The DV working principle based on thermal stratification essentially divides up a room into a vertical temperature gradient with the coolest air pooled at the bottom and the warmest at the top. This temperature gradient is clearly depicted in Figure 5-13, which has three layers of varying temperature. The occupants at the lower area of the lecture hall are in a colder zone of 17°C -20°C, the upper-level occupants are at an air temperature of 20°C -23°C, and the layer above the occupants is 23°C -26°C. The occupants are kept at suitable temperatures for thermal comfort, but there is a clear temperature difference between upper and lower-level occupants. This effect was explained in a simulation study paper by Niu, Chen and Gao [160], who discuss that this might not be ideal for occupants as the lower level occupants will receive more clean air compared to upper level occupants; when the cool air enters through the floor risers it can flow downwards, leaving little to no ventilation for the upper level occupants. The dispersion of particles in the lecture hall can further illustrate how the air travels in each ventilation configuration.

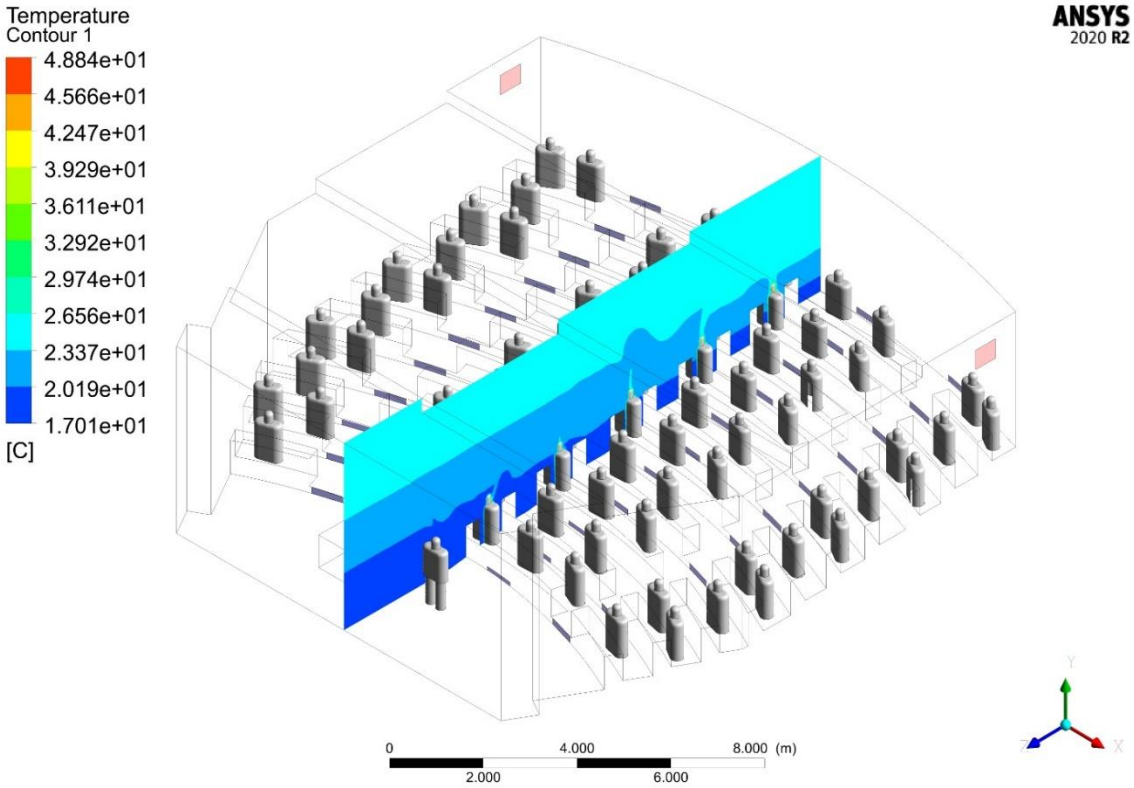

Figure 5-13: Temperature contour for the displacement ventilation case.

5.3.2. Particle Dispersion Results

The following sections present the results of particle dispersion and risk comparison for DV and MV configurations for infection sources at the back, middle, and front of the lecture hall.

5.3.2.1. Front Injection Case

The first set of simulations for both DV and MV configurations begins with a coughing infectious source at the front of the room. See Figure 5-14 where the cough begins to expel at 2 seconds of simulation time. The cough jet immediately begins to spread upwards and disperse for the MV case, while the dispersions is slower for the DV case. In both cases the heavier droplets (droplets in the size range of 60-100 μm) start falling downwards.

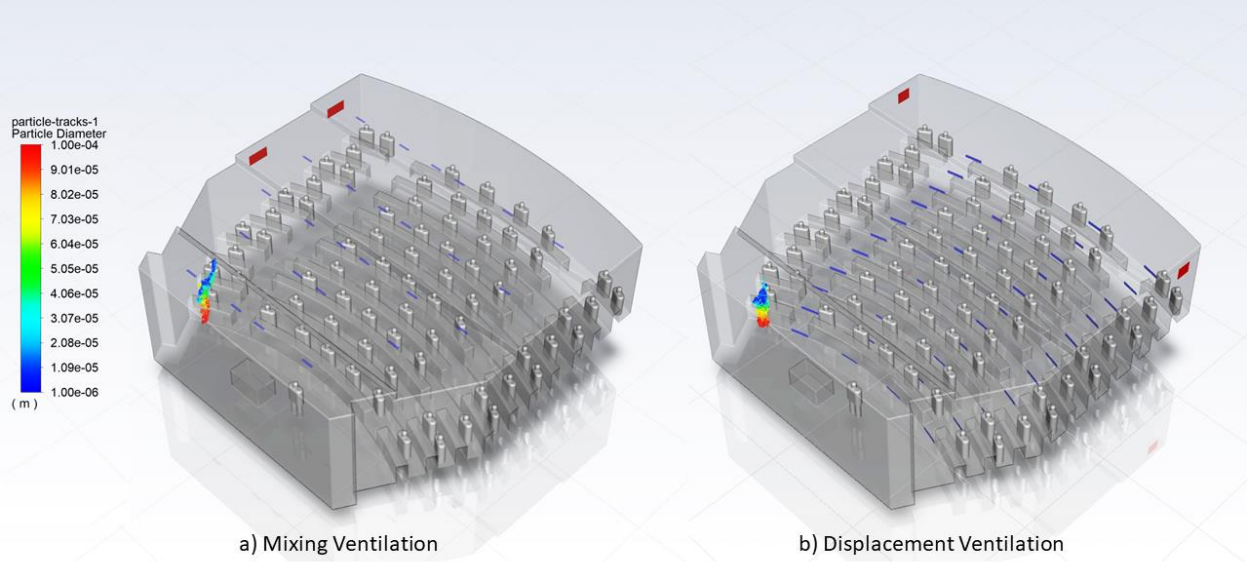

Figure 5-14: 2 seconds of simulation time for the infectious source at the front of the room for a) mixing ventilation case, and b) displacement ventilation case

After a minute (Figure *5-15*), the particle spread patterns have become considerably different. The MV case's particles have begun mixing with the air and recirculating over the rows in the front corner, as well as reaching upwards near the ceiling. This introduces risk to the 5 rows of occupants located behind the infectious occupant. It can also be noticed that some of the particles are approaching the air outlet, in which case, any risk introduced may not remain stagnated for too long. The particles in the DV case move more gradually as they drift backwards and upwards.

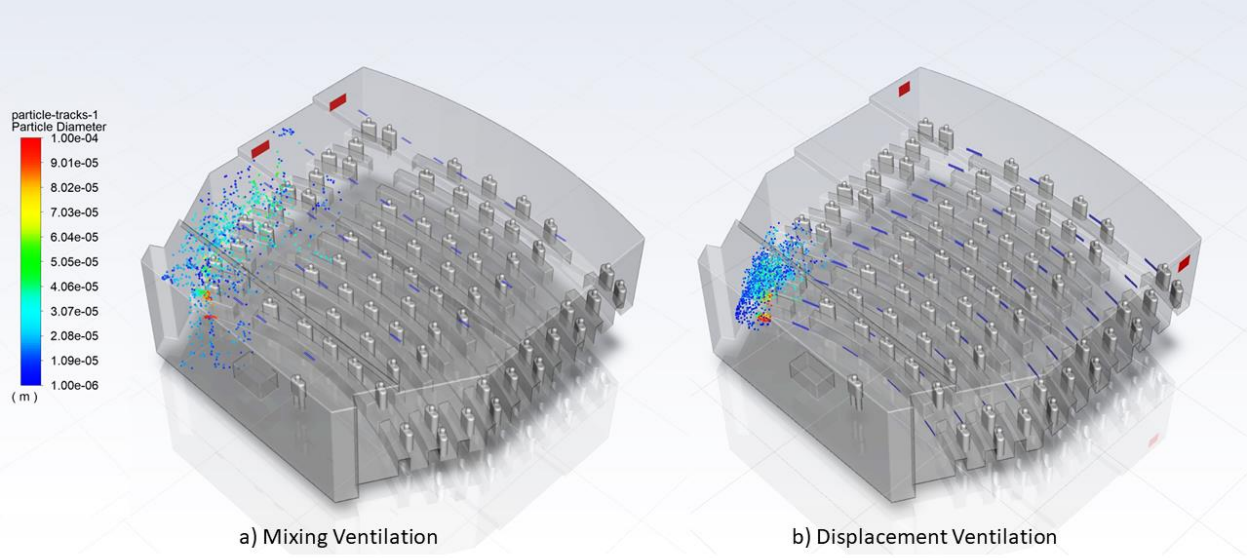

Figure 5-15: 1 minute of simulation time for the infectious source at the front of the room for a) mixing ventilation case, and b) displacement ventilation case

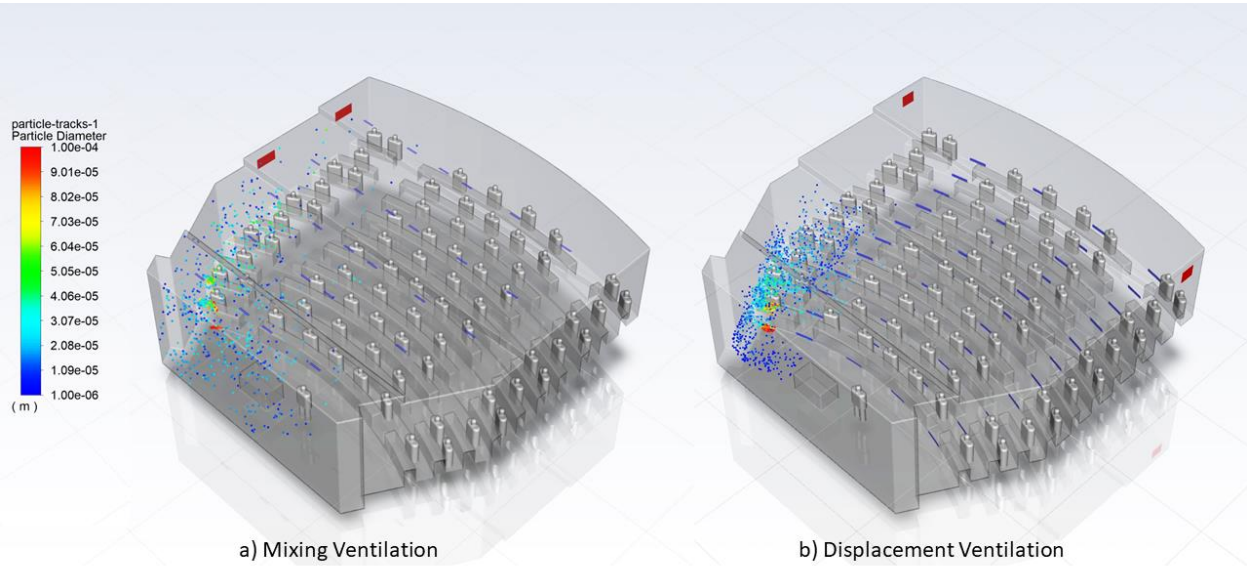

Figure 5-16: 2 minutes of simulation time for the infectious source at the front of the room for a) mixing ventilation case, and b) displacement ventilation case

By 3 minutes of simulation time (Figure 5-17), most of the particles in the MV case have either exited, or diluted and spread in small portions over the front and centre of the hall. Some particles have also reached the standing occupant and seem to be circulating in their breathing zone. On the other hand, the DV case looks very prone to transmission, as all the particles have

now slowly moved into the breathing zones of the rows behind the infectious occupant. Some of the particles are rising upwards but most are gradually moving backwards towards the air outlet. The particles also seem to be extending to the front of the room for the DV case, but have not yet reached the standing occupant.

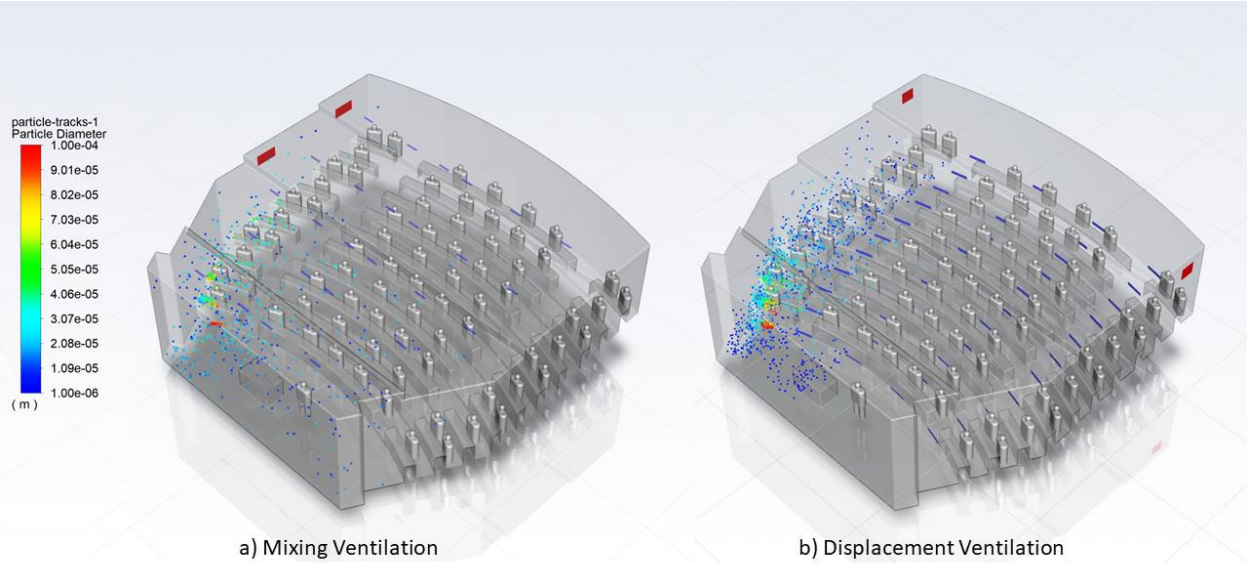

Figure 5-17: 3 minutes of simulation time for the infectious source at the front of the room for a) mixing ventilation case, and b) displacement ventilation case

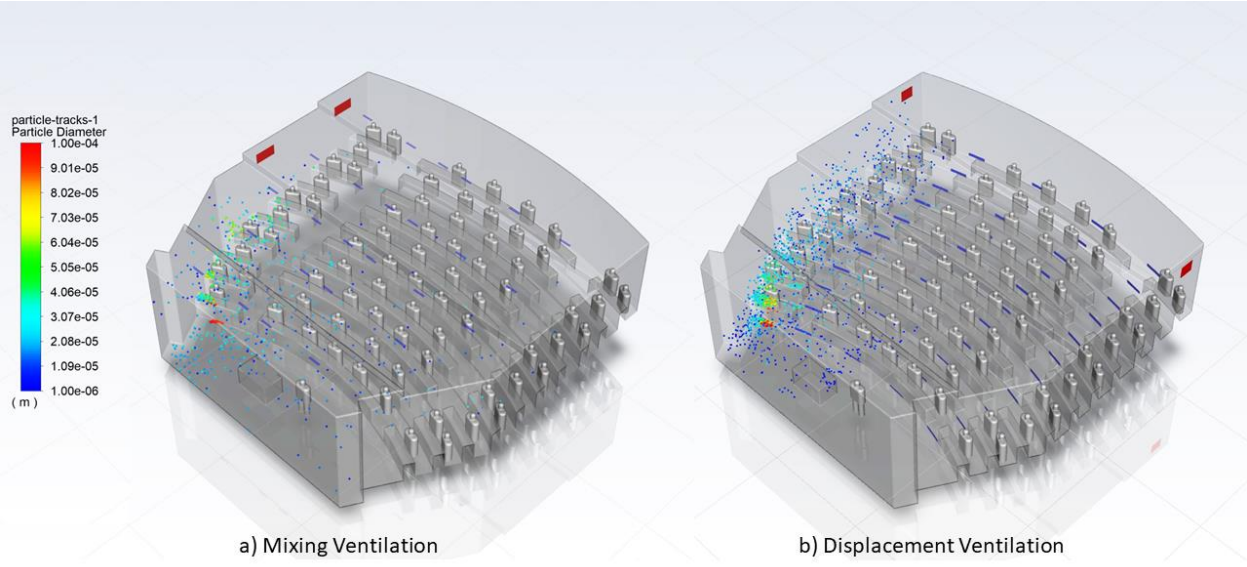

Figure 5-18: 4 minutes of simulation time for the infectious source at the front of the room for a) mixing ventilation case, and b) displacement ventilation case

At 5 minutes of simulation time (Figure 5-19), most of the suspended particles in the MV case have either escaped or deposited on surfaces. A very small proportion of particles are seen to reach the middle and other side of the room. As for the DV case, a small proportion of the particles have escaped, while most remain suspended in the breathing zones of the rows behind the infection source. A small amount of the particles have also flown up to the front-centre of the hall.

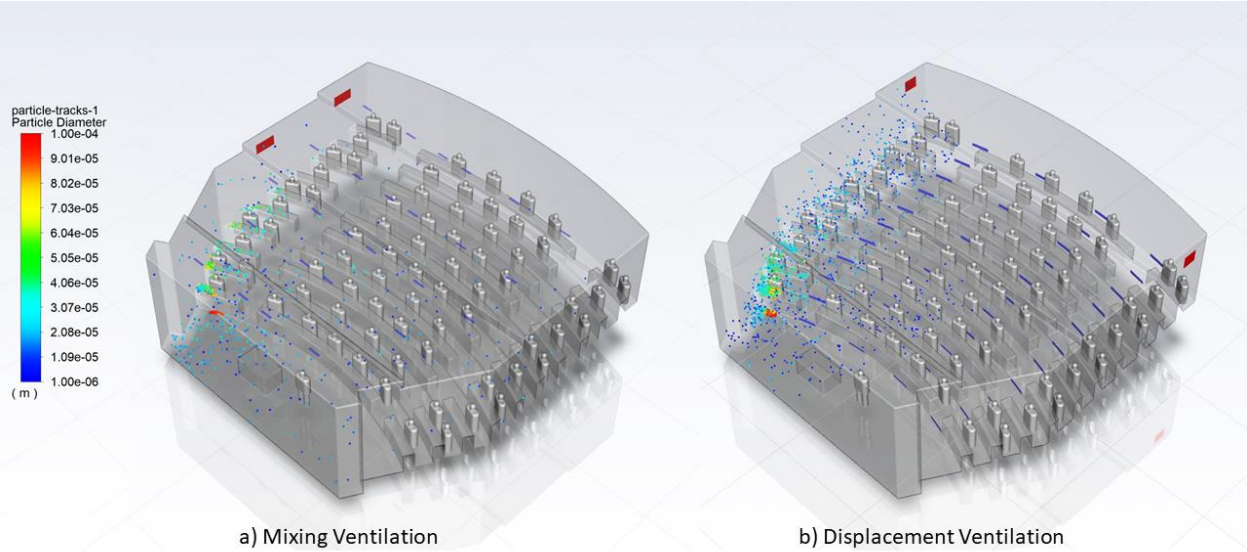

Figure 5-19: 5 minutes of simulation time for the infectious source at the front of the room for a) mixing ventilation case, and b) displacement ventilation case

The clear differences between the two configurations particle dispersion patterns come down to two factors: their working principles and the location of the air outlet. The working principle of MV configurations is based on high velocity mixing of fresh and contaminated air, which allows the particles to quickly mix, dilute and also spread to several areas. This has both risks and benefits from an airborne transmission perspective. Even though the particles are spread to areas very far from the initial source location, a lot of the particles are mixed and diluted with fresh air, which will inevitably reduce the infectious dose. In addition, the vigorous mixing lets the particles reach the air outlet which can then pull these particles out of the room. It should also be noted that the outlet was near the source occupant which allowed for a quick exit of the particles.

In terms of DV working principles, the ventilation is based on thermal stratification, i.e., cold air comes in from the stair riser diffusers very slowly and then the air moves up as it heats from the occupants' heat dissipation, and this upwards movement should essentially displace the old air with the new. This phenomenon seems to be happening, but the terraced style of the lecture

hall and the placement of the air outlet at the back of the room means the particles are slowly moving upwards and backwards exposing several occupants on the way. The aerosols are landing right in the breathing zones of the occupants behind the source occupant. If the room had a leveled floor design, perhaps all the particles would stay above the occupants' breathing zones. The DV results demonstrate that if this type of ventilation is used, susceptible occupants should remain at the same level or below the source occupant, as the risk of "lock-up phenomenon"—where infectious aerosols stagnate in a susceptible occupant's breathing zone [114]—is high and can easily cause secondary infections if the susceptible occupants' breathing zones in the lock-up zone.

5.3.2.2. Middle Injection Case

The following injection of particles was produced from an occupant located in the middle of the lecture hall, see Figure 5-20.

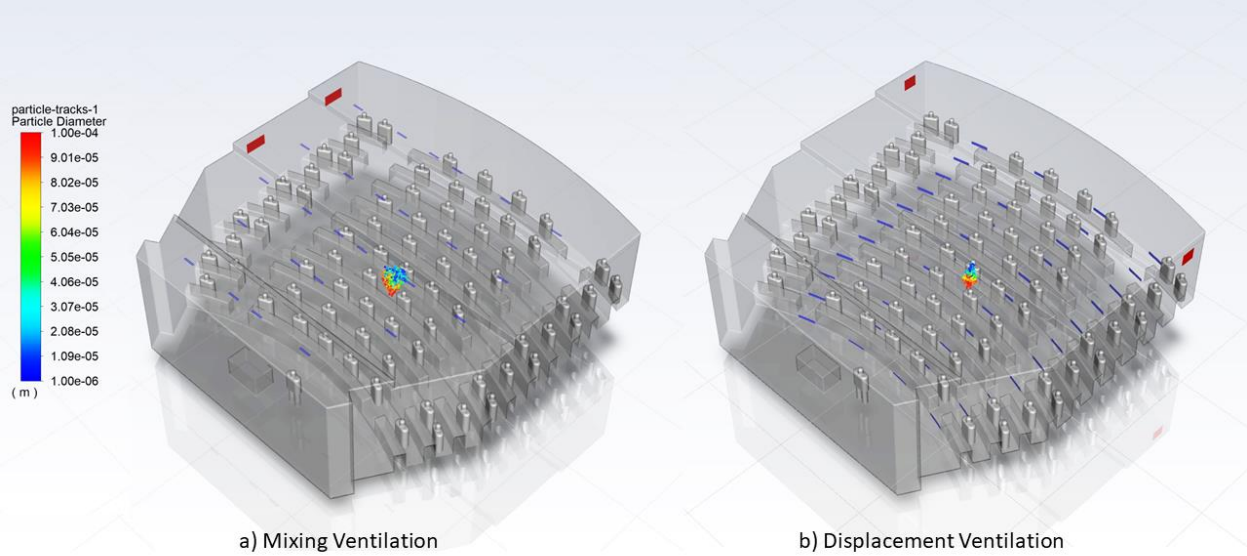

Figure 5-20: 2 seconds of simulation time for the infectious source in the middle of the lecture hall for a) mixing ventilation case, and b) displacement ventilation case

Within the first minute of particle dispersion, the spread area is significantly different between the MV and DV case, as seen in Figure 5-21. In the MV case, the air mixing spread out the aerosols over the entire middle and some back areas of the lecture hall. In contrast, the DV case shows a conservative spread that is gradually moving backwards.

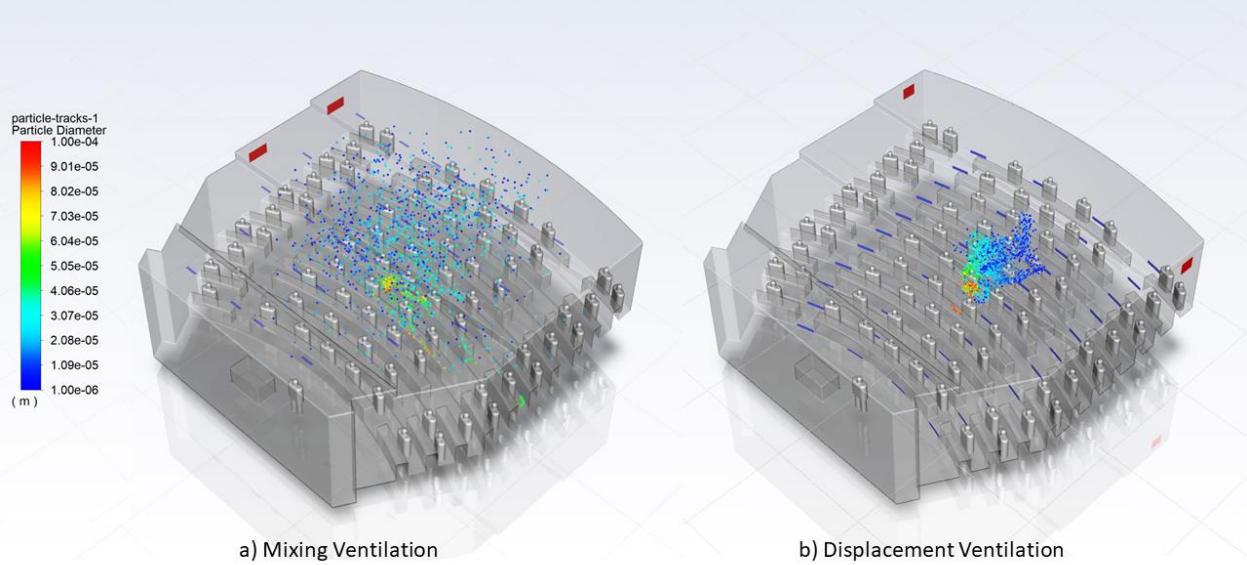

Figure 5-21: 1 minute of simulation time for the infectious source in the middle of the lecture hall for a) mixing ventilation case, and b) displacement ventilation case

By 2 minutes (Figure 5-21), the particles in the MV configuration have reached around 70% of the occupants breathing zones, while they try to exit out of the outlets on the left wall. The majority of particles are moving towards the outlet, causing the occupants on the left to be more exposed to any risk of infection. The occupants near the complete right wall are mostly untouched except for a few straggler particles. Looking at the DV case, all the occupants seated behind the source occupant are getting enveloped by the particle stream, risking extremely high exposure. However, the rest of the room remains completely untouched.

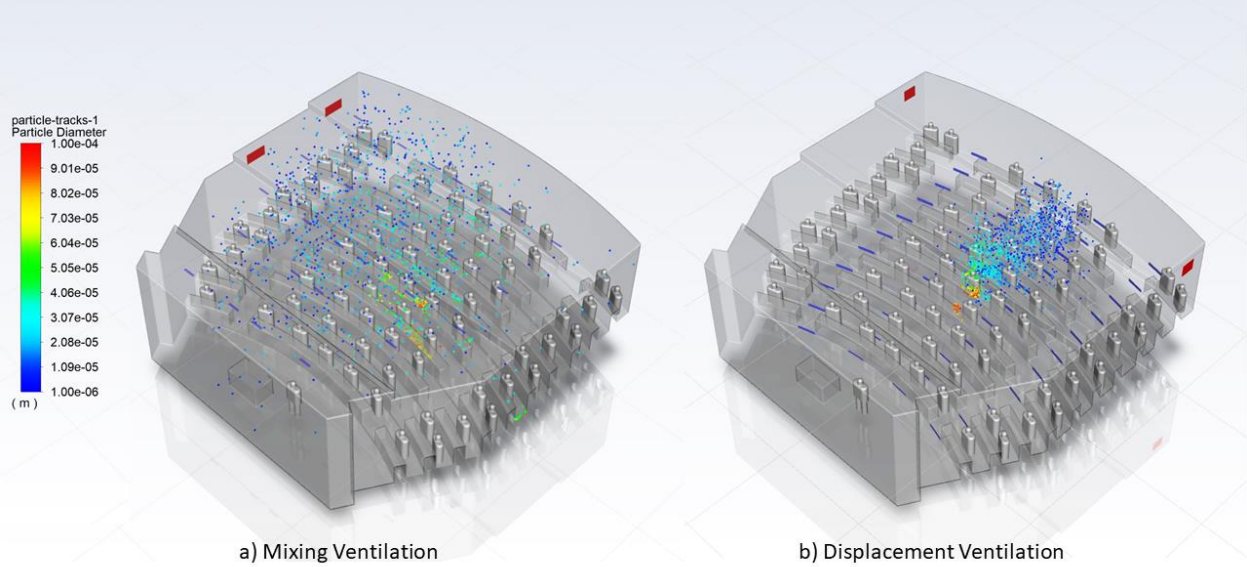

Figure 5-22: 2 minutes of simulation time for the infectious source in the middle of the lecture hall for a) mixing ventilation case, and b) displacement ventilation case

By 3 minutes (Figure 5-23), in the MV case the larger particles have settled on surfaces, while the smaller particles are on their way out. For the DV case, the smaller particle are now slowly making their way to the outlets on the 2 corners of each wall, while the larger particles have mostly settled on the desks of the two rows of occupants right behind the source occupant.

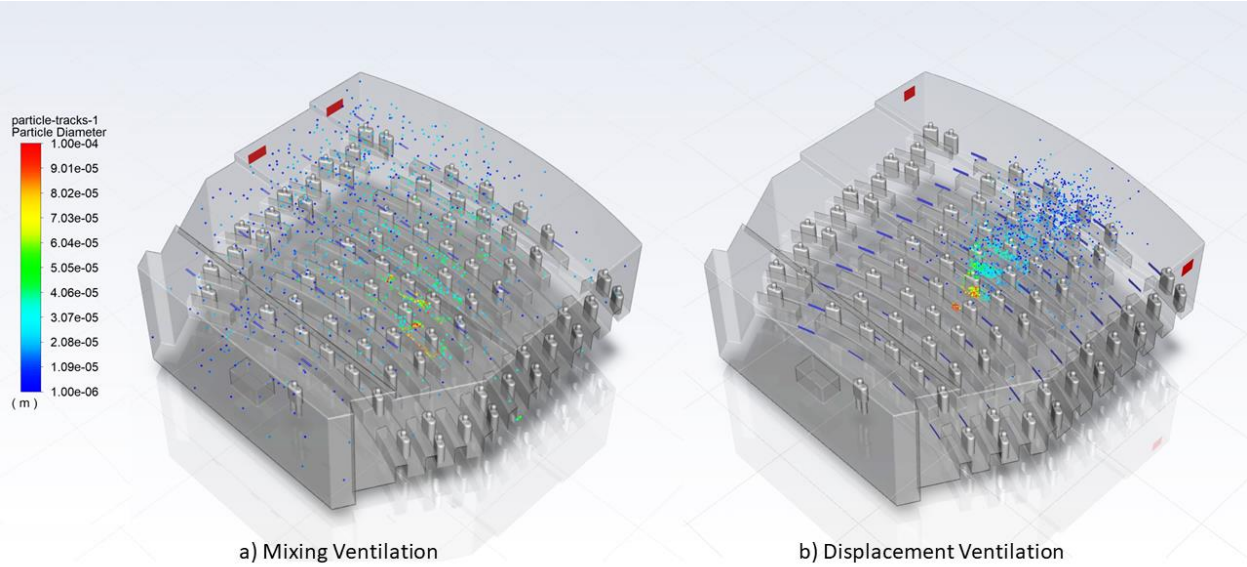

Figure 5-23: 3 minutes of simulation time for the infectious source in the middle of the lecture hall for a) mixing ventilation case, and b) displacement ventilation case

At 4 minutes (Figure 5-24), the particles are continuing their dispersion process for both cases.

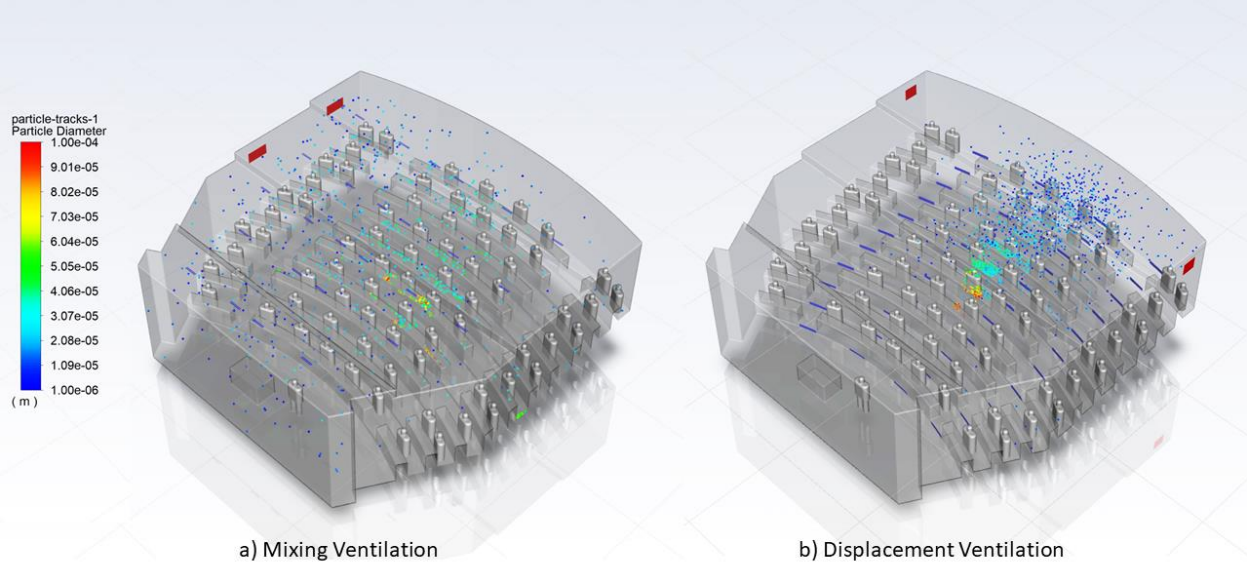

Figure 5-24: 4 minutes of simulation time for the infectious source in the middle of the lecture hall for a) mixing ventilation case, and b) displacement ventilation case

At the 5 minute mark (Figure 5-25), most of the smaller particles have cleared out in the MV case, except for a small amount that is diluted out and recirculating in the space. For the DV case, the particles have now reached the outlets and are beginning to exit, with the back rows being exposed in the process.

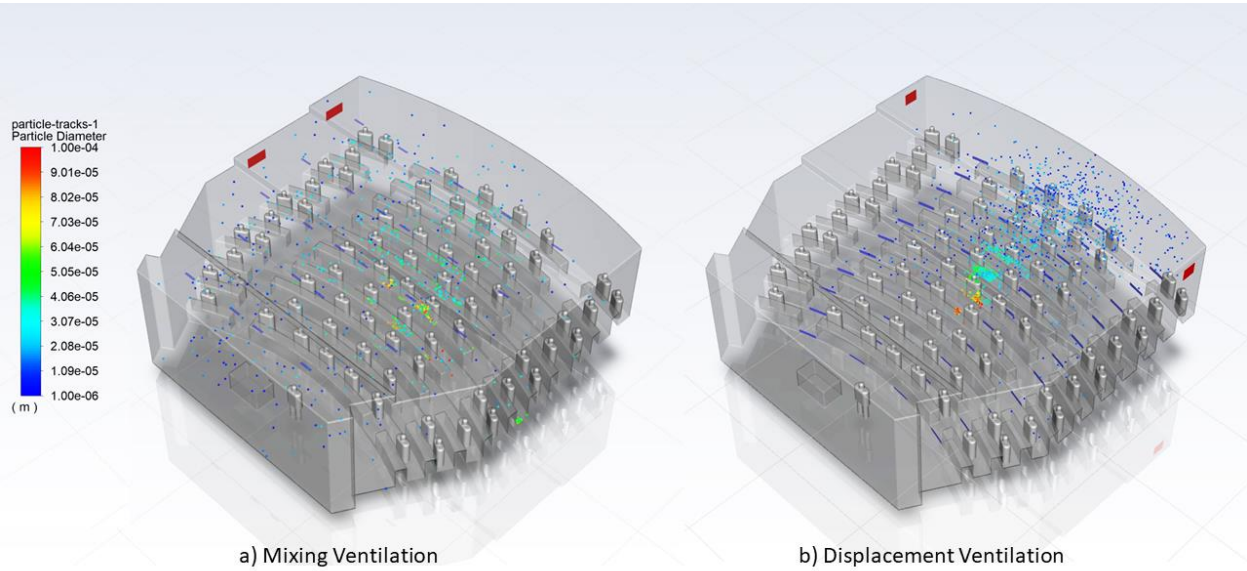

Figure 5-25: 5 minutes of simulation time for the infectious source in the middle of the lecture hall for a) mixing ventilation case, and b) displacement ventilation case

Particle dispersion results have varied for an infection source in the middle of the room, in comparison to that at the front of the room. The exposure of particles to occupants has been much higher, and more spread out for the MV case, but the removal rate of particles has been relatively similar. The particle dynamics for the DV case has been similar in the middle source injection site compared to the front: where the occupants behind the source occupant have all incurred doses of slow moving infectious particles, as the particles reach the outlets. Thus, most occupants in the MV case have received low doses of infectious aerosols for a short period of time, while in the DV case a proportion of the occupants have had a relatively longer exposure to a high concentration of infectious aerosols.

5.3.2.3. Back Injection Case

The following injection of particles was produced from an occupant at the back of the lecture hall, see Figure 5-26.

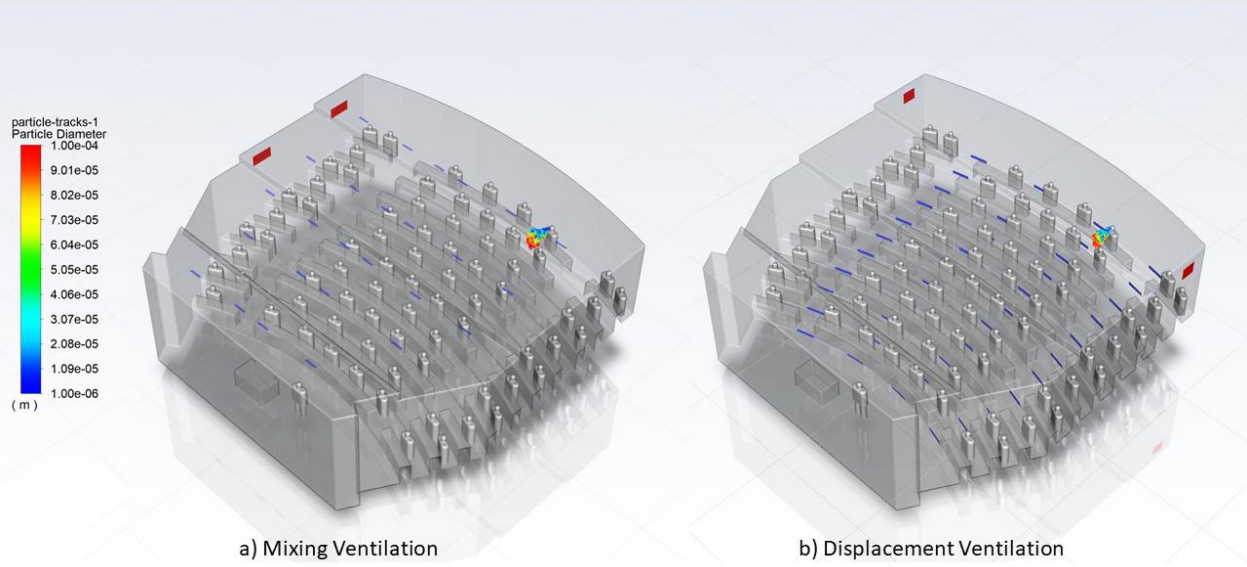

Figure 5-26: 2 seconds of simulation time for the infectious source at the back of the room for a) mixing ventilation case, and b) displacement ventilation case

For the MV case the source infection at the back of the lecture hall, within 1 minute (Figure 5-27) the particles are violently dispersed in the entire back section of the lecture hall. The particles are seen to reach 4 rows down as well as disperse sideways towards the return grilles. The particles in the displacement ventilation case are more conservatively spread, the particles are moving

upwards and towards the closest return grille on the right (from readers perspective). This is because the heat plumes and stratification induced by the displacement ventilation design propagate the aerosols to rise above the breathing zone.

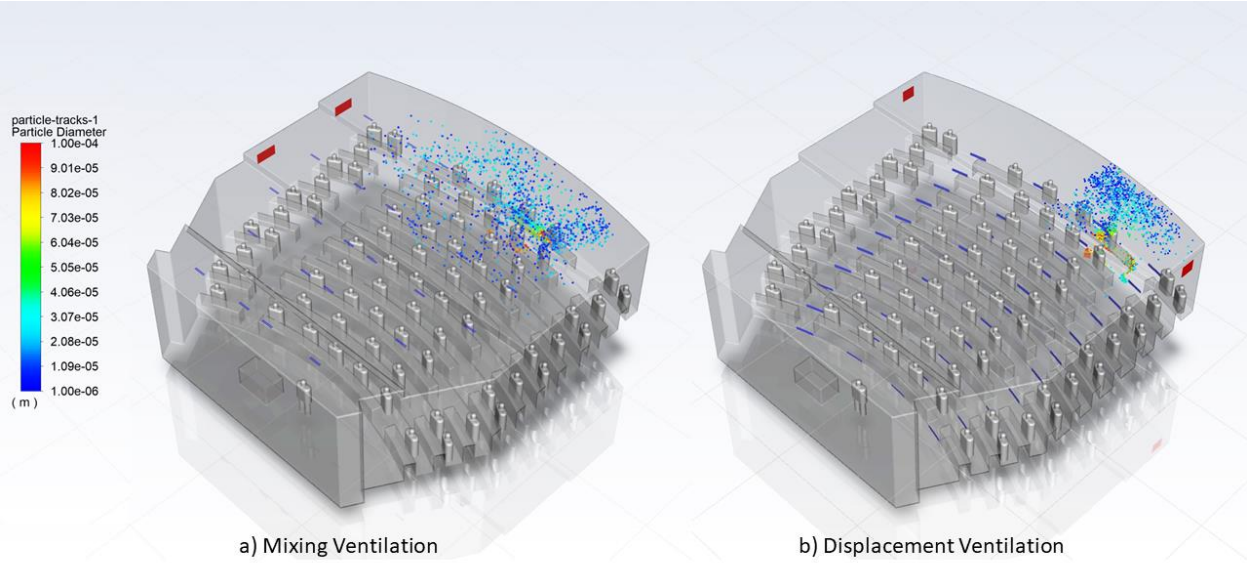

Figure 5-27: 1 minute of simulation time for the infectious source at the back of the room for a) mixing ventilation case, and b) displacement ventilation case

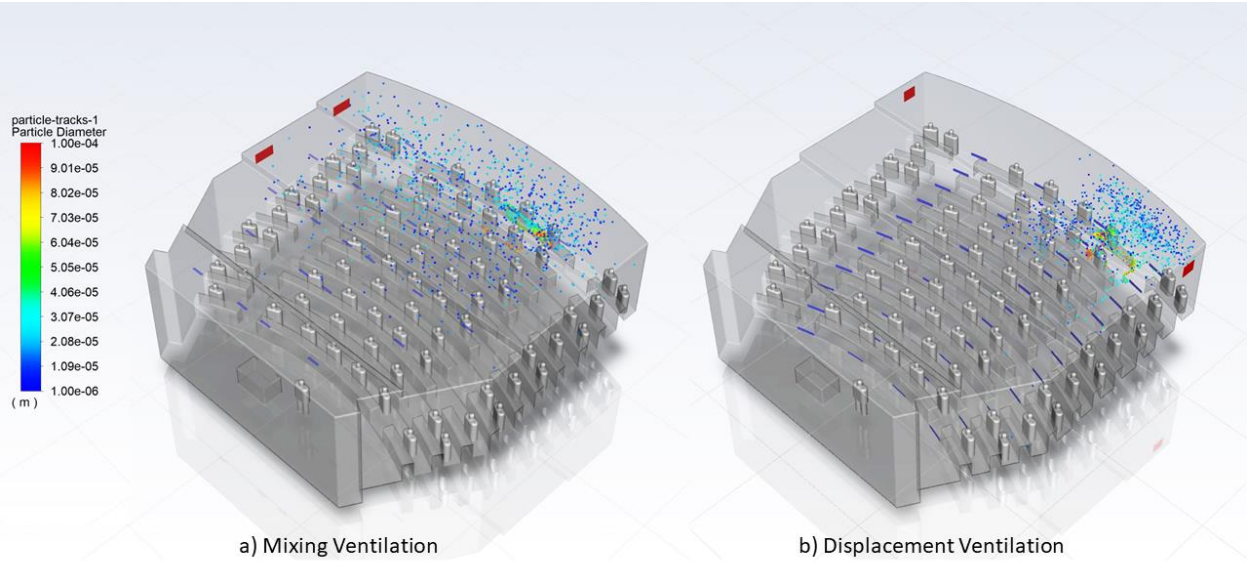

Figure 5-28: 2 minutes of simulation time for the infectious source at the back of the room for a) mixing ventilation case, and b) displacement ventilation case

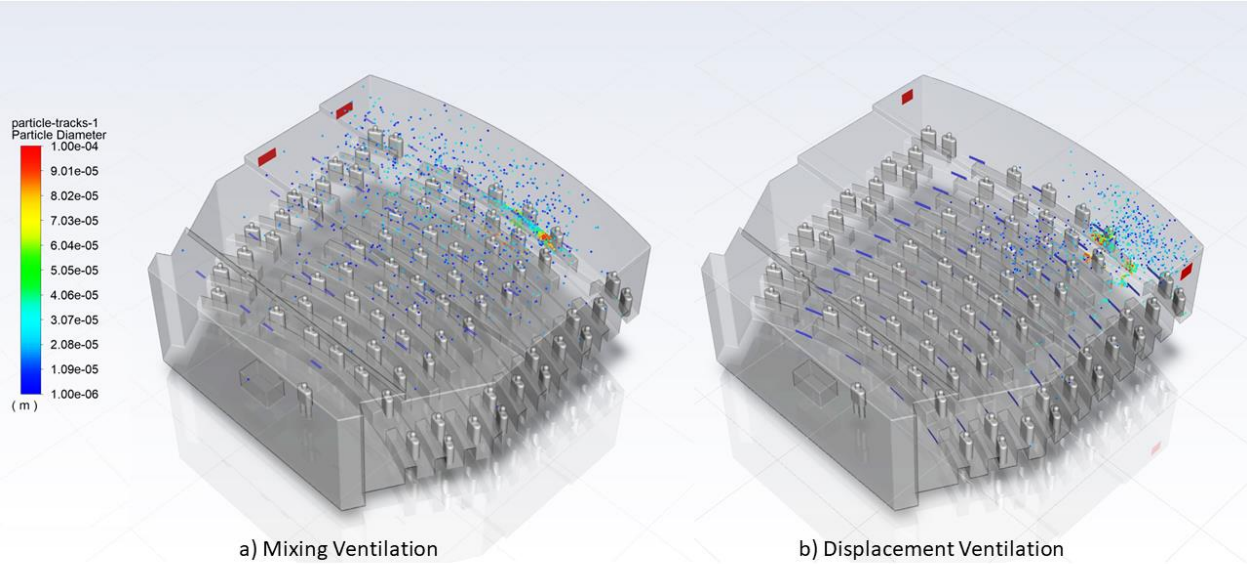

Figure 5-29: 3 minutes of simulation time for the infectious source at the back of the room for a) mixing ventilation case, and b) displacement ventilation case

As time progresses, the particles in the MV configuration start dispersing further to the front of the room in sparse amounts. While, for the DV case most particles do not escape the route towards the right outlet, but rather stagnate above the source occupant until they are pulled out by the outlet. Some particles in the DV configuration have found their way down the rows. In the MV case, by 4 minutes of time, a few particles had already reached the standing occupant at the front of the room.

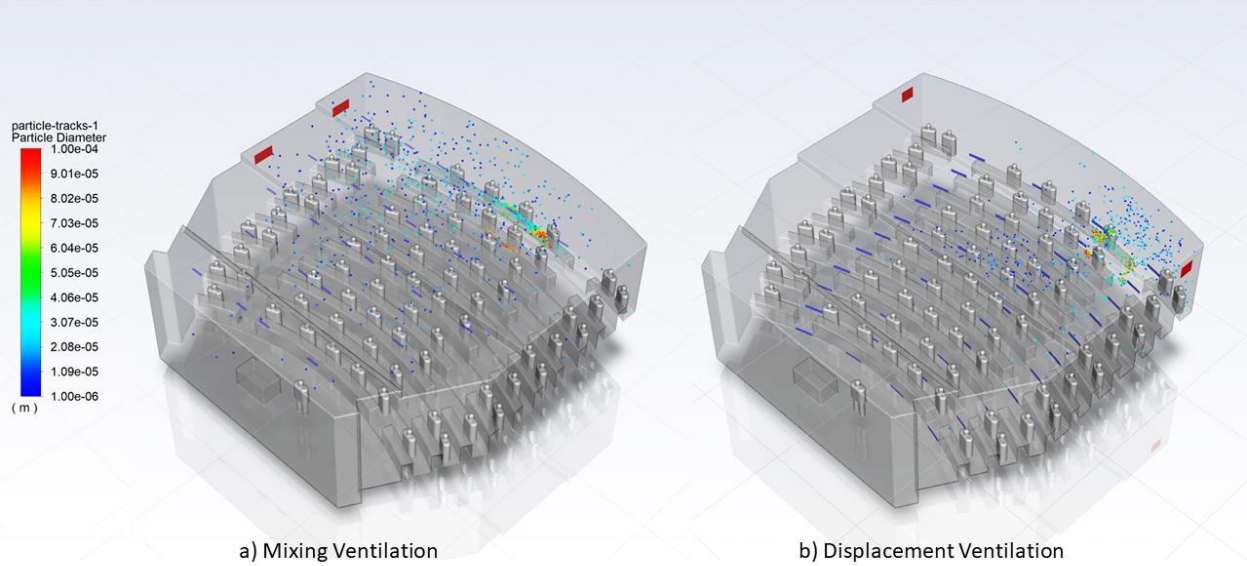

Figure 5-30: 4 minutes of simulation time for the infectious source at the back of the room for a) mixing ventilation case, and b) displacement ventilation case

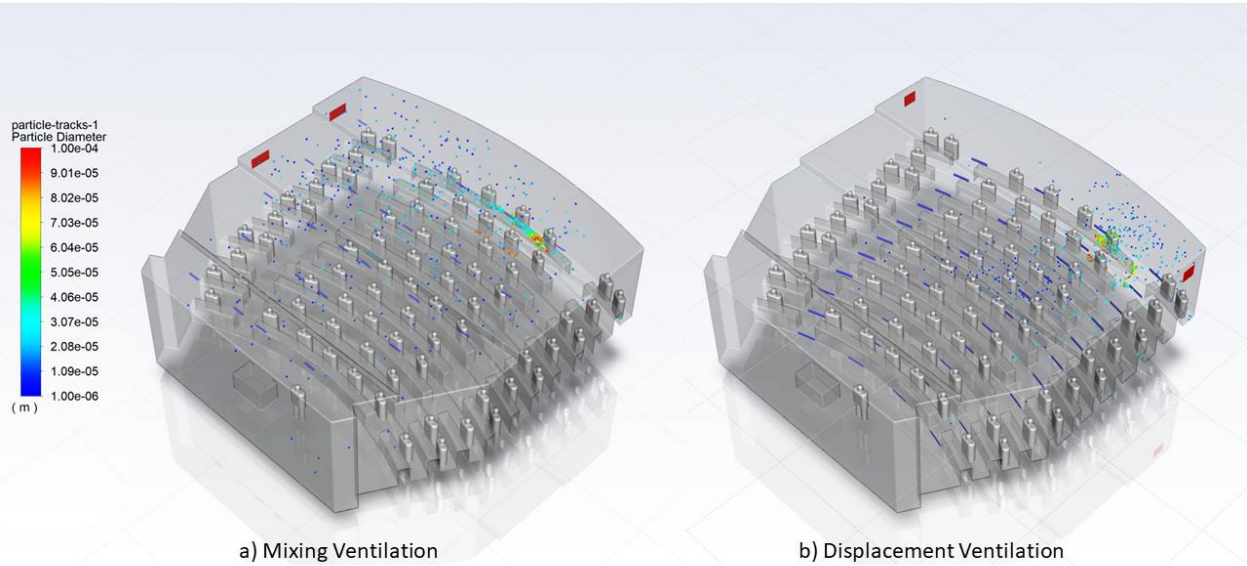

Figure 5-31: 5 minutes of simulation time for the infectious source at the back of the room for a) mixing ventilation case, and b) displacement ventilation case

As the simulation time reaches 5 minutes (Figure 5-31), the particles in both ventilation settings have partially cleared out and remain in sparse concentrations. The main difference in dispersion seen from the back injection set of simulations is that the particles reach the front of the lecture hall for the MV case. However, for the DV case a small concentration of particles moved

four rows down, while most particles concentrated over the source occupant, as they exited. In this case, the DV configuration performed most optimally because, firstly, the infectious source was located at the top of the lecture hall, so any lock-up of particles happened above and away from anyone's breathing zone. Secondly, the outlet was close to the infectious occupant, thus the particles were able to quickly exhaust out, performing favorably with the working principles of DV. The MV configuration however, was not ideal, because the exit was farther away, resulting in the particles mixing and spreading to a large area of the lecture hall before exiting. After 5 minutes many of the particles were still not able to escape, and rather recirculated and lingered at the back areas of the lecture hall.

The particle dispersion results above were effective to visualize the particle spread. However, it was difficult to observe the risk of infection posed to occupants within each scenario. A quantified risk of infection map will provide more insight as to which cases involved higher infection risk.

5.3.3. Risk Maps

The following figures include risk maps that are representative of the spatial distribution of infection risk in the lecture hall. The risk maps account for exposure to particles in the breathing zones of occupants, the duration of exposure and the quantity of exposure, thus providing an accurate representation of infection risk within the six cases studied.

The risk of infection is separated into 22 zones of equal area (see Figure 5-9). The zones are evaluated at heights based on the breathing zones of each level of occupants in the lecture hall. The risk value was determined with equation (9), to represent the risk of infection occupants in each zone are exposed to. The risk maps are colored by the level of risk: green-little to no risk, yellow-low risk, orange-medium risk, red-high risk.

Looking at the risk map for the case of an infection source at the front of the room (Figure 5-32), we see infection begins in zone A5, which has a risk value of 100% for both ventilation configurations. In the MV case the risk gets lower looking at the zones above A5 (i.e. A4, A3, A2 and A1), while for the DV case the risk lowers too, but the reduction in risk is not as significant as in the MV case. For instance, for MV in zones A3 and A4 the risks are 31.48% and 1.70% respectively, while for DV they are 73.68% and 45.34% respectively. They risk zones vary by a risk level for the two different ventilation cases. Another aspect that changes the outlook of risk

distribution is the spread of risk through the entire map. For MV all the zones except for C5, have a risk value above 0, which means that the infectious aerosols spread extensively through the lecture hall, even if a very small number of particles were distributed to the far-field zones. In contrast, for DV 9 zones in the upper right corner were untouched by particles in the breathing zone for the 5 mins of simulated time. The risk maps are reflective of the particle dispersion patterns seen in Figure 5-15-Figure 5-19: where the particles were diluted and widespread for MV—represented by the widespread distribution of low risk zones, and the particles were concentrated and moving upwards to the outlet for DV—represented by the high risk zones in row A.

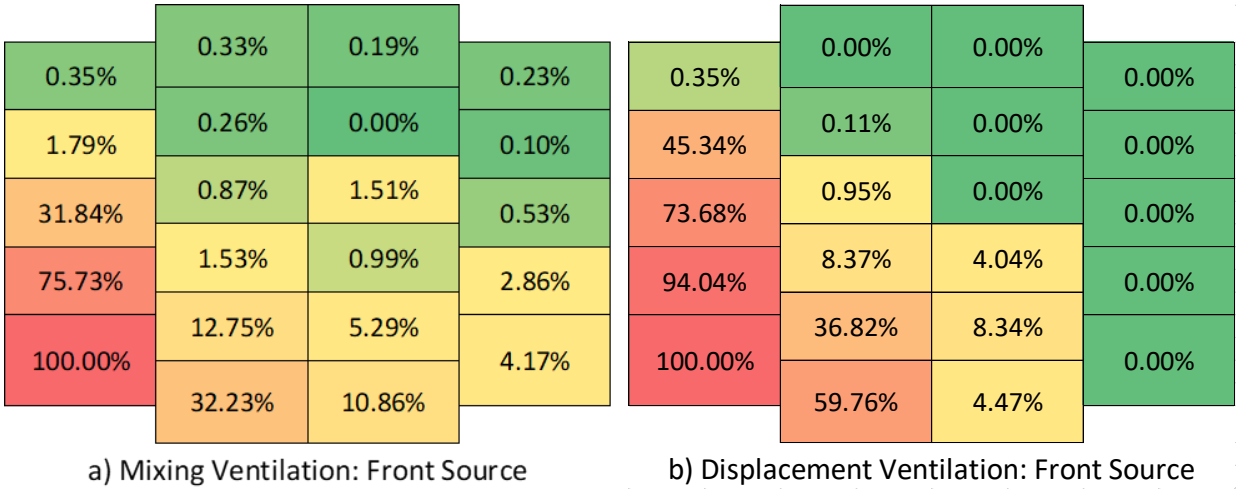

Figure 5-32: Risk map for an infection source located at the front of the lecture hall for a) mixing ventilation case, and b) displacement ventilation case

Looking at the risk map for the case of an infection source in the middle of the room (Figure 5-33), we see infection begins at the halfway point of zone B4 and C4, which have a risk value of 96% and 99% for MV, and 100% for both those zones in DV. The risk of infection is again widespread for MV similar to the case of infection source at the front (Figure 5-32 a), however in this case there are 4 more medium risk zones and 2 more high risk zones. For the DV case, there is one more high risk zone in the middle source case (4 zones) compared to the front source case, and the same number of medium risk zones (3 zones). There is also a similar portion of zones with around 0% risk in DV, for both front and middle case. Overall, in the middle infection source case, the risk was spread out and comparatively high for MV, while for DV the risk was high in the zones behind the source occupant, but the risk was conservatively spread. This risk distribution was reflected in the particle dispersion results as seen in Figure 5-21 to Figure 5-25, where the

particles spread out in high concentrations for MV, while it was compactly drifting backwards for DV.

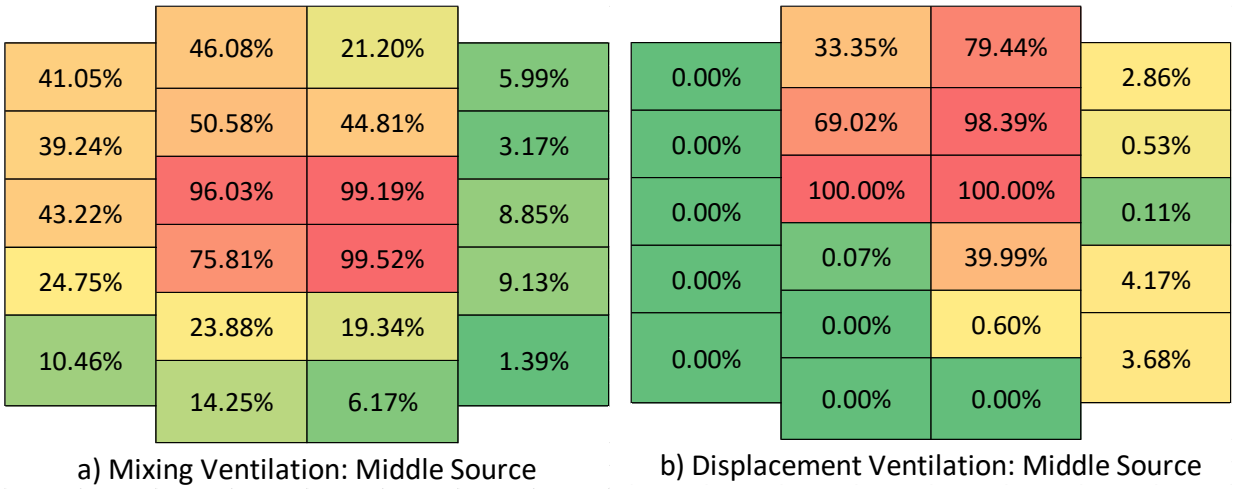

Figure 5-33: Risk map for an infection source in the middle of the lecture hall for a) mixing ventilation case, and b) displacement ventilation case

Looking at the risk map for the case of an infection source at the front of the room (Figure 5-34), we see infection begins in zone C1, which has a risk value of 100% for both ventilation configurations. In the MV case the risk is then spread out from the back towards the middle and left. This leads to 3 high risk zones, 4 medium risk zones and 6 low risk zones in the MV configuration. The DV configuration however has only 1 high risk zone, 2 medium risk zones and 6 low risk zones all of which have risk values significantly lower than the MV case. This drastic difference in risk distribution for the two cases can be explained by their working principles. In the MV case, right as the aerosols were expelled, they were mixed and dispersed aggressively, causing them to spread around the back areas of the lecture hall. On the other hand, the aerosols in the DV case were slowly lifted upwards due to thermal stratification, leading the aerosols to get "locked-up" at the height of the air outlet; thus, the particles were able to quickly exit without dispersing in the lecture hall.

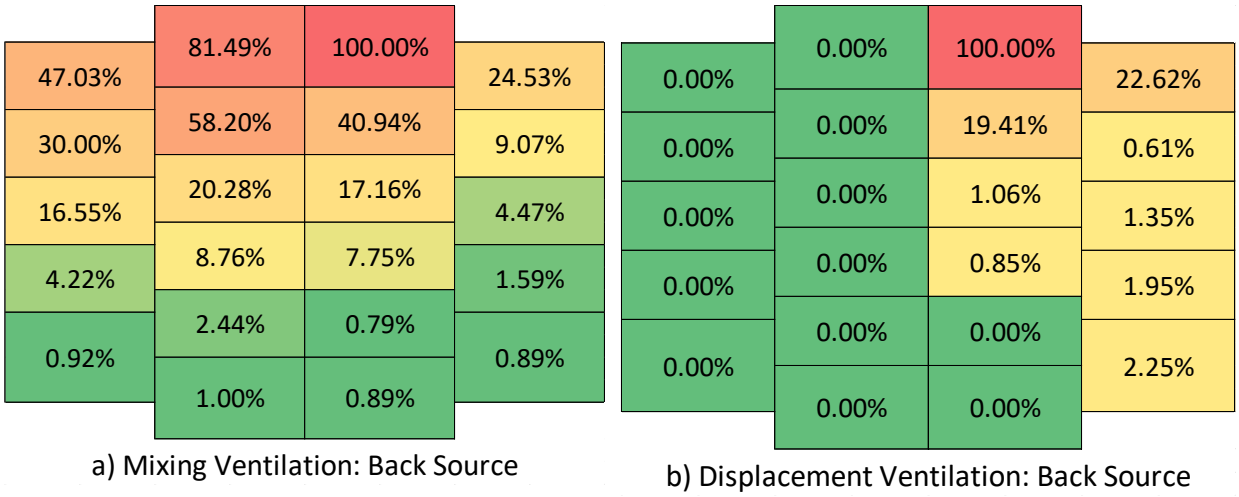

Figure 5-34: Risk map for an infection source at the back of the lecture hall for a) mixing ventilation case, and b) displacement ventilation case

Comparing the front, middle and back infection source locations it was demonstrated that the front infection source was optimal for the MV configuration, and the back infection source was optimal for the DV configuration. It was also observed that the outlet location had a significant impact on aerosol removal rates, as the settings where the outlet was closest to the coughing occupant had particles removed at a faster rate and limited particles spreading throughout the room. This was evident for the front infection source case in the MV configuration (see Figure 5-14 to Figure 5-19) and the back infection source case in the DV configuration (see Figure 5-27 to Figure 5-31).

Overall, the DV configuration is ideal if the infection source is known and can be placed closest to the outlet to limit dispersion and exposure to other occupants. Furthermore, if the room is terraced like a lecture hall in DV configurations, the highest locations should be dedicated for symptomatic occupants and the lowest for vulnerable occupants. That way the thermally stratified air flow will carry the expelled aerosols upwards, preventing any exposure to occupants' breathing zones.

The MV configuration is ideal for overall reduction in infection if the infection source is not known. This is because MV dilutes and mixes aerosols quickly and uniformly regardless of the position of the infection source. The probability of infection to all occupants in a MV configuration are comparatively lower to DV configurations. In DV configurations a small number of occupants that may be in the infection source's lock-up region get a high dosage and long period of exposure, which can overwhelm the immune system of occupants. This is depicted in the plot

in Figure 5-35, which shows the total number of particles (in the breathing zones) multiplied by their residence times, from 1 to 5 minutes, for the middle injection case. The mixing ventilation case has a lower residence time and number of particles than the displacement ventilation case 1 minute in. As the total number of particles in the breathing zone starts clearing out for both cases, there is a gradual reduction of the "particle number x residence time", and by 5 minutes the difference between the particle number over their residence time for DV is 2.6 factors higher than MV. In Figure 5-20 to Figure 5-25, the particles are seen to spread out for both cases, but for the MV case the particles were quickly dispersed and quickly deposited or were escaping. While, for the DV case the particles were slowly moving towards the outlets. Therefore, the higher residence times, and significant concentrations stagnating in the breathing zones of (the few) occupants resulted in the higher total "particle number x residence time" for DV in the plot (in Figure 5-35). Thus, in MV configurations the aerosols clear out rapidly, which reduce the risk of potential infection in comparison to DV configurations.

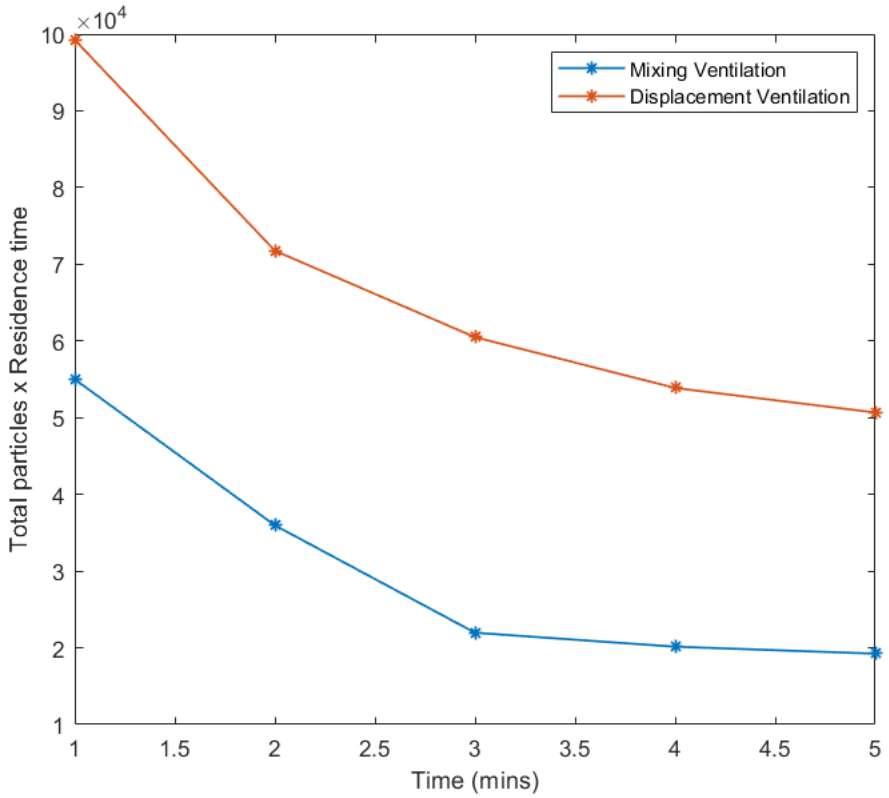

Figure 5-35: Total number of particles in the breathing zone for the middle source injection from 1-5 mins. The number of particles in the mixing ventilation case is shown in blue and the number of particles in the displacement ventilation case is shown in red.

The higher residence time of particles for DV configurations is also conducive to higher airborne infection spread through re-dispersion. The particles tend to slowly drift towards the outlets in a path, but as movement occurs in the lecture hall space, which often happens when students change classes, the path of contained particles will get disturbed and spread out. This means the high concentration of particles grouped together will then be dispersed into several areas of the lecture hall. Several occupants in the incoming class will now also be exposed to the infectious particles.

5.4. Conclusions and Future Work

This chapter modelled a lecture hall space from the Curtis Lecture Halls at York University campus. Six different cases were studied, two ventilation configurations: mixing (existing) and displacement ventilation, and three infection source locations: front, middle and back. The main objectives were to firstly, evaluate sensitivity of infection source locations with respect to the room and ventilation layout, and secondly identify any optimal scenarios for minimal airborne transmission risk within lecture halls. CFD was used to simulate the ventilation and particle dispersion, and a modified Wells-Riley risk equation was used to construct risk maps for the lecture hall separated into multiple risk zones.

The results showed a range of risk values based on the ventilation configuration as well as infection source locations. The results confirmed that infection source locations can be important based on the ventilation type, location of the outlet and the design of the room. Displacement ventilation had more magnified effects for the infection source location in comparison to the mixing ventilation configuration, where for the DV case the infection source location at the front exposed the most occupants to infection, and the infection source at the back quickly and efficiently removed most of the infectious particles out. The scenarios in both ventilation types with the infection source closest to the outlet performed the best.

The concluding decision for this study was that mixing ventilation is a better choice compared to displacement ventilation for infection minimization in lecture hall spaces. Two specific reasons contribute to this conclusion. Firstly, lecture hall spaces are terraced, so the occupants have different breathing heights, which sets DV configurations at a disadvantage; DV configurations raise the expelled contaminants above the infection source occupant causing a “lock-up” region. This cloud of raised infectious aerosols then flows right in the breathing zones

of the occupants sitting behind the source occupant, exposing them to a high dose of infectious particles. DV configurations risk serious infection for the occupants behind the source occupant since occupants get a high dose and long exposure of infectious aerosols. In comparison, MV configurations distribute the aerosols at small concentrations all over the space, reducing the risk of high exposure to most occupants. Secondly, lecture halls have a high turnover rate of occupants, and it has been observed that DV configurations have a higher residence time of aerosols: as the DV configuration slowly removes stagnated aerosols, there is a risk of re-dispersion of the path of aerosols when occupants change classes. Thus, when the aerosols are disturbed from their flow path, they will disperse and infect several occupants that were previously not in the lock-up zone.

Future work can consider other educational spaces such as small classrooms, labs, lounges, and open-concept workspaces. Other novel ventilation configurations in lecture halls can also be valuable to investigate, as well combining current ventilation configurations in lecture halls with control measures such as plexi-glass barriers and air cleaner locations. Lecture hall spaces are prevalent in many institutions, and as re-opening of educational spaces has become a priority, this study will help to inform on the risks of infection transmission in these spaces. Ensuring control measures such as masking, vaccination and social distancing within these spaces is crucial to reducing the risk of infection, with the most important measure: ensuring proper ventilation operation within occupied indoor spaces.

Chapter 6 A combined CFD-SIR method to model airborne transmission in indoor environments.

6.1. Introduction

During the early months of the pandemic when measures such as masking and social distancing, to mitigate transmission were not prevalent, it was up to the ventilation in indoor spaces to control the airborne infection spread. Most residences and public spaces have heating, ventilation, and air-conditioning (HVAC) systems that ensure the indoor air quality is maintained, with regular air inflow, filtration and exhaustion. Ventilation plays a major role in airborne transmission minimization if designed with effective removal of airborne contaminants in mind [111]. Additionally, each indoor space is different from the occupant locations, ventilation type and location, furniture layout and other obstructions [12] which is why one solution cannot be applied to all settings [11]. An important aspect to further consider for airborne transmission of viral particles is the location of the infection source with respect to the ventilation. The interaction between the ventilation induced air pathways and the respiratory aerosols from the infection source can have different outcomes for the airborne transmission risk in a room.

Currently infectious aerosol transport in various spaces is effectively measured through CFD (Computational Fluid Dynamics) studies, which can incorporate various ventilation settings, occupants heat fluxes and particle transport [18,110,147]. However, this method can be computationally expensive and require long simulation times, especially if long-term effects (such as several days) of infection spread need to be considered. Such long-term infection dynamics would be valuable in infection outbreaks where the same occupants remained in areas over multiple days with poor ventilation design, such as the COVID-19 outbreaks in the cruise ship [100]. A long-term infection dynamics model could also be valuable in spaces where occupants arrive daily/regularly and remain in the space for long periods of time thus propagating infection in the space, such as in office spaces [98].

Looking at the long-term dynamics of airborne transmitted diseases and the impact of control measures is simple when classic epidemiological models such as the Susceptible-Infected-Recovered (SIR), or Susceptible-Infected-Susceptible (SIS) model are used. With the emergence of the SARS-CoV-2 virus, epidemiological models have been instrumental in quantifying the

population-scale risks of the disease. For instance, the basic reproduction numbers helped determine whether an endemic would occur [163–165]and whether the implementation of control measures would eradicate or at the least slow down infection [166,167]. Furthermore, a study conducted by Aruffo et al. [168] of a theme-park showed how epidemic models can be scaled down to investigate smaller population sizes, resulting in venue specific control measures. They concluded that increasing cleaning rates would prevent the most infection transmission, as human-environment transmission was the highest. However, epidemic models are generalized for a large population with transmission rates that are all encompassing and do not reflect the intricacies of transmission. On the other hand, airborne transmission's complex dispersion patterns are simulated well with CFD. Coupling CFD results to classic epidemiological models is a method that can obtain both spatially distributed airborne transmission risk and long-term infection dynamics in a room's population. Noakes et al. [169] performed a similar method of airborne transmission analysis with epidemic models, however they used the Well's Riley equation to determine the airborne transmission risk, the drawbacks of which have been discussed earlier in this review. Noakes et al. [169] also discuss how such coupled models could be valuable for diseases where the incubation times are shorter or similar to exposure times, for instance, in hospital wards where nosocomial infections occur from highly contagious airborne diseases. Asanuma and Ito [35] performed a study that coupled unsteady CFD results of airborne contaminant concentrations to an SIR model through the transmission rates, resulting in optimistic results for the usability of a CFD and epidemic model coupling method to predict airborne transmission risks in a space. The method can then be used to further determine the variation in airborne transmission risk for a space based on the ventilation design and occupancy zones.

The current project proposes an airborne transmission risk estimation method that determines whether a certain ventilation and occupant layout will lead to a viral outbreak or quick eradication within the space. This risk model evaluates the impact of ventilation designs and infection source locations towards the long-term (several days of) risk distribution in the space. A key measure of the airborne transmission risk is defined through a *pseudo-reproduction number*. A pseudo-reproduction number mimics the "basic reproduction number" seen in epidemiological models, but it differs from the basic reproduction number because it is a measure of the simulated long-term effects of infection transmission dynamics in a small population in an indoor space, rather than a measure of infection transmission dynamics in a large-scale population. The method

will involve an initial CFD simulation coupled with a zone-specific Wells-Riley risk equation will output parameter values for the identification of various risk zones, as well as transmission rates among those risk zones. After which, these parameters will be used in a classic Susceptible-Infected-Removed (SIR) differential equations model to,

i) determine the risk and severity of outbreaks that are caused by airborne transmission and,
ii) identify possible measure that can be taken to minimize airborne transmission risk in the space.

6.2. Methodology

The mathematical model implemented within this study is a Susceptible-Infected-Removed (SIR) model, which incorporated host heterogeneity. Host heterogeneity was considered with respect to occupants identified to be within high risk, medium risk and low risk zones in the domain. The host heterogeneity was based on varying risk zones which allowed the model to incorporate spatial heterogeneity of airborne transmission risk in a domain. The domain was a square (6 x 6) m room sectioned into 9 separate zones for risk evaluation. Three cases were considered:

1) Original-with 2 air outlets at the back of the room and with full occupancy,
2) Extra Outlets-with 4 air outlets distributed symmetrically at the back and front of the room with full occupancy, and
3) Removed Occupants-with 2 air outlets at the back of the room and the front 3 zones of occupants vacated (see Figure 6-1 below for all the three case's layouts).

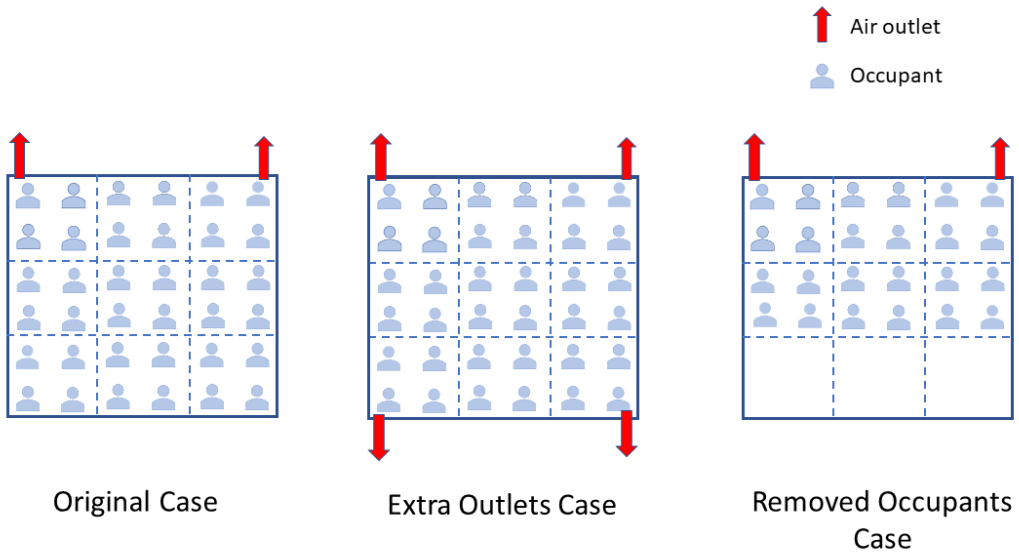

Figure 6-1: Layout of the domains for the three cases: original case, extra outlets case and removed occupants case. The red arrows indicate the location and direction of air outlets and the blue heads indicate occupants. The domain is separated into 9 zones with the dotted lines.

The progression of the study began with the risk distribution results of the original case with the air outlets at the back and full occupancy. From those results it was noted that the front zones accumulated more particles thus becoming high risk zones. Based on the original case results, control measures were implemented to see the effects they had on the risk distribution infection progression. Two different control measure were implemented:

a. *Adding extra outlets in the front of the room*- it was evident from the results that the zones closest to the air outlets had the lowest concentration of particles in the breathing zone. Thus, a control measure of changing the ventilation layout by installing additional outlets in the front would reduce the high risk and medium risk zones to be low risk zones in the front of the room.
b. *Removing occupants from the front of the room*- considering the front of the room had higher risk of infection, vacating occupants from those zones would provide an overall lower pseudo-reproduction number for the room.

6.2.1. Assumptions

The following assumptions are considered in the model:

i) The cases are assumed to take place during the early months of the pandemic, hence masking and social distancing are not included.

ii) The particle dynamics results for an hour are stretched to assume the same conditions apply for 30 days, which results in a long-term pseudo-reproduction number.

iii) The occupants do not travel between different risk zones, i.e., the occupants do not change from being in the high-risk zone to medium or low risk zone, an occupant will remain in the same risk zone for the duration of the simulation.

iv) The transmission rates are average rates of an infectious individual affecting a susceptible individual from different/same zones; the transmission rates of two different pairs of high risk to low risk zones can vary but an average between the two will be assumed.

v) The simulation is run for 100 seconds (which is when most particles clear out) then multiplied by six to assume the scenario of particle expulsion is repeated every ten minutes for an hour of evaluation.

vi) The incubation time for the Coronavirus disease is approximately 5 days which is the average time taken for an individual infected with COVID-19 to become symptomatic [170]. After the individual becomes symptomatic, they are removed from the space at a rate of 0.2 removals/day.

6.2.2. Flow Diagram

The following figure (Figure 6-2) demonstrates the flow diagram for the model. The subscripts H, M and L indicate high, medium and low risk zone occupants. The first set of boxes represent the occupants that are susceptible in the high, medium, and low risk zones indicated as: S_H, S_M, S_L, respectively. When the susceptible occupants become infected, they then enter their respective infected classes in the high, medium, and low risk zones indicated as: I_H, I_M, I_L, respectively. Finally, the removed class: R, representing all infected individuals that leave the space (assumed to be quarantined once symptoms appear). B represents the infection transmission rates of occupants from the Susceptible class to the Infected class, and γ represents the removal rates of occupants from the Infected class to Removed class. The subscripts on β represent the susceptible and infection source risk groups, respectively.

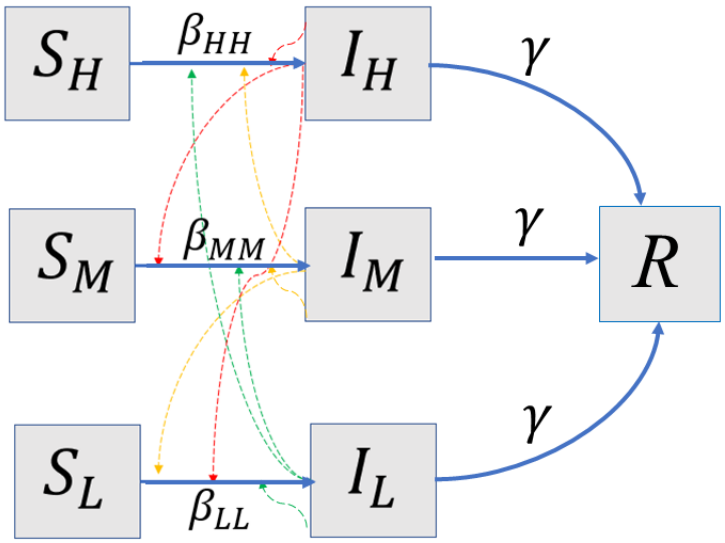

Figure 6-2: SIR flow diagram for high, medium and low risk zones. The solid blue arrows indicate the progression of occupants in different risk zone from their respective Susceptible class to the Infected class and finally to the Removed class. The dotted arrows represent the infection transmission routes from Infecteds of each risk zone to Susceptibles of each risk zone.

The arrows indicate the infected occupants from each risk zone able to infect the susceptible occupants in each of the three risk zones: the red arrow indicates infection from infected occupants in the high risk zones, yellow represents infection from infected occupants in medium risk zones and green represents infection from occupants in the low risk zones. The parameters for the transmission rates corresponding to each arrow has not been indicated in the flow diagram below, refer to the contact matrix (see matrix (1)) below for all the transmission routes.

6.2.3. Equations and Parameters

6.2.3.1. Ordinary Differential Equations (ODE)

The transmission rates for the various cases were put into a contact matrix accounting for the 9 permutations of transmission rates (see below). The diagonal of the matrix $(\beta_H, \beta_{MM}, \beta_{LL})$ are the transmission rates for infectious classes infecting susceptible classes within the same risk zones. The first row of the contact matrix, $(\beta_{HH}, \beta_{HM}, \beta_{HL})$ are the transmission rates from

infectious classes of high, medium and low (will be referred to as "*x*" from now on), respectively, infecting susceptible occupants in the high risk zone. The second row, $(\beta_{MH}, \beta_{MM}, \beta_{ML})$ are the transmission rates from *x* infectious classes infecting susceptible occupants in the medium risk zone. From the third row, $(\beta_{LH}, \beta_{LM}, \beta_{LL})$ are the transmission rates from *x* infectious classes, infecting susceptible occupants in the low risk zone. The matrix is not symmetric, as the high risk occupants will most likely infect the most occupants while low risk occupants the least, hence the first column will dominate the matrix.

$$\beta = \begin{bmatrix} \beta_{HH} & \beta_{HM} & \beta_{HL} \\ \beta_{MH} & \beta_{MM} & \beta_{ML} \\ \beta_{LH} & \beta_{LM} & \beta_{LL} \end{bmatrix} \tag{10}$$

The following equations (see equation (11) to equation (16)) are the ordinary differential equations representing the change in the susceptible and infectious populations in the three risk groups. The transmission rates are multiplied by the respective infected proportions of occupants from each risk zone, which is summed to represent the overall βI for each susceptible host type. Then the βI terms are multiplied with the proportion of susceptibles, S_x in the *x* risk group which is the number of susceptibles in *x* risk group over the total number of people N in the room. The γ term is the removal rate, which is set to 0.2 for all cases, based on the average time taken for COVID-19 infected individuals to develop symptoms (incubation period). The assumption is that once occupants become symptomatic, they are removed from the room.

$$\frac{dS_H}{dt} = -(\beta_{HH} I_H + \beta_{HM} I_M + \beta_{HL} I_L)\, S_H \tag{11}$$

$$\frac{dS_M}{dt} = -(\beta_{MH} I_H + \beta_{MM} I_M + \beta_{ML} I_L) S_M \tag{12}$$

$$\frac{dS_L}{dt} = -(\beta_{LH} I_H + \beta_{LM} I_M + \beta_{LL} I_L) S_L \tag{13}$$

$$\frac{dI_H}{dt} = (\beta_{HH}I_H + \beta_{HM}I_M + \beta_{HL}I_L)\, S_H - \gamma I_H \quad (14)$$

$$\frac{dI_M}{dt} = (\beta_{MH}I_H + \beta_{MM}I_M + \beta_{ML}I_L)S_M - \gamma I_M \quad (15)$$

$$\frac{dI_L}{dt} = (\beta_{LH}I_H + \beta_{LM}I_M + \beta_{LL}I_L)S_L - \gamma I_L \quad (16)$$

$$\frac{dR}{dt} = \gamma I_H + \gamma I_M + \gamma I_L \quad (17)$$

The eigenvector (see below) can then be derived from the Jacobian matrix, and the respective values, I_H^s, I_M^s, I_L^s will represent the distribution of infections caused by each risk zone in the slaved region only.

$$\text{Eigenvector} = \begin{bmatrix} I_H^s \\ I_M^s \\ I_L^s \end{bmatrix} \quad (18)$$

6.2.3.2. Pseudo-Reproduction Number

The pseudo-reproduction number can be calculated by, first deriving the Jacobian matrix for the infection ODEs:

$$J = \begin{bmatrix} \beta_{HH}n_H - \gamma & \beta_{HM}n_H & \beta_{HL}n_H \\ \beta_{MH}n_M & \beta_{MM}n_M - \gamma & \beta_{ML}n_M \\ \beta_{LH}n_L & \beta_{LM}n_L & \beta_{LL}n_L - \gamma \end{bmatrix} \quad (19)$$

Further calculating the respective pseudo-reproduction numbers, R_0^x, which represents the number of secondary infections caused by a primary infection from *x* risk zone, as seen in equations (20)-(23) below.

$$R_p^H = \frac{(\beta_{HH}n_H + \beta_{MH}n_M + \beta_{LH}n_L)}{\gamma} \quad (20)$$

$$R_p^M = \frac{(\beta_{HM}n_H + \beta_{MM}n_M + \beta_{LM}n_L)}{\gamma} \quad (21)$$

$$R_p^L = \frac{(\beta_{HL}n_H + \beta_{ML}n_M + \beta_{LL}n_L)}{\gamma} \quad (22)$$

After finding the respective pseudo-reproduction numbers contributed by *x* risk zones, the effective pseudo-reproduction number can be calculated as the summation of $R_0^x \cdot I_x^S$ from each *x* risk zone, as seen in equation (23) below:

$$R_p = R_p^H I_H^S + R_p^M I_M^S + R_p^L I_L^S \quad (23)$$

6.2.4. Computational Fluid Dynamics (CFD) Setup

The CFD domain was designed as a (6 x 6) m room, divided into 9 zones. Each zone has 4 occupants each, consisting of a total of 36 occupants (see Figure 6-3 below).

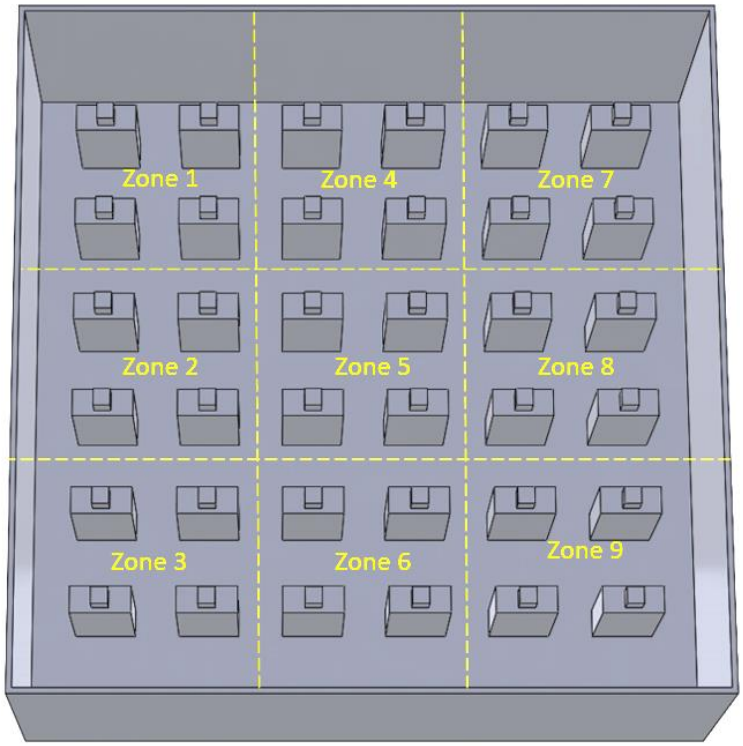

Figure 6-3: The CFD domain in top view, with equal sized zones 1 to 9 divided by the dotted lines. High, medium and low risk will be based on these zones.

In terms of the ventilation design, the room was designed with 6 air inlets on the ceiling with KFD-KLD 1000-2 linear slot diffusers, that have an effective area of 0.0191 m^2 [15]. The assigned boundary condition is a velocity inlet with 1.9 m/s of air flowing in. The air outlets are located at the bottom two corners at the back of the room with dimensions (40 x 25) cm, assigned as pressure outlets (see Figure 6-4 below of the domain in isometric view with indicated inlets and outlets).

6.2.4.1.Meshing

The domain is meshed with unstructured tetrahedral cells with element sizes of 5 cm. The inlets are refined to have element sizes of 0.95 cm. Prism layers are added to the domain walls with default settings, ensuring a maximum of 15 layers and a growth rate of 1.2. There were a total of 6.26 million elements and 1.3 million nodes in the domain.

6.2.4.2.Numerical Modelling Setup

The general setup followed the same methodology as described in section 3.1.2. To simulate airborne transmission 9 particles with diameters of 1 μm were injected from the centers of each zone, for a total of 99 particles tracked in the domain. The total number of particles is small, which raises concerns in terms of statistical significance of the particle distributions in the domain, but due to the large amount of data needed to process and considering the limited time, the simulation resorted to a small population of particles. The particles were injected in a single stream at 0.02 m/s in the z-direction for a period of 1 second (simulated time), after which the particles were tracked for a span of 100 seconds. The mass flow rate of the particles was $1x10^{-20}$ kg/s. The contact matrix is calculated through the allocation of particles in the various zones of the domain. The particles are spread all over the domain, but only particles suspended or entered in the breathing zone—in this case $\pm 60\ cm$ (y-axis in Figure 6-4) from the manikin shoulders—are considered. These particles are then further filtered out based on their location in x and z coordinates, to determine which zone they are located in (see Figure 6-3 for the separate zones). The particles are tracked based on the source zone they are released (injected) from, and so the distribution of particles over time with respect to their source injections are plotted for each zone to identify the high, medium, and low risk zones as well as derive parameters for the contact matrix.

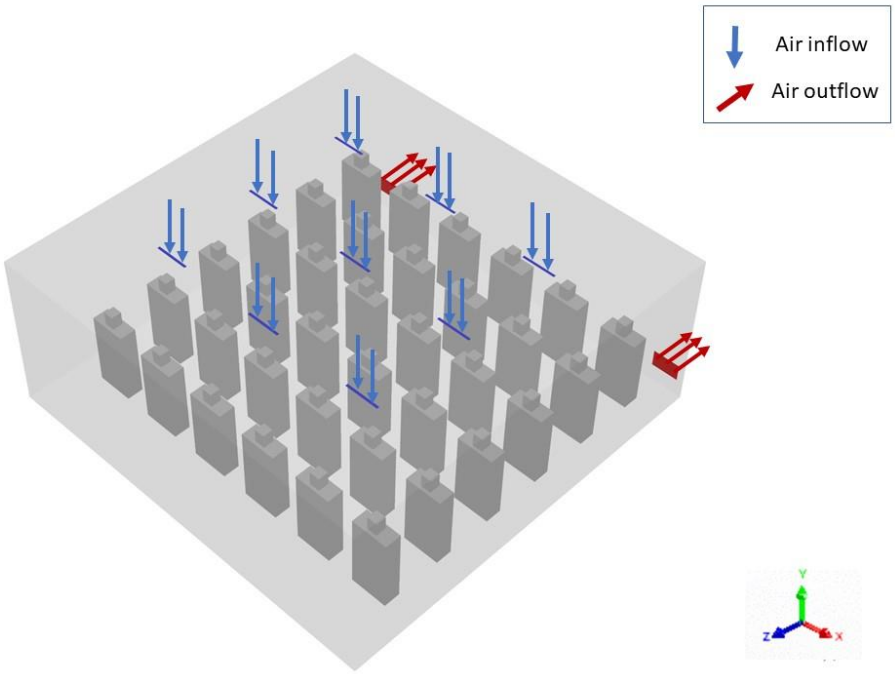

Figure 6-4: CFD domain in isometric view with 9 inlets indicated with blue downwards pointing arrows and 2 outlets indicated with red arrows in the negative direction of the z-axis. The cuboids with cubed heads are the simplified geometry for the occupants.

6.2.5. Risk Modelling

The risk of infection for the occupants were measured using a modified form of the Wells-Riley equation acquired from Buonanno et al.[143], see equation (24) below. The function for risk of infection (R, %) is dependent on time, and evaluated for each zone of the lecture hall.

$$R = \left(1 - \exp\left(-\mathrm{IR} \int_{T_i}^{T} n(t)dt\right)\right)(\%) \tag{24}$$

IR (m^3/s), represents the inhalation rate of the occupants, which is set to 1.36 x 10^{-4} m^3/s (0.49 m^3/h), based on the resting inhalation rate average for males and females [143]. In this study a unity infection term is assumed, so the quanta concentration in $n(t)$ (quanta/m^3), is equivalent to the particle concentration (number of particles/m^3) [26]. In other words, one particle will result in one quantum of infection. The quanta concentration is integrated over time, specifically by the residence time of each particle as it enters a zone at time T_i and leaves the zone at time T.

The risk value was then quantified by accounting for the total number of particles in the breathing zone every time step (*i.e.*, every 1 second for the current case), for a total of 100 seconds.

The integral of quanta concentration from T_i and T was then reflected by the particle counter. The total risk for an hour is then calculated by assuming particle expulsion events occur every 10 minutes during an hour of exposure, thus the time integrated quanta concentrations are multiplied by 6 then inserted into the risk equation.

6.2.6. Contact matrix derivation

In order to derive the contact matrix, the risk distributions are referred to. The evaluation of high, medium and low risk zones is based on the quanta retention from particles generated in the source zones. Thus, if particles stagnate in the zones they were injected in, those zones have poor ventilation and are considered high risk zones; and, if particles are quickly removed from their source zones, they are considered low risk zones with effective ventilation. The risk zones will be based on relative risk distributions. In this specific case, zones with greater than 25% risk are considered high risk, zones with risk between 12.5% and 25% are considered medium risk and less than 12.5% are considered low risk. These values were derived based on the occupancy in each zone (of 4). Thus, a high risk zone will cause a transmission rate of 1 or higher, medium risk will result in a transmission rate between 0.5 and 1 and low risk will contribute to a risk less than 0.5. The values for transmission rates of each zone from its own injection, as well as from other zones can then be derived.

Table 6-1: Risk ranges and number of Infecteds for low, medium and high risk zones.

Risk Zone	Range (%)	Number of Infected Individuals (Susceptibles x Risk%)
Low Risk	Less than 12.5	Less than 0.5
Medium Risk	Between 12.5 and 25	Between 0.5 and 1
High Risk	Greater than 25	Greater than 1

Referring to assumption ii, that stated the transmission rates are average rates of an infectious individual affecting a susceptible individual from different/same zones. Hence for β_{HL}:

1. the particles from all the low risk zones in each high risk zone is summed,
2. then the total of all particles from low risk zones in high risk zones is divided by the total number of high risk zones,
3. multiplied by 6—to account for the risk during an hour of exposure with particle expulsion every 10 minutes.

4. Then the value is inserted into equation (24)—to derive the total risk percentage of risk from low risk zone Infecteds to high risk zone Susceptibles.
5. This risk value is multiplied by the total number of Susceptibles in each zone (which is 4) to finally result in a transmission rate—that conveys the number cases that can result in a 4 occupancy zone.

6.3. Results and Discussion

6.3.1. Particle Distributions

The particle distribution results are acquired from the CFD simulations and filtered to include the particles only in the breathing zone as they are the main contributors of infection. The particles dispersed, settled, stagnated, or exited from the room and that is reflected through the particles integrated over their residence times. This data collection method for particle distribution is preferred as in airborne transmission scenarios, the concentration of particles, as well as residence time of particles are both contributors towards higher infection risk; a small concentration of particles exposed to occupants for a long period of time can have a similar risk of infection as a large concentration of particles exposed for a short period.

Referring to the particle distribution histogram in Figure 6-5, the particles concentrations integrated over their residence times for each of the 9 zones in the room are demonstrated (as labelled in the y-axis). From here forth the particle number multiplied over the residence time will simply be referred to as "particle concentrations." As described in the CFD methodology, the particle distribution data is collected based on their source injection x, y, and z coordinates, therefore, the x-axis is labelled in accordance with their source zone. All three cases of particle distributions are included in the histogram to allow for comparison. The blue bars indicate particle distribution results for the original setup case, the red bars indicate the results for the case with extra outlets added at the front and the yellow bars indicate the case with occupants removed from the front of the room.

For most of the zones, excluding zone 1, 7 and 9 (for the extra outlets case) the dominant particle concentrations are from the zone's own particle source. Zones 1 and 7 are the closest to the air outlets which explains why their particle concentrations from their source injections are relatively low; the particles were quickly exhausted out and did not linger in the breathing zone.

Also, zones 1 and 7 have more particles from neighboring zones in comparison to the other zones, which is also explained by the location of air outlets, as particles are attracted towards and carried out by the airflow pathways induced by the air outlets. Identifying some high risk zones, zone 3 and 9 for the original case, and zone 4 for the removed occupants case, have particle concentrations of 500 to 600 tracked from their own sources. This means that after the particles were injected out, they lingered in the breathing zone for a while. These are examples of high risk zones as the occupants in those zones (for the specific cases) were at a high risk for infection.

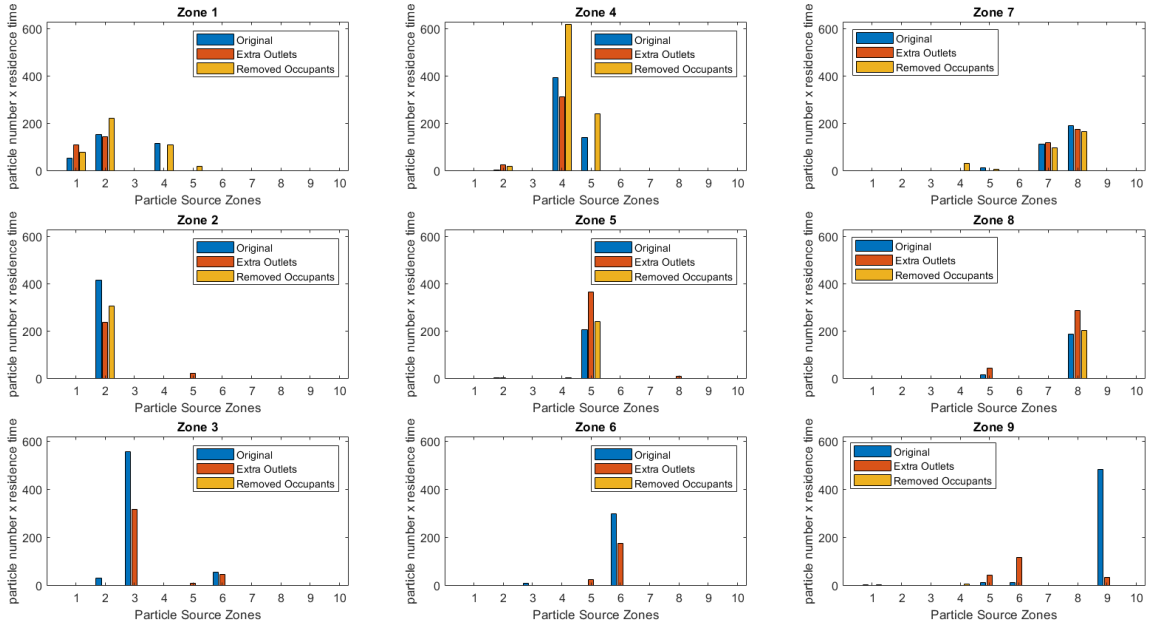

Figure 6-5: Histograms for particle distributions in each zone for all three cases: original setup, adding extra outlets and removing occupants from zones 3,6 and 9.

The results from each case tell a story for how the particles dispersed in the room. Looking at the original case first, we see zones 3 and 9 at the bottom with the highest concentration of particles. The zones upwards slowly reduce in particle concentrations, with zones 1 and 7 where the air outlets were located with the least height of particle concentrations. On the other hand, zones 1 and 7 have a high diversity of particle sources as zone 1 has particles from 1 (own source particles), 2 and 4, while zone 7 has particles from zones 5, 7 (own source particles) and 8. This leads to the inference that the particles could not escape from the front zones (3, 6 and 9) and remained there, while the particles from the middle zones were close enough to the outlets that

they were pulled into zones with the outlets (zones 1 and 7) and some of them were able to escape. Zone 4 had a relatively high particle concentration, which may be because the pull from the two outlets (in zones 1 and 7) were symmetrical thus a resultant zero net force was created for the particles in zone 4.

The extra outlets case has similar patterns to the original case with diverse sources injections for particles in the zones adjacent to outlets (in this case, zones 1, 3, 7 and 9). However, the main and valuable takeaway from the extra outlets case is that the control measure of adding extra outlets in the front of the room reduced the particle concentrations by 42.8% for zone 3, 40% for zone 6 and 93% for zone 9, all of which are quite significant. Another difference between the original case and extra outlets case is the particles in the middle zones, specifically zone 5 and 8, which have a higher particle concentration than the original and removed occupants case. This could have been caused by the equal pull from opposite outlets, which keeps the particles stagnated in the middle.

In terms of the removed occupants case, the results are similar enough to the original case. This is expected as the ventilation layout has not changed, so the particle concentration differences between the original and removed occupants case in zones 1, 2, 4, 5, 7 and 8 (zones where particles were injected and occupied for the Removed Occupants case) should only be because of stochastic effects in turbulence. If the occupants in the domain were simulated to produce heat fluxes, there would be changes due to the difference in heat flux with reduced occupants, but since the energy equation was neglected for simplicity and simulation time reductions no heat flux changes need to be considered for the differences in results. The only significant difference is that there are no visible particle concentrations for zones 3, 6 and 9. There is a very small particle concentration (with a value of 7 from injection 4) in zone 9 for the removed occupants case, which resulted from the air circulation in the room due to turbulence effects.

6.3.2. Risk Zones

The particle concentrations from each zone's own particles were then converted into risk zones to determine the risk of infection in the zones, as well as to translate the results into transmission rates for the epidemiological model. The following images (Figure 6-7-Figure 6-8) show the risk of infection in each zone based on Buonanno et al.'s modification of the Wells-Riley risk equation (see equation (24)). As discussed in the methodology, risk group identification is based on three

ranges: risk values of 0-12.5% are considered low risk zones and the risk value is coloured in green in the figures (Figure 6-6 to Figure 6-8), risk values of 12.5-25% are considered medium risk zones and are coloured in yellow and risk values greater than 25% are considered high risk zones and are coloured in red.

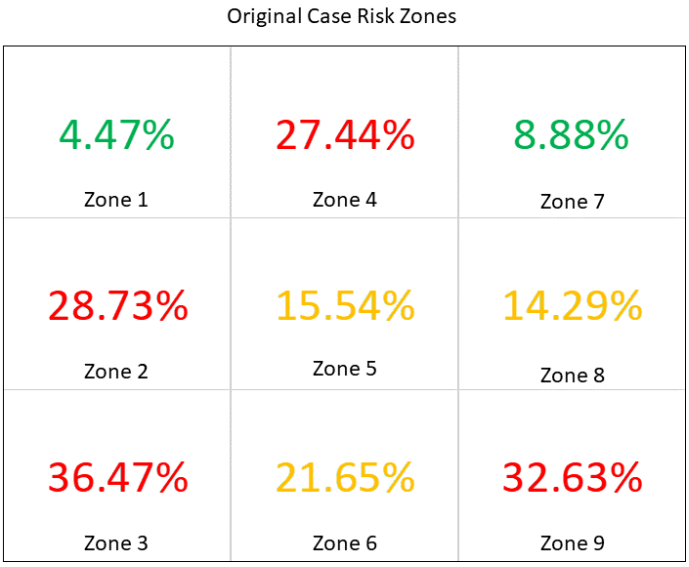

Figure 6-6: Risk values for zones 1-9 in the Original setup case.

Figure 6-6 shows the risk distribution in each zone for the original case. The case consists of 2 low risk zones, 3 medium risk zones and 4 high risk zones. Zones 1 and 7 are identified as low risk zones because as seen in Figure 6-5 above the particle concentrations for their own source injections were very low and the particles exited those zones quickly and efficiently. Zones 3 and 9 are identified as high risk zones, which aligns with the particles concentration results seen in Figure 6-5, where the particles could not escape and stagnated in high concentrations. The particle retention in zones 2, 3, 4 and 9 were significant enough to increase the risk of infection above 25% thus considered to have a high risk of infection to occupants.

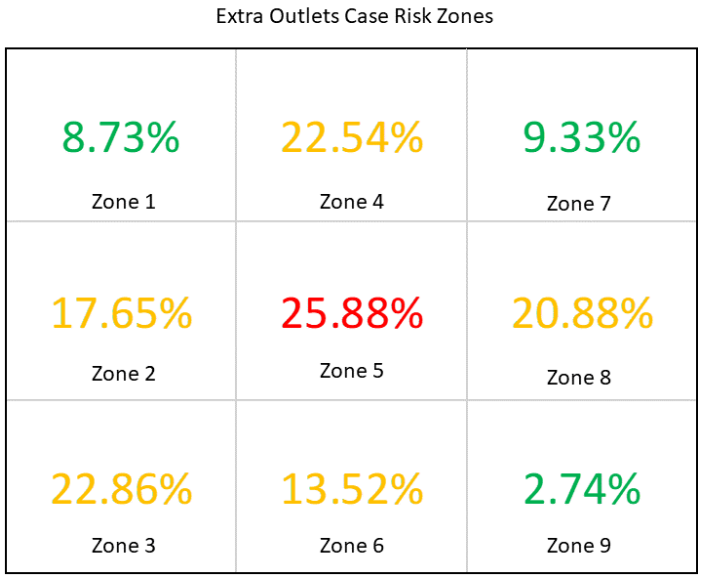

Figure 6-7: Risk values for zones 1-9 in the Extra Outlets case.

Figure 6-7 shows the risk distribution in each zone for the extra outlets case. This case consists of 3 low risk zones, 5 medium risk zones and only 1 high risk zone. This a significant improvement in risk compared to the original case (Figure 6-6), as the high risk zones (zone 2, 3, 4 and 9) are now medium or low risk zones. Also, the highest risk was 36.47% for the original case, but it is only 25.88% for the extra outlets case. The extra outlets case has 3 low risk zones which are the zones adjacent to air outlets, signifying the impact of the air outlets. Zone 3 which is also adjacent to an air outlet may not have reduced to a low risk zone but has reduced from a high risk zone (36.47%) to a medium risk zone (22.86%). One issue that should be pointed out is that zone 5 which was a medium risk zone in the original case is now a high risk zone in the extra outlets case. As explained in the histogram results, the symmetry of air outlets on all four corners (in zones 1, 3, 7 and 9) result in a net zero airflow for the middle zones, especially the centre of the room, which lead to particles stagnating in zone 5.

Figure 6-8 shows the risk distribution in each zone for the removed occupants case. This case has 5 low risk zones, 3 medium risk zones and 1 high risk zone. This is much improved from the two cases above (the original and extra outlets case). There are three low risk zones (zone 3, 6 and 9) with 0% risk, which is expected as there were no occupants or particle sources in those zones, so the zones remained untouched by particles. Comparing to the original case (Figure 6-6) which had the same ventilation layout, the risk zones are similar, except for zone 2, which was a high risk zone in the original case but is a medium risk zone in the removed occupants case. There

was some improvement in risk due to stochastic effects. However, zone 4 worsened in the removed occupants case in comparison to the original case where the risk increased from 27.44% to 39.61%. This suggests that a control measure may be necessary for zone 4, such as placing an air cleaner or vacating occupants in that zone.

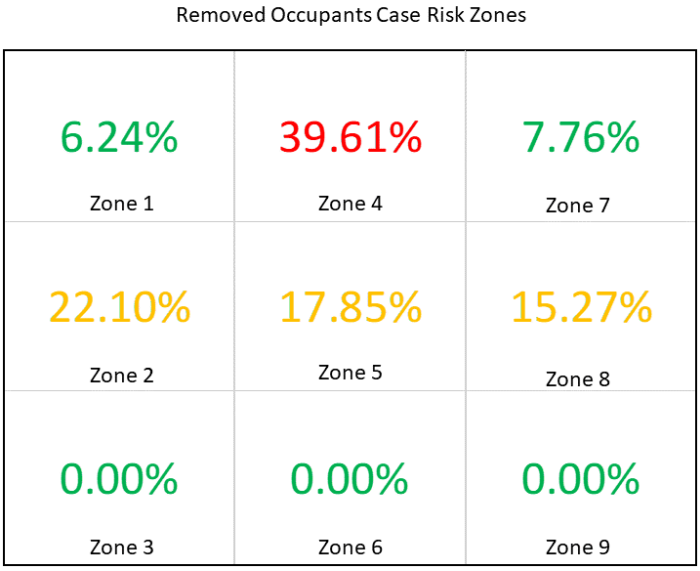

Figure 6-8: Risk values for zones 1-9 in the Removed Occupants case.

Vacating occupants in certain zones of a room may look promising, but it is not always feasible, especially in places where space is limited, and many people need to be accommodated. In those cases, an alternative option could be to place occupants that are masking, vaccinated or have immunity in those zones, which would have similar effects to removing occupants entirely and reducing the overall risk. Those occupants are less likely to contribute to infection or get infected.

In all the cases seen above, there is a lack of symmetry, which is because of the stochastic effects of turbulence. This demonstrates that airborne risk distribution is not necessarily predictable, and these models provide an estimate of the risk. Thus, CFD is valuable in reducing the margins of error, but there could still be several other factors and stochastic patterns that can impact the airborne disease spread.

6.3.3. Epidemiological Model

The following step in the method was to translate the risk values above into transmission rates. Thus, the risk values with identified risk zones were converted to transmission rates with the

steps described in the *contact matrix derivation*. This process was completed for all three cases and all nine permutations of the contact matrix, resulting in the following contact matrices for the original, extra outlets and removed occupants cases:

$$\beta = \begin{bmatrix} \beta_{HH} & \beta_{HM} & \beta_{HL} \\ \beta_{MH} & \beta_{MM} & \beta_{ML} \\ \beta_{LH} & \beta_{LM} & \beta_{LL} \end{bmatrix} = \begin{bmatrix} 1.28 & 0.19 & 0.0057 \\ 0.025 & 0.71 & 0.0044 \\ 0.43 & 0.32 & 0.27 \end{bmatrix}$$

Parameter 1: Contact Matrix for the Original case.

$$\beta = \begin{bmatrix} \beta_{HH} & \beta_{HM} & \beta_{HL} \\ \beta_{MH} & \beta_{MM} & \beta_{ML} \\ \beta_{LH} & \beta_{LM} & \beta_{LL} \end{bmatrix} = \begin{bmatrix} 1.03 & 0.052 & 0.016 \\ 0.07 & 0.83 & 0.0046 \\ 0.053 & 0.46 & 0.29 \end{bmatrix}$$

Parameter 2: Contact Matrix for the Extra Outlets case.

$$\beta = \begin{bmatrix} \beta_{HH} & \beta_{HM} & \beta_{HL} \\ \beta_{MH} & \beta_{MM} & \beta_{ML} \\ \beta_{LH} & \beta_{LM} & \beta_{LL} \end{bmatrix} = \begin{bmatrix} 1.58 & 0.77 & 0.013 \\ 0.0054 & 0.74 & 0.0033 \\ 0.099 & 0.27 & 0.061 \end{bmatrix}$$

Parameter 3: Contact Matrix for the Removed Occupants case.

The diagonals for all three cases are the transmission rates for Infected Individuals infecting Susceptibles in the same risk zones. The values align well with the ranges determined in Table 6-1, which confirms the derivation method for the contact matrices. The transmission rates above are then used in the ODEs in equation (11)-(17) to result in the SI plots below. The SI plots are shown for 30 days, assuming 1 event occurs per day. The initial number of susceptibles is based on the risk maps from Figure 6-6-Figure 6-8, for instance the Original case has two low risk zones, therefore the initial number of Susceptibles in the low risk zones are $2 * 4 = 8$ susceptible occupants. The infected occupant is not taken from the number of occupants in the room but is assumed to be an extra occupant.

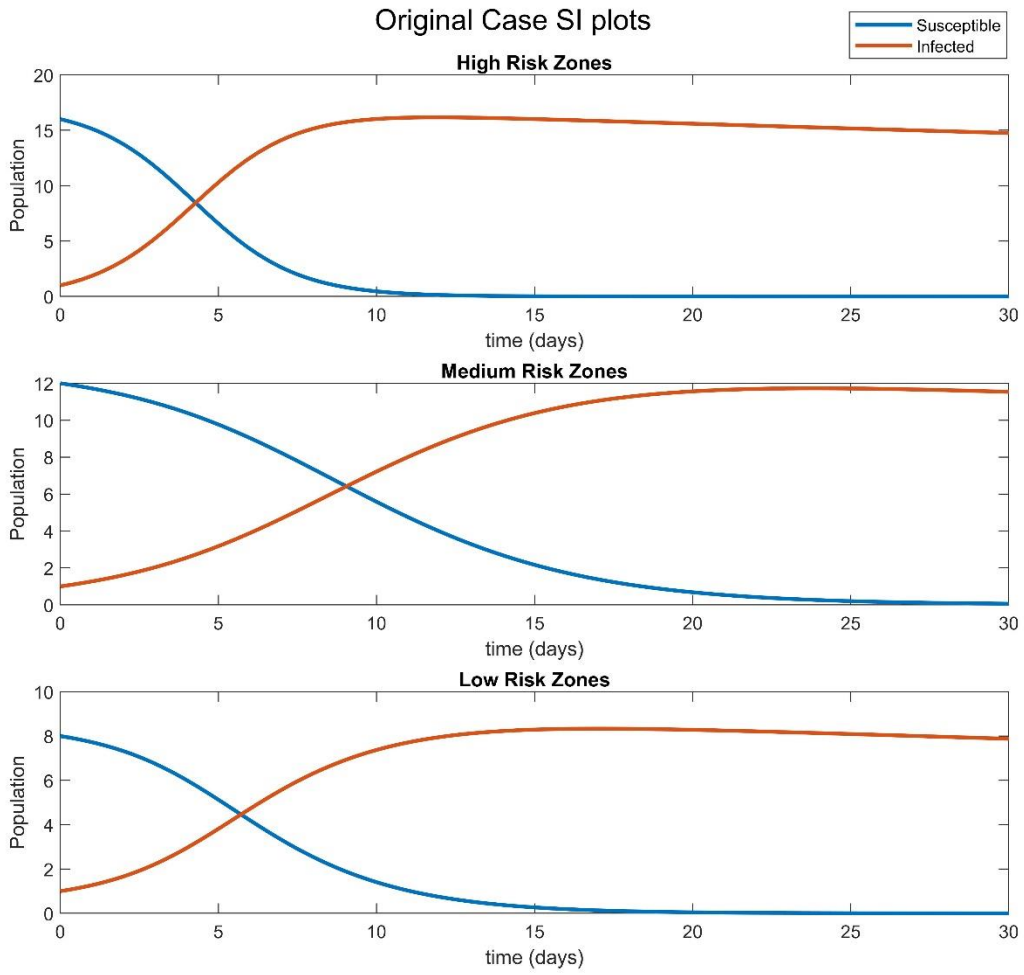

Figure 6-9: Original Case SI plots for high, medium and low risk zones.

Figure 6-9 shows the progression of Susceptibles becoming Infected for the Original case in each risk group. In the high risk zones, by 4 days half of the susceptibles have been infected. To infect of the Susceptibles the medium and low risk zones took around 9 and 5 days respectively. The high risk zone Susceptibles became infected quickly because of the exposure from high risk zones, which was evident from the transmission rate (β_{HH}) of 1.28. The low risk zones were also quick to develop infection because many particles were being transmitted from the high and medium risk zones to the low risk zones. This also explains why the Susceptibles in the medium risk zones were slower to get infected; the transmission rates from other risk zones to medium risk zones were comparatively low.

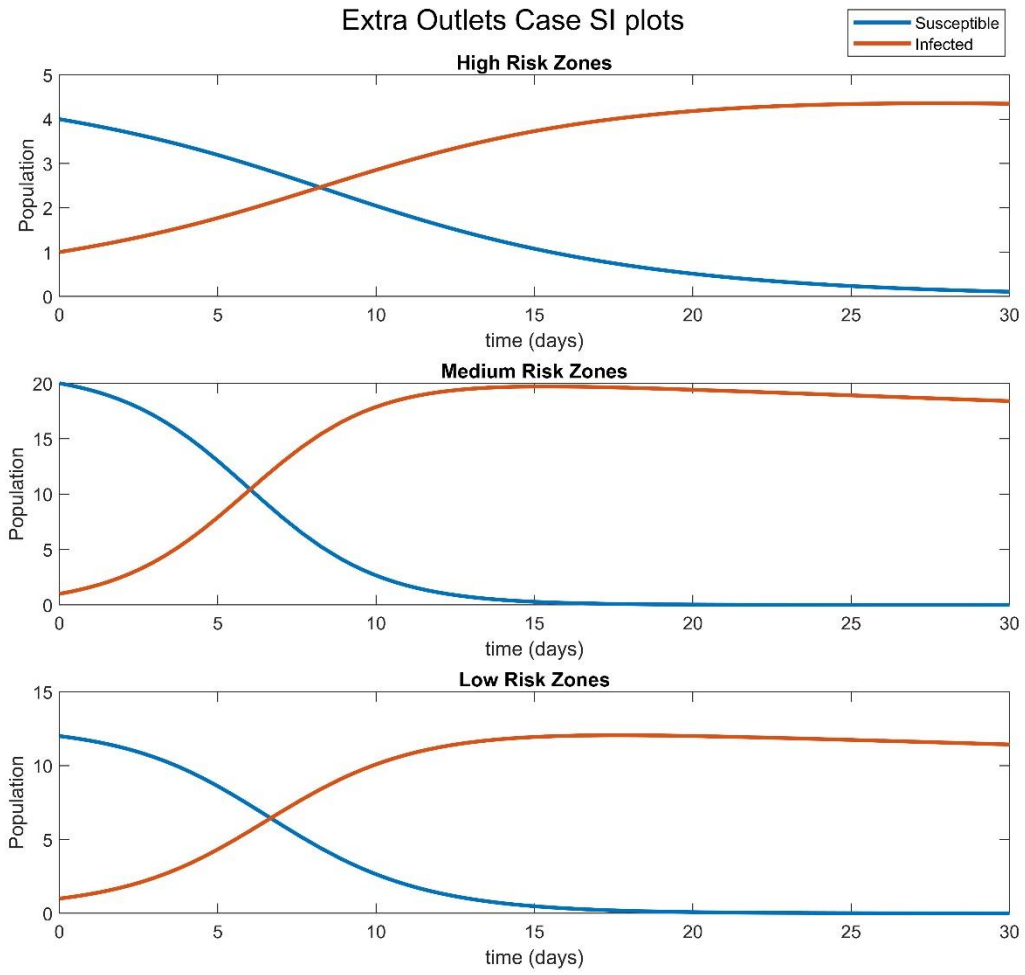

Figure 6-10: Extra Outlets Case SI plots for high, medium and low risk zones.

Figure 6-10 shows the progression of Susceptibles becoming Infected for the Extra Outlets case in each risk group. In the high risk zones, by 8 days half of the susceptibles have been infected, while the medium and low risk zones both took around 6 days. The high risk zone performed better for "infection half-life" (*i.e.* time of infection for half the population), mainly because of the size of the population; since there was only 1 high risk zone in the domain the total of high risk Susceptibles were only 4. On the other hand, the low risk Susceptibles were quick to become infected because of the high number of medium risk zones whose transmission rate towards low risk zones was comparatively high (β_{LM} was 0.46).

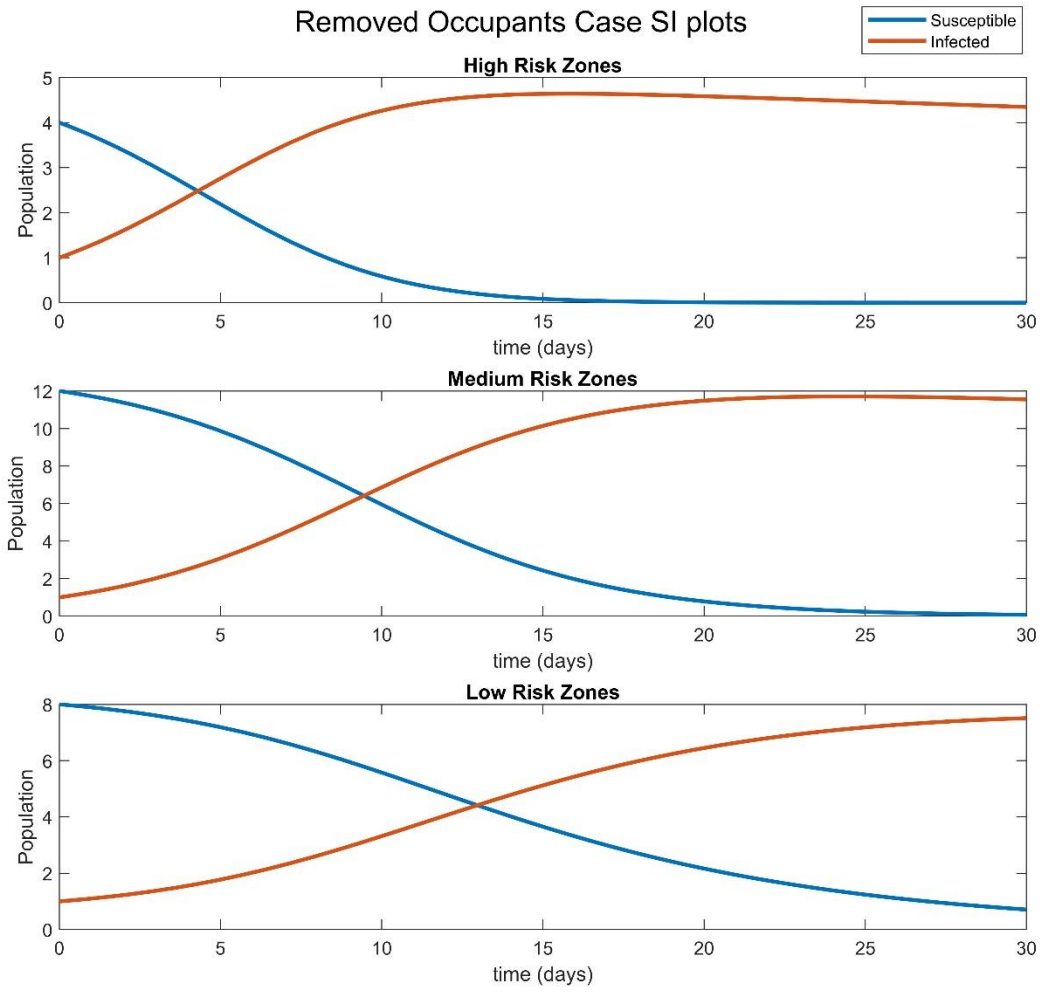

Figure 6-11: Removed Occupants Case SI plots for high, medium and low risk zones

Figure 6-11Figure 6-10 shows the progression of Susceptibles becoming Infected for the Removed Occupants case in each risk group. By 2.5 days half of the susceptibles have been infected in the high risk zones, while the medium and low risk zones took 6 and 8 days respectively. In this case there was only 1 high risk zone, but the transmission rate from high risk zone Infecteds to high risk zone Susceptibles was significant (β_{HH} was 1.58), which lead to more than double the infection rate compared to the Extra outlets case, for the same number of high risk zones. The medium and low risk zones had slower rates of infection in comparison to the high risk zone.

6.3.3.1.Pseudo-Reproduction Numbers

With the derived transmission rates, the resultant pseudo-reproduction numbers can be calculated for the Original case and the implemented control measures. Table 6-2 lists the pseudo-

reproduction numbers for the Original case, Extra Outlets case and Removed Occupants case. The effective pseudo-reproduction numbers are included as well as the pseudo-reproduction numbers due to infections from each risk zone.

Table 6-2: Pseudo-reproduction numbers for the Original case, adding extra air outlets and removing occupants from the front zones. R_p is the effective pseudo-reproduction number, R_0^H, R_0^M, R_0^L are the pseudo-reproduction numbers from the high, medium, and low risk zones respectively.

Case	R_0	R_0^H	R_0^M	R_0^L
Original	3.71	3.36	1.96	0.32
Extra Outlets	3.02	0.86	3.10	0.51
Removed Occupants	2.82	1.50	2.94	0.12

The resulting pseudo-reproduction numbers are within the bounds of the reproduction numbers seen for earlier variants of COVID-19 in literature of [2-5]. Both control measures have resulted in improved pseudo-reproduction numbers from the Original case. The pseudo-reproduction number for the Extra Outlets case is reduced from the Original case by 18.6%. The control measure of installing extra outlets is proven to be effective by reducing transmission from high risk zones (R_0^H) by 74% from the Original case. However, the medium and low risk pseudo-reproduction numbers increased for the Extra Outlets case by 58% and 59% respectively, from the Original case. From the risk maps (Figure 6-6 and Figure 6-7), it was observed that the reduction in the high risk zones needed to be compensated by the medium and low risk zones, which resulted in an increase in pseudo-reproduction numbers for those zones.

The pseudo-reproduction number for the Removed Occupants case has reduced from the Original case by 24%, and reduced from the Extra Outlets case by 6.6.%. A reduction is also seen in the pseudo-reproduction numbers from the high and low risk zones between the Original and Removed Occupants cases: there is a 55% reduction in the high risk zone's pseudo-reproduction number and a 63% reduction in the low risk zone's pseudo-reproduction number. However, the medium risk zone's pseudo-reproduction number increased by 50%. Regardless of the increase in the medium risk's pseudo-reproduction number, the overall contribution was still most optimal with the smallest overall pseudo-reproduction number for the Removed Occupants case. This was due to the small number of risk zones, thus leading to fewer susceptible occupants. Three of the risk zones were completely vacated (zones 3, 6 and 9) with no risk of infection or transmission, which lead to an overall reduction in infection transmission for the Removed Occupants case.

According to the pseudo-reproduction numbers the optimal control measure is then to reduce occupancy in high risk zones of the room. Measures such as vaccination, masking and placing occupants that have gained natural immunity in high risk zones is an alternative to vacating occupants, as it would have the same effect; occupants that are masking or have immunity are less likely to get infected or transmit infection. On the other hand, adding extra outlets may also be effective if placed strategically. As seen from the results, the zones adjacent to air outlets reduced in risk significantly, but the middle zones increased in risk because of the equal pull from the outlets on both sides resulting in particle stagnancy. Increasing the number of outlets and/or placing outlets close to high risk regions is useful for minimizing infection risk, but changing the ventilation layout in existing buildings may be unfeasible. In those cases, installing air cleaners are a good replacement for air outlets, as air cleaners can remove infectious particles from the air. Air cleaners are also a cheap and easy to install method which has been recommended by ASHRAE [43] to minimize the airborne transmission risk when placed in appropriate zones.

6.4. Conclusion and Future Works

The objective of this study was to develop a method that can predict the airborne transmission risk in an indoor space, to then evaluate the long-term infection dynamics through the population within that space. The method was intended to output an all-encompassing pseudo-reproduction number, which can help determine the overall airborne transmission risk in a space. Furthermore, implementing the method on different cases can identify minimum risk configurations, or point to the most effective control measures for a specific indoor space. The method couples particle dispersion data acquired from CFD studies to classic epidemiological models. The coupled method results in an airborne transmission risk analysis that considers both the intricate aerosol dispersion pathways, and the long-term effects of these dispersion patterns on a space's population.

For the method, CFD studies of the particle dispersion were conducted in the domain with particles sources in each zone. The particle locations and residence times were then converted to zone specific risk values with a modified Wells-Riley risk equation derived by Buonanno et al. [143]. The risk values were then used to identify high, medium and low risk zones, as well as translate the risk values into transmission rates for a host heterogenous contact matrix. The transmission rates connected the CFD data to the SIR epidemic model, which finally resulted in

the pseudo-reproduction numbers. The method was applied to a domain which was a (6 x 6) m room (in area), with 36 occupants separated into 9 equal zones in the room. The method was applied to three different cases: with two air outlets at the back of the room and full occupancy (Original case), with four air outlets located symmetrically at the back and the front of the room with full occupancy (Extra Outlets case), and lastly, with two air outlets at the back of the room and reduced occupancy (Removed Occupants case). The Extra Outlets and Removed Occupants cases were designed to consider the effects of control measures based on the results of the Original case.

All three cases resulted in varying risk distributions and pseudo-reproduction numbers. The pseudo-reproduction numbers were 3.71, 3.02 and 2.82 for the Original, Extra Outlets and Removed Occupants cases, respectively. Evidently, it was concluded that the Removed Occupancy case performed most optimally. The Removed Occupancy case's optimal performance is two-fold: it was assumed that the occupants in the three frontal zones were completely vacated, which meant that there were three less sources of infection, as well as 12 fewer susceptible occupants in the room that could get infected. Thus, the overall risk of infection reduced through the transmission rates and through the total number of occupants (N). This solution can equally be applied to occupants that have either gained immunity (through vaccination or infection) or are masking and following infection safety recommendations. The control measure of using extra outlets was also seen to be effective, as it reduced the risk of infection in the zones adjacent to the outlets. However, the measure also increased risk in certain zones because of the improper placement of the outlets. The four outlets were placed symmetrically and opposite to each other, which created a ventilation dead zone in the middle and lead to particle stagnancy in the middle zones. This issue can also be encountered when placing air cleaners in a built environment. The issue can be avoided through proper ventilation layout planning and preliminary CFD studies to ensure the ventilation works effectively to ensure thermal comfort for occupants and reduce the risk of particle stagnation.

In terms of future work, validation with past outbreaks and experimental validation of particle dispersion can increase confidence for this methodology. Other aspects that were neglected or simplified in the current study were the transient nature of risk and the thermal comfort of occupants. In this study, it was assumed that the risk zones determined from the initial analysis and remained at steady state after that. However, risk zones can change based on occupants'

removal, and changes in occupants' behaviours. The heat flux and thermal comfort of occupants were not considered to simplify the ventilation design.

The method presented is a new approach to airborne transmission risk modelling that combines the two dominant methods of risk modelling seen in literature for airborne transmission: CFD and epidemiological models. CFD studies look at micro-scale physics of infectious aerosol transport, while epidemic models look at long-term infection dynamics in a population. This method is a first attempt of combining CFD and epidemic models for airborne transmission risk analysis (specifically in indoor environments) with the potential for several modifications to adapt to different conditions. Amid the COVID-19 pandemic, this method can provide useful information regarding the potential for outbreaks in indoor environments, the zones contributing to high transmission rates and control measures that will be most effective at reducing the risk of infection. The risk of airborne transmission is often random and can be impacted by many physical, environmental and host factors, hence this method is a gross estimation of airborne transmission risk.

Chapter 7 Summary, Conclusion and Future Works

This thesis study set forth with three main objectives, firstly to further understand how airborne transmitted infection propagates in indoor environments. Another important objective that followed, was then to find methods to minimize airborne transmitted infection, thus reducing the effects of COVID-19 through airborne routes. The focus was on determining the impacts of ventilation layout and infection source locations (with respect to the room and ventilation layout) on the airborne transmitted infection risk in indoor spaces. A final objective was to find a method for ease of comparison between different ventilation layouts or control measures, to decide on the most optimal layout for airborne transmission risk reduction.

The study began by determining the sensitivity of ventilation layout, by analyzing the CFD results of particle dispersion and particle history (deposited on surfaces, escaped or suspended in air) in a small office when an outlet was added to the ceiling. Three different configurations were investigated: the existing layout, an overhead outlet added with respect to the occupant, and an outlet added further away from the occupant. The results demonstrated that the particle dispersion patterns can change significantly based on the existence and location of the outlet. Any ventilation component changes the airflow patterns in the space, and the particles are carried with respect to those changes. Particles can coagulate, deposit or disperse widely based on the ventilation induced airflow patterns.

The study proceeded to study the impact of ventilation type and infection source location. A lecture hall was simulated for two different ventilation types: mixing ventilation and displacement ventilation, and three different infection source locations. The spatially and temporally varying infection risk based on the particle distributions were quantified with a zonal Wells-Riley model risk map. The results showed mixing ventilation with source infections in the front of the room to perform most optimally with rapid dilution and removal of particles. The configuration with displacement ventilation and infection source location at the back of the room also performed ideally, with quick and contained removal of expelled particles. Overall, the results indicated that an infection source located near the air outlets provides the best-case scenario, as particles are quickly removed from the space without significant dispersion to other occupants. Furthermore, mixing and displacement ventilation had very different particle distribution results, which is explained by their unique working principles. Displacement ventilation contained the expelled particles and carried the particles upwards and backwards which lead to high exposures

of particles right in the breathing zones of susceptible occupants seated behind the infection source. Mixing ventilation on the other hand, dispersed the particles extensively, but also diluted them, thus reducing infectious dose exposures to most occupants. It was concluded that mixing ventilation is more appropriate for lecture hall settings.

A CFD-SIR coupled risk model was then developed to incorporate the findings: that ventilation layout and infection source location can impact the distribution of infection risk in a space. The objective was to develop a method to determine the airborne transmission risk in an indoor space, to then evaluate the long-term infection dynamics through the population within that space. The model included steps to divide the evaluated indoor space into multiple zones, with infection sources in each zone. CFD studies were run on the domain to determine the resultant particle dispersion patterns for the ventilation layout. The particle dispersion and accumulation results were discriminated by their source injections to identify high, medium, and low risk zones. The results also indicated which zones contributed particles towards their neighboring zones. The average particle accumulation results from respective zones were translated into transmission rates to be modelled into an epidemic SIR model. Pseudo-reproduction numbers were then acquired from the SIR model. The model was applied to a square domain with 36 occupants, for three different scenarios: with two outlets at the back of the room, with four outlets separated equally in the front and back of the room, and with two outlets and reduced occupancy; the resultant pseudo-reproduction numbers were 3.71, 3.02 and 2.82, respectively. The model evaluated the risk of infection in a room with long-term infection dynamics considered, resolved the dependency of infection source location and quantified the risk of infection considering the ventilation layout and additional control measures. Further work is required to validate the model and apply it to other settings. The model may be long and cumbersome, with areas of further improvement, but currently it provides a method to easily compare between different control measures, considering several factors boiled down to a simple pseudo-reproduction number.

Considering the work done in this thesis, it can be concluded that if the viral stability can be retained for more than 3 hours [64], expelled aerosols can travel significantly further than 2 m in distance, as particles dispersed extensively for both the office space and lecture hall settings in less than 5 minutes. It was also noted that the ventilation layout and configuration can significantly impact the pattern by which the expelled aerosols are transported within the space. This means HVAC and building designers need to be concerned with the most optimal layouts to minimize the

dispersion of airborne particulates when planning the ventilation design. Additionally, the risk of airborne transmitted infection can drastically change based on the infection source location with the respect to the room and the ventilation layout. So, when simulating and planning for ventilation layouts to reduce airborne transmitted infection, several different areas for infection source location should be considered.

In terms of suggested ventilation types, mixing ventilation is a safe bet when there is lack of resources to evaluate different ventilation configurations, as it is less dependent on infection source location in comparison to displacement/stratified ventilation setups. However, displacement ventilation can be very beneficial in a levelled floor setting (all occupants have the same breathing height) with air outlets in the room. If super spreaders can be identified in the space, such as the speakers in the room, symptomatic occupants (in hospital waiting rooms), unvaccinated occupants and occupants not practicing masking or other hygiene measures, can be located near the room's air outlets and far from the air inlets. This ensures the air in the room has a clean-to-dirty airflow pathway. But most important to note that, there is no "one-solution-fits-all" technique for minimizing airborne transmission in all spaces, which is why future work is crucial.

7.1. Future Work

Validation is important for any CFD study to ensure that the results can be extrapolated towards real events. In the case of this thesis study, the temperature distributions, the airflow pathways, and the particle transport patterns needed to be validated. A thorough validation study was conducted with Yin et al.'s experimental data of an isolation ward [128]. However, several components could have been lost in translation with third-party data, as well as applying the methodology to a whole new domain. During the thesis study experimental work was unfeasible with limited lab access, and frequent lockdowns during the pandemic. For future work, an in-lab validation study will be more useful, as the sources of error can easily be identified, and the simulation domain can be validated (instead of methodology translation from a validation domain to a different simulated domain).

In terms of research progress, many other public indoor spaces should be simulated and studied to evaluate the factors contributing towards high risk of airborne infection transmission. The current thesis study was limited to an office space and lecture hall. Evaluating the effects of

ventilation type and infection source location in more indoor spaces would add or further confirm conclusions claimed within this thesis. More control measures such as air cleaner and plexi-glass barriers would have added value to the study. Indoor spaces where outbreaks occurred during the pandemic should also be investigated as retrospective studies; places such as call-centers, meat packing plants and other highly congregated spaces can be simulated, to identify the main contributors to such outbreaks. The developed CFD-SIR risk model can also be applied to these spaces to identify the best control measures to be implemented. Further work can be done to identify any novel ventilation strategies and other control measures that are effective at removing expelled aerosols and contaminants in indoor spaces.

This study is concluded with the hope that research will be continued, to gain progress in the fields of indoor air and airborne transmission minimization techniques. The history of negligence towards airborne transmission pathways and the lack of research to prevent airborne transmitted infection led to the controversy, ill-preparedness and misinformation seen during the COVID-19 pandemic. This research study and the work done by other researchers since the SARS-CoV-2 virus emerged, has emphasized one important fact, that we are not ready for another infectious airborne transmitted disease anytime soon. Significant work needs to be done towards research, design, standardization and regulation of building air and airborne transmission control measures. This work is very much needed for a future that is more prepared for emerging airborne transmitted diseases.

References

[1] T. Fisher *et al.*, “WHO-convened Global Study of Origins of SARS-CoV-2,” 2021.

[2] S. Singh *et al.*, “How an outbreak became a pandemic: a chronological analysis of crucial junctures and international obligations in the early months of the COVID-19 pandemic.,” *Lancet*, vol. 398, no. 10316, pp. 2109–2124, Dec. 2021, doi: 10.1016/S0140-6736(21)01897-3.

[3] W. H. O. (WHO), “Modes of transmission of virus causing COVID-19: implications for IPC precaution recommendations,” *Geneva: World Health Organization;*, vol. Available, no. March, pp. 19–21, 2020, doi: 10.1056/NEJMc2004973.Cheng.

[4] J. L. Jimenez *et al.*, “What were the historical reasons for the resistance to recognizing airborne transmission during the COVID -19 pandemic? ,” *Indoor Air*, vol. 32, no. 8, pp. 1–18, 2022, doi: 10.1111/ina.13070.

[5] World Health Organization, “FACT: COVID-19 is NOT AIRBORNE,” *Twitter*, Mar. 28, 2020. [Online]. Available: https://twitter.com/who/status/1243972193169616898

[6] L. Morawska and D. K. Milton, “It is Time to Address Airborne Transmission of COVID-19,” pp. 1–41, 2020.

[7] D. Lewis, “Why the WHO took two years to say COVID is airborne,” *Nature*, vol. 604, no. 7904, pp. 26–31, 2022, doi: 10.1038/d41586-022-00925-7.

[8] K. Randall *et al.*, “How did we get here: What are droplets and aerosols and how far do they go? A historical perspective on the transmission of respiratory infectious diseases,” *Interface Focus*, vol. 11, no. 6, 2021, doi: 10.1098/rsfs.2021.0049.

[9] L. Morawska, “Droplet fate in indoor environments, or can we prevent the spread of infection?,” *Indoor Air*, vol. 16, no. 5, pp. 335–347, 2006, doi: 10.1111/j.1600-0668.2006.00432.x.

[10] L. Morawska *et al.*, “A paradigm shift to combat indoor respiratory infection,” *Science (1979)*, vol. 372, no. 6543, pp. 689–691, 2021, doi: 10.1126/science.abg2025.

[11] “Airborne Transmission of SARS-CoV-2: Proceedings of a Workshop in Brief,” *Airborne Transmission of SARS-CoV-2*, 2020, doi: 10.17226/25958.

[12] K. Khankari, “Analysis of Airflow Patterns and Probability of Infection in Indoor Spaces – A Concept of Aerodynamic Containment,” in *ASHRAE Annual Conference*, 2021.

[13] J. M. Mahesh Jayaweera, Hasini Perera, and Buddhika Gunawardana, “Transmission of COVID-19 virus by droplets and aerosols: A critical review on the unresolved dichotomy,” *Ann Oncol*, no. January, pp. 19–21, 2020, doi: 10.1007/s00134-020-05991-x.Bizzarro.

[14] K. W. D. Cheong and S. Y. Phua, “Development of ventilation design strategy for effective removal of pollutant in the isolation room of a hospital,” *Build Environ*, vol. 41, no. 9, pp. 1161–1170, 2006, doi: 10.1016/j.buildenv.2005.05.007.

[15] Y. E. Cetin, M. Avci, and O. Aydin, “Influence of ventilation strategies on dispersion and removal of fine particles: An experimental and simulation study,” *Sci Technol Built Environ*, vol. 26, no. 3, pp. 349–365, 2020, doi: 10.1080/23744731.2019.1701332.

[16] R. He *et al.*, “Airborne transmission of COVID-19 and mitigation using box fan air cleaners in a poorly ventilated classroom,” *Physics of Fluids*, vol. 33, no. 5, pp. 1–14, 2021, doi: 10.1063/5.0050058.

[17] D. S. Thatiparti, U. Ghia, and K. R. Mead, “Computational fluid dynamics study on the influence of an alternate ventilation configuration on the possible flow path of infectious cough aerosols in a mock airborne infection isolation room,” *Sci Technol Built Environ*, vol. 23, no. 2, pp. 355–366, 2017, doi: 10.1080/23744731.2016.1222212.

[18] S. Shao *et al.*, “Risk assessment of airborne transmission of COVID-19 by asymptomatic individuals under different practical settings,” *J Aerosol Sci*, vol. 151, no. August 2020, p. 105661, 2021, doi: 10.1016/j.jaerosci.2020.105661.

[19] S. Zhu *et al.*, “An advanced numerical model for the assessment of airborne transmission of influenza in bus microenvironments,” *Building and Environment*, vol. 47, no. 1. pp. 67–75, 2012. doi: 10.1016/j.buildenv.2011.05.003.

[20] A. A. Aliabadi *et al.*, “Preventing Airborne Disease Transmission-Review of Methods for Ventilation Design in Health Care Facilities Aliabadi et al 2011.pdf.”

[21] J. Zhang, “Integrating IAQ control strategies to reduce the risk of asymptomatic SARS CoV-2 infections in classrooms and open plan offices,” *Sci Technol Built Environ*, vol. 26, no. 8, pp. 1013–1018, 2020, doi: 10.1080/23744731.2020.1794499.

[22] A. Novoselac and J. Srebric, “Comparison of air exchange efficiency and contaminant removal effectiveness as IAQ indices,” *ASHRAE Trans*, vol. 109 PART 2, no. 4663, pp. 339–349, 2003.

[23] R. K. Bhagat *et al.*, “Effects of ventilation on the indoor spread of COVID-19,” *J Fluid Mech*, vol. 903, 2020, doi: 10.1017/jfm.2020.720.

[24] Q. He *et al.*, “CFD study of exhaled droplet transmission between occupants under different ventilation strategies in a typical office room.pdf.” Build. Environ., pp. 397–408, 2011. [Online]. Available: doi:10.1016/j.buildenv.2010.08.003

[25] M. Abuhegazy *et al.*, “Numerical investigation of aerosol transport in a classroom with relevance to COVID-19,” *Physics of Fluids*, vol. 32, no. 10, 2020, doi: 10.1063/5.0029118.

[26] Y. Yan *et al.*, “Evaluation of airborne disease infection risks in an airliner cabin using the Lagrangian-based Wells-Riley approach,” *Build Environ*, vol. 121, pp. 79–92, 2017, doi: 10.1016/j.buildenv.2017.05.013.

[27] K. Talaat *et al.*, “Simulation of aerosol transmission on a Boeing 737 airplane with intervention measures for COVID-19 mitigation Simulation of aerosol transmission on a Boeing 737 airplane with intervention measures for COVID-19 mitigation,” vol. 033312, no. February, 2021, doi: 10.1063/5.0044720.

[28] F. Cui *et al.*, “Transport and fate of virus-laden particles in a supermarket: Recommendations for risk reduction of COVID-19 spreading,” *Journal of Environmental Engineering*, vol. 147, no. 4, pp. 1–15, 2021, doi: 10.1061/(ASCE)EE.1943-7870.0001870.

[29] E. C. Riley, G. Murphy, and R. L. Riley, “Airboren spread of measles in a suburban elementary school,” *Am J Epidemiol*, vol. 107, no. 5, pp. 421–432, May 1978, doi: 10.1093/oxfordjournals.aje.a112560.

[30] W. F. Wells, “On air-borne infection: study II. droplets and droplet nuclei.,” *Am J Epidemiol*, vol. 20, no. 3, pp. 611–618, Nov. 1934, doi: 10.1093/oxfordjournals.aje.a118097.

[31] A. Henriques *et al.*, “Modelling airborne transmission of SARS-CoV-2 using CARA: Risk assessment for enclosed spaces,” *Interface Focus*, vol. 12, no. 2, 2022, doi: 10.1098/rsfs.2021.0076.

[32] M. Z. Bazant and J. W. M. Bush, “A guideline to limit indoor airborne transmission of COVID-19,” *Proc Natl Acad Sci U S A*, vol. 118, no. 17, 2021, doi: 10.1073/pnas.2018995118.

[33] R. Mittal, C. Meneveau, and W. Wu, “A mathematical framework for estimating risk of airborne transmission of COVID-19 with application to face mask use and social distancing,” *Physics of Fluids*, vol. 32, no. 10, 2020, doi: 10.1063/5.0025476.

[34] X. Li *et al.*, “A spatiotemporally resolved infection risk model for airborne transmission of COVID-19 variants in indoor spaces,” *Science of the Total Environment*, vol. 812, p. 152592, 2022, doi: 10.1016/j.scitotenv.2021.152592.

[35] H. Asanuma and K. Ito, “Integrated Approach of CFD and SIR Epidemiological Model for Infectious Transmission Analysis in Hospital,” in *Towards Optimal Airtightness Performance*, 2011, pp. 170–173.

[36] C. Noakes and A. Sleigh, “Applying the Wells-Riley equation to the risk of airborne infection in hospital environments : The importance of stochastic and proximity effects,” 2008.

[37] World Health Organization, “WHO Coronavirus (COVID-19) Dashboard,” *WHO Health Emergency Dashboard*. https://covid19.who.int/

[38] J. C. Castillo *et al.*, “Market design to accelerate COVID-19 vaccine supply.,” *Science*, vol. 371, no. 6534, pp. 1107–1109, Mar. 2021, doi: 10.1126/science.abg0889.

[39] G. Gopinath, “Reopening from the great lockdown: Uneven and Uncertain recovery,” *IMF Blog*, 2020. [Online]. Available: https://www.imf.org/en/Blogs/Articles/2020/06/24/blog-weo-update-reopening-from-the-great-lockdown-uneven-and-uncertain-recovery

[40] R. Tellier *et al.*, “Recognition of aerosol transmission of infectious agents: A commentary,” *BMC Infect Dis*, vol. 19, no. 1, pp. 1–9, 2019, doi: 10.1186/s12879-019-3707-y.

[41] G. Seminara *et al.*, *Biological fluid dynamics of airborne COVID-19 infection*, vol. 31, no. 3. Springer International Publishing, 2020.

[42] P. Bahl *et al.*, “Airborne or Droplet Precautions for Health Workers Treating Coronavirus Disease 2019?,” *J Infect Dis*, Apr. 2020, doi: 10.1093/infdis/jiaa189.

[43] E. J. Stewart *et al.*, “ASHRAE Position Document on,” 2012.

[44] X. Xie *et al.*, “How far droplets can move in indoor environments,” *Indoor Air*, vol. 17, pp. 211–2256, 2007, doi: 10.1111/j.1600-0668.2006.00469.x.

[45] J. P. Duguid, “The size and the duration of air-carriage of respiratory droplets and droplet-nuclei,” *Journal of Hygiene*, vol. 44, no. 6, pp. 471–479, 1946, doi: 10.1017/S0022172400019288.

[46] M. E. Rosti *et al.*, “Fluid dynamics of COVID-19 airborne infection suggests urgent data for a scientific design of social distancing,” *Sci Rep*, vol. 10, no. 1, pp. 1–9, 2020, doi: 10.1038/s41598-020-80078-7.

[47] S. Yang *et al.*, “The size and concentration of droplets generated by coughing in human subjects.,” *J Aerosol Med*, vol. 20, no. 4, pp. 484–494, 2007, doi: 10.1089/jam.2007.0610.

[48] X. Xie *et al.*, “Exhaled droplets due to talking and coughing (Xie et al, 2009).pdf,” *J R Soc Interface*, vol. 6, no. October, pp. 703–714, 2009.

[49] G. R. Johnson *et al.*, “Modality of human expired aerosol size distributions,” *J Aerosol Sci*, vol. 42, no. 12, pp. 839–851, 2011, doi: 10.1016/j.jaerosci.2011.07.009.

[50] J. P. Duguid, “The numbers and the sites of origin of the droplets expelled during expiratory activities.,” *Edinb Med J*, vol. 52, no. 11, pp. 385–401, Nov. 1945.

[51] L. Liu *et al.*, “Evaporation and dispersion of respiratory droplets from coughing,” *Indoor Air*, vol. 27, no. 1, pp. 179–190, 2017, doi: 10.1111/ina.12297.

[52] A. C. Lowen *et al.*, “Influenza virus transmission is dependent on relative humidity and temperature,” *PLoS Pathog*, vol. 3, no. 10, pp. 1470–1476, 2007, doi: 10.1371/journal.ppat.0030151.

[53] P. Mecenas *et al.*, “Effects of temperature and humidity on the spread of COVID-19: A systematic review,” *PLoS ONE*, vol. 15, no. 9 September. 2020. doi: 10.1371/journal.pone.0238339.

[54] T. Yao and Z. Lin, “An experimental and numerical study on the effect of air terminal layout on the performance of stratum ventilation,” *Build Environ*, vol. 82, pp. 75–86, 2014, doi: 10.1016/j.buildenv.2014.08.016.

[55] S. Yuan, S. C. Jiang, and Z. L. Li, “Do Humidity and Temperature Impact the Spread of the Novel Coronavirus?,” *Front Public Health*, vol. 8, no. May, pp. 8–11, 2020, doi: 10.3389/fpubh.2020.00240.

[56] W. Yang and L. C. Marr, “Dynamics of Airborne influenza A viruses indoors and dependence on humidity,” *PLoS One*, vol. 6, no. 6, 2011, doi: 10.1371/journal.pone.0021481.

[57] A. Ahlawat, A. Wiedensohler, and S. K. Mishra, “An overview on the role of relative humidity in airborne transmission of sars-cov-2 in indoor environments,” *Aerosol Air Qual Res*, vol. 20, no. 9, pp. 1856–1861, 2020, doi: 10.4209/aaqr.2020.06.0302.

[58] K. Lin and L. C. Marr, “Humidity-Dependent Decay of Viruses, but Not Bacteria, in Aerosols and Droplets Follows Disinfection Kinetics,” *Environ Sci Technol*, vol. 54, no. 2, pp. 1024–1032, 2020, doi: 10.1021/acs.est.9b04959.

[59] ASHRAE, “Ashrae Epidemic Task Force. Healthcare,” *Ashrae*, p. 2021, 2021, [Online]. Available: https://www.ashrae.org/file library/technical resources/covid-19/ashrae-filtration_disinfection-c19-guidance.pdf

[60] C. C. Tseng and C. S. Li, “Inactivation of viruses on surfaces by ultraviolet germicidal irradiation,” *J Occup Environ Hyg.*, vol. 4, no. 6, pp. 400–405, 2007, doi: 10.1080/15459620701329012.

[61] C. M. Walker and G. Ko, “Effect of ultraviolet germicidal irradiation on viral aerosols,” *Environ Sci Technol*, vol. 41, no. 15, pp. 5460–5465, 2007, doi: 10.1021/es070056u.

[62] C. W. Lo *et al.*, “UVC disinfects SARS-CoV-2 by induction of viral genome damage without apparent effects on viral morphology and proteins,” *Sci Rep*, vol. 11, no. 1, pp. 1–11, 2021, doi: 10.1038/s41598-021-93231-7.

[63] M. Schuit *et al.*, “Airborne SARS-CoV-2 is rapidly inactivated by simulated sunlight,” *Journal of Infectious Diseases*, vol. 222, no. 4, pp. 564–571, 2020, doi: 10.1093/infdis/jiaa334.

[64] van Doremalen N, Bushmaker T, Morris DH, “Aerosol and Surface Stability of SARS-CoV-2 as Compared with SARS-CoV-1,” *N Engl J Med*, pp. 0–2, 2020.

[65] M. Yao *et al.*, “On airborne transmission and control of SARS-Cov-2,” *Sci Total Environ*, vol. 731, p. 139178, 2020, doi: 10.1016/j.scitotenv.2020.139178.

[66] P. Piscitelli *et al.*, “The role of outdoor and indoor air quality in the spread of SARS-CoV-2: Overview and recommendations by the research group on COVID-19 and particulate matter (RESCOP commission),” *Environ Res*, vol. 211, no. February, 2022, doi: 10.1016/j.envres.2022.113038.

[67] J. Wei and Y. Li, “Enhanced spread of expiratory droplets by turbulence in a cough jet,” *Build Environ*, vol. 93, no. P2, pp. 86–96, 2015, doi: 10.1016/j.buildenv.2015.06.018.

[68] L. Bourouiba, E. Dehandschoewercker, and J. W. M. Bush, “Violent expiratory events: On coughing and sneezing,” *J Fluid Mech*, vol. 745, no. April, pp. 537–563, 2014, doi: 10.1017/jfm.2014.88.

[69] J. K. Gupta, C. H. Lin, and Q. Chen, “Flow dynamics and characterization of a cough,” *Indoor Air*, vol. 19, no. 6, pp. 517–525, 2009, doi: 10.1111/j.1600-0668.2009.00619.x.

[70] J. W. Tang *et al.*, “A schlieren optical study of the human cough with and without wearing masks for aerosol infection control,” *J R Soc Interface*, vol. 6, no. SUPPL. 6, pp. 727–736, 2009, doi: 10.1098/rsif.2009.0295.focus.

[71] J. Wei and Y. Li, “Human cough as a two-stage jet and its role in particle transport,” *PLoS One*, vol. 12, no. 1, pp. 1–15, 2017, doi: 10.1371/journal.pone.0169235.

[72] S. W. Zhu, S. Kato, and J. H. Yang, “Study on transport characteristics of saliva droplets produced by coughing in a calm indoor environment,” *Build Environ*, vol. 41, no. 12, pp. 1691–1702, 2006, doi: 10.1016/j.buildenv.2005.06.024.

[73] M. Vansciver, S. Miller, and J. Hertzberg, “Particle image velocimetry of human cough,” *Aerosol Science and Technology*, vol. 45, no. 3, pp. 415–422, 2011, doi: 10.1080/02786826.2010.542785.

[74] A. A. Aliabadi *et al.*, “CFD simulation of human coughs and sneezes: A study in droplet dispersion, heat, and mass transfer,” *ASME International Mechanical Engineering Congress and Exposition, Proceedings (IMECE)*, vol. 7, no. PARTS A AND B, pp. 1051–1060, 2010, doi: 10.1115/IMECE2010-37331.

[75] L. Bourouiba, “The Fluid Dynamics of Disease Transmission,” *Annual Review of Fluid Mechanics*, vol. 53. pp. 473–508, 2021. doi: 10.1146/annurev-fluid-060220-113712.

[76] Y. Tang, “Computational Fluid Dynamics Study of Aerosol Transport and Deposition Mechanisms,” 2012.

[77] Ansys®, “15.2.1 Discrete Phase: Equations of Motion for Particles,” in *ANSYS Fluent Theory Guide 12.0*, ANSYS, Inc., 2009.

[78] Y. Tang and B. Guo, “Computational fluid dynamics simulation of aerosol transport and deposition,” *Frontiers of Environmental Science and Engineering in China*, vol. 5, no. 3, pp. 362–377, 2011, doi: 10.1007/s11783-011-0365-8.

[79] P. G. Saffman, “The lift on a small sphere in a slow shear flow,” *J Fluid Mech*, vol. 22, no. 2, pp. 385–400, 1965, doi: 10.1017/S0022112065000824.

[80] A. Tsuda, F. S. Henry, and J. P. Butler, “Particle transport and deposition: Basic physics of particle kinetics,” *Compr Physiol*, vol. 3, no. 4, pp. 1437–1471, 2013, doi: 10.1002/cphy.c100085.

[81] H. Q. McLean *et al.*, “Prevention of Measles, Rubella, Congenital Rubella Syndrome, and Mumps, 2013,” *Morbidity and Mortality Weekly Report*, vol. 62, no. 4, pp. 1–34, 2013.

[82] P. L. Remington *et al.*, “Airborne Transmission of Measles in a Physician’s Office,” *JAMA*, vol. 253, no. 11, pp. 1574–1577, 1985, doi: 10.1001/jama.1985.03350350068022.

[83] “Air,” *Centers for Disease Control and Prevention*. https://www.cdc.gov/infectioncontrol/guidelines/environmental/background/air.html#c2c (accessed Jun. 23, 2022).

[84] A. A. Gershon *et al.*, “Varicella zoster virus infection,” *Nat Rev Dis Primers*, vol. 1, p. 15016, Jul. 2015, doi: 10.1038/nrdp.2015.16.

[85] E. A. Nardell, “Transmission and Institutional Infection Control of Tuberculosis,” *Cold Spring Harb Perspect Med*, vol. 6, no. 2, pp. a018192–a018192, Aug. 2015, doi: 10.1101/cshperspect.a018192.

[86] S. Herfst *et al.*, “Airborne Transmission of Influenza A/H5N1 Virus Between Ferrets,” *Science (1979)*, vol. 336, no. 6088, pp. 1534–1541, 2012, doi: 10.1126/science.1213362.

[87] B. J. Cowling *et al.*, “Aerosol transmission is an important mode of influenza A virus spread,” *Nat Commun*, 1935, doi: 10.1038/ncomms2922.

[88] R. Tellier, “Review of aerosol transmission of influenza A virus,” *Emerg Infect Dis*, vol. 12, no. 11, pp. 1657–1662, 2006, doi: 10.3201/eid1211.060426.

[89] R. Tellier, “Aerosol transmission of influenza A virus: A review of new studies,” *J R Soc Interface*, vol. 6, no. SUPPL. 6, 2009, doi: 10.1098/rsif.2009.0302.focus.

[90] H. Kulkarni *et al.*, “Evidence of respiratory syncytial virus spread by aerosol time to revisit infection control strategies?,” *Am J Respir Crit Care Med*, vol. 194, no. 3, pp. 308–316, Aug. 2016, doi: 10.1164/RCCM.201509-1833OC/SUPPL_FILE/DISCLOSURES.PDF.

[91] T. A. Myatt *et al.*, “Airborne rhinovirus detection and effect of ultraviolet irradiation on detection by a semi-nested RT-PCR assay,” *BMC Public Health*, vol. 3, no. 1, p. 5, 2003, doi: 10.1186/1471-2458-3-5.

[92] S.-H. Kim *et al.*, “Extensive Viable Middle East Respiratory Syndrome (MERS) Coronavirus Contamination in Air and Surrounding Environment in MERS Isolation Wards,” *Clinical Infectious Diseases*, vol. 63, no. 3, pp. 363–369, Aug. 2016, doi: 10.1093/cid/ciw239.

[93] I. T. S. Yu *et al.*, “Evidence of Airborne Transmission of the Severe Acute Respiratory Syndrome Virus,” *New England Journal of Medicine*, vol. 350, no. 17, pp. 1731–1739, 2004, doi: 10.1056/NEJMoa032867.

[94] S. J. Olsen *et al.*, “Transmission of the Severe Acute Respiratory Syndrome on Aircraft,” *New England Journal of Medicine*, vol. 349, no. 25, pp. 2416–2422, 2003, doi: 10.1056/NEJMoa031349.

[95] T. F. Booth *et al.*, “Detection of Airborne Severe Acute Respiratory Syndrome (SARS) Coronavirus and Environmental Contamination in SARS Outbreak Units,” *J Infect Dis*, vol. 191, no. 9, pp. 1472–1477, 2005, doi: 10.1086/429634.

[96] J. S. Kutter *et al.*, “SARS-CoV and SARS-CoV-2 are transmitted through the air between ferrets over more than one meter distance,” *Nat Commun*, vol. 12, no. 1, 2021, doi: 10.1038/s41467-021-21918-6.

[97] S. J. Smither *et al.*, “Experimental aerosol survival of SARS-CoV-2 in artificial saliva and tissue culture media at medium and high humidity,” *Emerg Microbes Infect*, vol. 9, no. 1, pp. 1415–1417, 2020, doi: 10.1080/22221751.2020.1777906.

[98] S. Y. Park *et al.*, “Coronavirus disease outbreak in call center, South Korea,” *Emerg Infect Dis*, vol. 26, no. 8, pp. 1666–1670, 2020, doi: 10.3201/eid2608.201274.

[99] C. A. Taylor, C. Boulos, and D. Almond, “Livestock plants and COVID-19 transmission,” *Proceedings of the National Academy of Sciences*, vol. 117, no. 50, pp. 31706–31715, 2020, doi: 10.1073/pnas.2010115117.

[100] E. Dahl, “Coronavirus (Covid-19) outbreak on the cruise ship Diamond Princess.,” *International maritime health*, vol. 71, no. 1. Poland, pp. 5–8, 2020. doi: 10.5603/MH.2020.0003.

[101] J. L. Santarpia *et al.*, “Aerosol and surface Transmission Potential of SARS-CoV-2,” *Https://Doi.Org/10.1101/2020.03.23.20039446* ., pp. 1–19, 2020.

[102] Z. D. Guo *et al.*, “Aerosol and Surface Distribution of Severe Acute Respiratory Syndrome Coronavirus 2 in Hospital Wards, Wuhan, China, 2020,” *Emerg Infect Dis*, vol. 26, no. 7, pp. 1586–1591, 2020, doi: 10.3201/eid2607.200885.

[103] J. A. Lednicky *et al.*, “Viable SARS-CoV-2 in the air of a hospital room with COVID-19 patients,” *International Journal of Infectious Diseases*, no. 1, pp. 1–20, 2020, doi: 10.1016/j.ijid.2020.09.025.

[104] S. W. X. Ong *et al.*, "Air, Surface Environmental, and Personal Protective Equipment Contamination by Severe Acute Respiratory Syndrome Coronavirus 2 (SARS-CoV-2) From a Symptomatic Patient," *JAMA*, vol. 323, no. 16, pp. 1610–1612, Apr. 2020, doi: 10.1001/jama.2020.3227.

[105] Y. Liu *et al.*, "Aerodynamic analysis of SARS-CoV-2 in two Wuhan hospitals," *Nature*, vol. 582, no. 7813, pp. 557–560, 2020, doi: 10.1038/s41586-020-2271-3.

[106] P. K. Nag, *Office Buildings: Health, Safety and Environment*, vol. 203, no. 8. 2019.

[107] L. Morawska *et al.*, "How can airborne transmission of COVID-19 indoors be minimised?," *Environ Int*, vol. 142, no. May, 2020, doi: 10.1016/j.envint.2020.105832.

[108] T. Lipinski *et al.*, "Review of ventilation strategies to reduce the risk of disease transmission in high occupancy buildings," *International Journal of Thermofluids*, vol. 7–8, p. 100045, 2020, doi: 10.1016/j.ijft.2020.100045.

[109] J. Muthusamy *et al.*, "Implication of coughing dynamics on safe social distancing in an indoor environment-A numerical perspective," *Build Environ*, vol. 206, p. 108280, Dec. 2021, doi: 10.1016/j.buildenv.2021.108280.

[110] Y. Li *et al.*, "Running title : Aerosol transmission of SARS-CoV-2 Evidence for probable aerosol transmission of SARS-CoV-2 in a poorly ventilated restaurant," pp. 1–19, 2020.

[111] F. Memarzadeh and W. Xu, "Role of air changes per hour (ACH) in possible transmission of airborne infections," *Building Simulation*, vol. 5, no. 1. 2012. doi: 10.1007/s12273-011-0053-4.

[112] REHVA, "COVID-19 Ventilation Calculator," no. November, pp. 1–12, 2020, [Online]. Available: https://www.rehva.eu/covid19-ventilation-calculator

[113] S. Liu *et al.*, "Investigation of airborne particle exposure in an office with mixing and displacement ventilation," *Sustain Cities Soc*, vol. 79, no. January, p. 103718, 2022, doi: 10.1016/j.scs.2022.103718.

[114] J. M. Villafruela *et al.*, "Assessment of displacement ventilation systems in airborne infection risk in hospital rooms," *PLoS One*, vol. 14, no. 1, pp. 1–18, 2019, doi: 10.1371/journal.pone.0211390.

[115] S. Taylor, "COVID-19 White Paper How is COVID-19 transmitted ?," pp. 1–30, 2020, [Online]. Available: https://taylorengineers.com/taylor-engineering-covid-19-whitepaper

[116] L. Morawska *et al.*, “How can airborne transmission of COVID-19 indoors be minimised?,” *Environ Int*, vol. 142, p. 105832, 2020, doi: 10.1016/j.envint.2020.105832.

[117] D. T. Liu *et al.*, “Portable HEPA Purifiers to Eliminate Airborne SARS-CoV-2: A Systematic Review,” *Otolaryngology - Head and Neck Surgery (United States)*, vol. 166, no. 4. pp. 615–622, 2022. doi: 10.1177/01945998211022636.

[118] W. G. Lindsley *et al.*, “Efficacy of Portable Air Cleaners and Masking for Reducing Indoor Exposure to Simulated Exhaled SARS-CoV-2 Aerosols — United States, 2021,” *MMWR Morb Mortal Wkly Rep*, vol. 70, no. 27, pp. 972–976, 2021, doi: 10.15585/mmwr.mm7027e1.

[119] R. Kosonen *et al.*, “Mixing Ventilation – New REHVA Guidebook No 19,” *REHVA Journal*, vol. 50, no. 4, pp. 64–67, 2013.

[120] Price Industries, “Engineering Guide Displacement Ventilation,” *Price Engineer’s HVAC Handbook*, vol. 1, no. 4, pp. 1–48, 2011.

[121] N. Gao, J. Niu, and L. Morawska, “Distribution of respiratory droplets in enclosed environments under different air distribution methods,” *Build Simul*, vol. 1, no. 4, pp. 326–335, 2008, doi: 10.1007/s12273-008-8328-0.

[122] S. Ren, S. Tian, and X. Meng, “Comparison of Displacement Ventilation, Mixing Ventilation and Underfloor Air Distribution System,” no. Icache, pp. 79–82, 2015, doi: 10.2991/icache-15.2015.16.

[123] H. Qian and X. Zheng, “Ventilation control for airborne transmission of human exhaled bio-aerosols in buildings,” *Journal of Thoracic Disease*, vol. 10. pp. S2295–S2304, 2018. doi: 10.21037/jtd.2018.01.24.

[124] Z. Lin *et al.*, “Investigation into anti-airborne infection performance of stratum ventilation,” *Build Environ*, vol. 54, pp. 29–38, 2012, doi: 10.1016/j.buildenv.2012.01.017.

[125] L. Tian *et al.*, “Numerical investigation of indoor aerosol particle dispersion under stratum ventilation and under displacement ventilation,” *Indoor and Built Environment*, vol. 18, no. 4, pp. 360–375, 2009, doi: 10.1177/1420326X09337335.

[126] X. Tian *et al.* “Multi-indicator evaluation on ventilation effectiveness of three ventilation methods: An experimental study,” *Build Environ*, vol. 180, no. July, p. 107015, 2020, doi: 10.1016/j.buildenv.2020.107015.

[127] G. A. Somsen *et al.*, “Small droplet aerosols in poorly ventilated spaces and SARS-CoV-2 transmission,” *Lancet Respir Med*, vol. 8, no. 7, pp. 658–659, 2020.

[128] Y. Yin *et al.*, “Experimental study on displacement and mixing ventilation systems for a patient ward,” *HVAC and R Research*, vol. 15, no. 6, pp. 1175–1191, 2009, doi: 10.1080/10789669.2009.10390885.

[129] H. Qian and X. Zheng, “Ventilation control for airborne transmission of human exhaled bio-aerosols in buildings,” *J Thorac Dis*, vol. 10, no. Suppl 19, pp. S2295–S2304, 2018, doi: 10.21037/jtd.2018.01.24.

[130] J. M. Villafruela *et al.* “Assessment of displacement ventilation systems in airborne infection risk in hospital rooms,” *PLoS ONE*, vol. 14, no. 1. 2019.

[131] A. A. Aliabadi *et al.*, “Hybrid Ventilation Design for a dining hall using computational fluid dynamics (CFD),” *Proceedings of The Canadian Society for Mechanical Engineering (CSME) International Congress*, no. June, pp. 1–6, 2014, doi: 10.13140/2.1.3784.1608.

[132] Y. Lu, M. Oladokun, and Z. Lin, “Reducing the exposure risk in hospital wards by applying stratum ventilation system,” *Build Environ*, vol. 183, no. June, p. 107204, 2020, doi: 10.1016/j.buildenv.2020.107204.

[133] “Displacement Flow Recessed Diffuser - Displacement - Price Industries.” https://www.priceindustries.com/displacement/products/1-way-displacement-diffuser-recessed-applications (accessed May 24, 2022).

[134] J. Li *et al.*, “Global airflow field distribution in a cabin mock-up measured via large-scale 2D-PIV,” *Build Environ*, vol. 93, no. P2, pp. 234–244, Nov. 2015, doi: 10.1016/J.BUILDENV.2015.06.030.

[135] H. K. Versteeg *et al.*, “Using Phase Doppler Anemometry and High Speed Imaging to Analyze MDI Spray Plume Dynamics,” *Respiratory Drug Delivery Europe*, 2017, [Online]. Available: https://dspace.lboro.ac.uk/dspace-jspui/bitstream/2134/24258/3/S.14.Versteeg.MR.pdf

[136] I. Olmedo *et al.*, “Distribution of exhaled contaminants and personal exposure in a room using three different air distribution strategies,” *Indoor Air*, vol. 22, no. 1, pp. 64–76, 2012, doi: 10.1111/j.1600-0668.2011.00736.x.

[137] D. S. Hui *et al.*, “Exhaled Air Dispersion during Coughing with and without Wearing a Surgical or N95 Mask,” *PLoS One*, vol. 7, no. 12, pp. 1–7, 2012, doi: 10.1371/journal.pone.0050845.

[138] B. Y. D. Rothamer *et al.*, “Minimizing Transmission In High Occupant Density Settings , Part 1,” no. May, 2021.

[139] B. C. Singer *et al.*, “Measured influence of overhead HVAC on exposure to airborne contaminants from simulated speaking in a meeting and a classroom,” *Indoor Air*, vol. 32, no. 1, pp. 1–18, 2022, doi: 10.1111/ina.12917.

[140] W. F. Wells, “Airborne Contagion and Air Hygiene. An Ecological Study of Droplet Infections.,” *Airborne Contagion and Air Hygiene. An Ecological Study of Droplet Infections.*, 1955.

[141] G. N. Sze To and C. Y. H. Chao, “Review and comparison between the Wells-Riley and dose-response approaches to risk assessment of infectious respiratory diseases,” *Indoor Air*, vol. 20, no. 1. pp. 2–16, 2010. doi: 10.1111/j.1600-0668.2009.00621.x.

[142] S. Chaudhuri, S. Basu, and A. Saha, “Analyzing the dominant SARS-CoV-2 transmission routes towards an ab initio SEIR model,” vol. 123306, no. November, 2020, doi: 10.1063/5.0034032.

[143] G. Buonanno, L. Stabile, and L. Morawska, “Estimation of airborne viral emission: Quanta emission rate of SARS-CoV-2 for infection risk assessment,” *Environ Int*, vol. 141, no. April, p. 105794, 2020, doi: 10.1016/j.envint.2020.105794.

[144] A. Foster and M. Kinzel, “Estimating COVID-19 exposure in a classroom setting: A comparison between mathematical and numerical models,” *Physics of Fluids*, vol. 33, no. 2, 2021, doi: 10.1063/5.0040755.

[145] C. J. Noakes and P. Andrew Sleigh, “Mathematical models for assessing the role of airflow on the risk of airborne infection in hospital wards,” *J R Soc Interface*, vol. 6, no. SUPPL. 6, 2009, doi: 10.1098/rsif.2009.0305.focus.

[146] R. W. C. P. Verstappen and A. E. P. Veldman, “Direct Numerical Simulation of Turbulence at Lower Costs,” *J Eng Math*, vol. 32, no. 2, pp. 143–159, 1997.

[147] H. Liu *et al.*, “Simulation-based study of COVID-19 outbreak associated with air-conditioning in a restaurant,” *Physics of Fluids*, vol. 33, no. 2, 2021, doi: 10.1063/5.0040188.

[148] X. Yang *et al.*, “Transmission of pathogen-laden expiratory droplets in a coach bus,” *J Hazard Mater*, vol. 397, no. March, p. 122609, 2020.

[149] S. Mazumdar *et al.*, “Impact of moving objects on contaminant concentration distributions in an inpatient ward with displacement ventilation,” *HVAC and R Research*, vol. 16, no. 5, pp. 545–563, 2010.

[150] H. Qian *et al.*, “Spatial distribution of infection risk of SARS transmission in a hospital ward,” *Build Environ*, vol. 44, no. 8, pp. 1651–1658, 2009, doi: 10.1016/j.buildenv.2008.11.002.

[151] D. C. Angela *et al.*, “Boeing-Computational-Fluid-Dynamics-Modeling-and-the-Transport-of-Cough-Particles-in-an-Aircraft-Cabin,” *Airbus*. 2020.

[152] J. K. Gupta, C. H. Lin, and Q. Chen, “Risk assessment of airborne infectious diseases in aircraft cabins,” *Indoor Air*, vol. 22, no. 5, pp. 388–395, 2012, doi: 10.1111/j.1600-0668.2012.00773.x.

[153] J. D. Posner, C. R. Buchanan, and D. Dunn-Rankin, “Measurement and prediction of indoor air flow in a model room,” *Energy Build*, vol. 35, no. 5, pp. 515–526, 2003, doi: 10.1016/S0378-7788(02)00163-9.

[154] D. Blay, S. Mergur, and C. Niculae, *Confined turbulent mixed convection in the presence of horizontal buoyant wall jet*. Fundamentals of Mixed Convection (American Society of Mechanical Engineers), 1992. [Online]. Available: https://books.google.ca/books?id=gBpRAAAAMAAJ

[155] Ansys®, “Academic Research Fluent.” 2020.

[156] Q. Chen, “Comparison of different k-ε models for indoor air flow computations,” *Numerical Heat Transfer, Part B: Fundamentals*, vol. 28, no. 3, pp. 353–369, 1995.

[157] Ansys®, “4.4.2 Turbulence: RNG k-epsilon Model,” in *ANSYS Fluent Theory Guide 12.0*, ANSYS, Inc., 2009.

[158] M. Chmielewski and M. Gieras, “Three-zonal Wall Function for k-ε Turbulence Models,” *Computational Methods in Science and Technology*, vol. 19, no. 2, pp. 107–114, 2013, doi: 10.12921/cmst.2013.19.02.107-114.

[159] Ansys®, “15.1. Discrete Phase: Introduction,” in *ANSYS Fluent Theory Guide 12.0*, ANSYS, Inc., 2009.

[160] Y. Cheng, J. Niu, and N. Gao, “Stratified air distribution systems in a large lecture theatre: A numerical method to optimize thermal comfort and maximize energy saving,” *Energy Build*, vol. 55, pp. 515–525, 2012.

[161] M. Ruud, “Infection probability of COVID-19 in a large lecture room with mechanical ventilation,” no. April, pp. 51–54, 2021.

[162] “Room Designer - Software - Price Industries.” https://www.priceindustries.com/software/room-designer/ (accessed May 24, 2022).

[163] B. Tang *et al.*, “An updated estimation of the risk of transmission of the novel coronavirus (2019-nCov),” *Infect Dis Model*, vol. 5, pp. 248–255, 2020, doi: https://doi.org/10.1016/j.idm.2020.02.001.

[164] I. Locatelli, B. Trächsel, and V. Rousson, “Estimating the basic reproduction number for COVID-19 in Western Europe,” *PLoS One*, vol. 16, no. 3 March, pp. 1–9, 2021, doi: 10.1371/journal.pone.0248731.

[165] M. T. Meehan *et al.*, “Modelling insights into the COVID-19 pandemic,” *Paediatr Respir Rev*, vol. 35, pp. 64–69, 2020, doi: 10.1016/j.prrv.2020.06.014.

[166] I. Harizi, S. Berkane, and A. Tayebi, “Modeling the Effect of Population-Wide Vaccination on the Evolution of COVID-19 Epidemic in Canada,” *medRxiv*, 2021, doi: 10.1101/2021.02.05.21250572.

[167] M. Prague *et al.*, “Population modeling of early COVID-19 epidemic dynamics in French regions and estimation of the lockdown impact on infection rate,” *medRxiv*, p. 2020.04.21.20073536, 2020, [Online]. Available: http://medrxiv.org/content/early/2020/04/24/2020.04.21.20073536.abstract

[168] E. Aruffo *et al.*, “COVID-19 transmission in a theme-park,” *medRxiv*, no. April, p. 2021.04.15.21255560, 2021, [Online]. Available: http://medrxiv.org/content/early/2021/04/20/2021.04.15.21255560.abstract

[169] C. J. Noakes *et al.*, “Modelling the transmission of airborne infections in enclosed spaces.,” *Epidemiol Infect*, vol. 134, no. 5, pp. 1082–1091, Oct. 2006, doi: 10.1017/S0950268806005875.

[170] S. A. Laurel *et al.*, “The Incubation Period of Coronavirus Disease 2019 (COVID-19) From Publicly Reported Confirmed Cases: Estimation and Application,” *Ann Intern Med*, vol. 172, no. 9, pp. 577–582, 2020, doi: 10.7326/M20-0504.